AFIT/GE/ENG/93J-03

AD-A266 718

DEVELOPMENT OF AN AIR-TO-AIR REFUELING
AUTOMATIC FLIGHT CONTROL SYSTEM USING
QUANTITATIVE FEEDBACK THEORY

THESIS

Dennis W. Trosen
Captain, USAF

AFIT/GE/ENG/93J-03

93-15348

93 7 08 002

DEVELOPMENT OF AN AIR-TO-AIR REFUELING

AUTOMATIC FLIGHT CONTROL SYSTEM USING

QUANTITATIVE FEEDBACK THEORY

THESIS

Presented to the Faculty of the School of Engineering

of the Air Force Institute of Technology

Air University

In Partial Fulfillment of the

Requirements for the Degree of

Master of Science in Electrical Engineering

Dennis W Trosen, B.S.E.E.

Captain, USAF

June, 1993

Accesion For		
NTIS CRA&I	☑	
DTIC TAB	☐	
Unannounced	☐	
Justification		
By		
Distribution /		
Availability Codes		
Dist	Avail and / or Special	
A-1		

Acknowledgements

I send thanks to my parents, Patricia and Kenneth Trosen, for shaping me into the man

I am today.

Prof Houpis and Prof Pachter, thank you for the knowledge to accomplish this thesis.

Kevin and Sean , you waited patiently for me, I love you and "daddy's all studied".

I dedicate this work to my wife, Chris whose love and understanding provides my

motivation, you make my life whole, I love you very much.

Dennis W. Trosen

Table of Contents

List of Figures

List of Tables

Abstract

Quantitative Feedback Theory and the improved method Quantitative Feedback

Theory are enhanced to include the rejection of disturbance at the system output. The

enhanced Quantitative Feedback Theory and improved method Quantitative Feedback

Theory processes are applied to the design of an automatic flight control system to

regulate position of the C-135B fuel receiving aircraft relative to the tanker during air-to-

air refueling. A simple feedback control system is developed that will achieve stable

position regulation. State-space aircraft models are generated. An "inner loop" autopilot

is designed to reduce the piant cutoff frequency and provide the system inputs for the

Quantitative Feedback Theory compensators. Disturbance models representing disturbance

due to wind gusts and refueling are developed. The flight control system is designed

using the enhanced Quantitative Feedback Theory equations. Linear simulations are

performed on $MATRIX_x$, and nonlinear simulations are run on EASY5x. The results of

the simulations show excellent results. The simulation results indicate that air-to-air

automatic flight control system are technically achievable, and that implementation in

US/ F aircraft is possible.

DEVELOPMENT OF AN AIR-TO-AIR REFUELING

AUTOMATIC FLIGHT CONTROL SYSTEM USING

QUANTITATIVE FEEDBACK THEORY

I. Introduction

1.1 Background

The United States Air Force (USAF) has the mission of transporting large quantities of material and troops over great distances. To meet this requirement, the USAF maintains a fleet of large cargo/transport aircraft. Refueling these aircraft during flight provides unlimited range of operation for this fleet of aircraft. However, long flights and multiple air-to-air refuelings can seriously strain and fatigue the pilot, decreasing flight safety, and extending recovery time between missions.

Cargo/transport aircraft are generally large and have high moments of inertia. Piloting a large, high inertia aircraft during air-to-air refueling requires intense concentration. The pilot must maintain a very precise position relative to the tanker. He/she maintains position visually, applying the appropriate control inputs when changes in position occur. The pilot must compensate for changes in aircraft dynamics due to taking on fuel, specifically, changes in center-of-gravity and moments of inertia I_{xx} and I_{yy}. Besides dynamic changes, the pilot must contend with maintaining position in the presence of wind gusts. Since these aircraft can take on large amounts of fuel, up to 250,000 pounds, air-to-air refueling can take up to 30 minutes. Compound this over long flights and multiple refuelings, the pilot's fatigue level increases and can reach an unsafe

1-1

level, endangering the flight crew, and possibly impact USAF's capability to perform its mission.

One way to ease the pilot workload is to implement an automatic flight control system (AFCS) for air-to-air refueling. The AFCS needs to be able to maintain a precise position of the fuel receiving aircraft (receiver) relative to the tanker in the presence of such disturbances as wind gusts and mass changes. In this thesis, an AFCS is designed to precisely regulate position relative to the tanker by applying the control synthesis techniques of Quantitative Feedback Theory (QFT). QFT is a design technique developed by Dr. Isaac Horowitz that quantifies the plant uncertainties and/or disturbances and uses this information to design feedback compensation to achieve stability, robustness, and desired system performance in the face of parametric uncertainty and disturbances[2].

For the regulation problem, a multiple-input multiple-output (MIMO) QFT design method is developed to address the disturbances entering the system at the output. Dr. Horowitz's original MIMO QFT development modeled all disturbances as entering the system at the input of the plant [3]. In this thesis, MIMO QFT is expanded to account for disturbances at the system output.

The sponsor for this thesis is the Flight Dynamics Directorate, Wright Laboratory, Wright-Patterson AFB, OH.

1.2 **Problem Statement**

During air-to-air refueling, the receiver aircraft will change position relative to the tanker. The pilot must pay close attention and take corrective action to maintain position. Excessive changes in position will disconnect the boom from the receiver. An AFCS

must be designed to regulate the receiver's position, thus reducing the pilot workload and fatigue factor. By using MIMO QFT, an AFCS is designed that operates throughout the range of the changing aircraft dynamics and rejects disturbances including those at the output [3].

1.3 Assumptions

The following assumptions are made for this thesis.

- Only the desired outputs are of interest for final performance.

- The robustness of the CAD packages used, MIMO/QFT, EASY5, MATRIX$_x$ and Mathematica are adequate for the design process.

- Position of the receiver aircraft relative to the tanker during air-to-air refueling can be accurately measured.

The first assumption is required in applying MIMO QFT. The second assumption is concerned with the limits of CAD packages and their numerical robustness. The third assumption is required because no sensors are currently in place to measure the position of the receiver relative to the tanker.

1.4 Research Objectives

This thesis (1) develops aircraft models for the QFT design from a published document [1] containing C-135 cargo aircraft stability derivatives tables and plots, (2) presents a design for multi-channel control laws using MIMO QFT for several flight conditions with special emphasis on changing aircraft center-of-gravity and weight, (3) simulates the design for linear and nonlinear performance on MATRIX$_x$, and nonlinear

performance on EASY5x, (4) evaluates the new control law, and (5) validates the development of MIMO QFT design with disturbances at the output.

1.5 Scope

This thesis applies the MIMO QFT technique to the design of an AFCS regulator for the three-dimensional separation (x, y, and z) of a C-135B (receiver) cargo aircraft relative to a tanker. The AFCS applies only to the receiver and is independent of the tanker in as much as the tanker is used as the point of reference. MIMO QFT design techniques are developed for disturbances at the system output. The present MIMO/QFT CAD package [4] is modified to incorporate the output disturbance development. The AFCS is designed to reject disturbances at the x, y, and z outputs in order to keep the receiver aircraft in a volume specified as the area of boom operation [1]. Models are developed for disturbances due to wind gusts and receiving fuel. The MIMO QFT plant is the C-135B bare-aircraft model augmented by a typical Mach-hold, altitude-hold, wing-leveler autopilot. QFT compensators control the reference signal of the autopilot to achieve "formation maintenance" during air-to-air refueling. The control system is simulated for linear performance in MATRIX$_x$. A full six-degree-of-freedom nonlinear simulation is performed in EASY5x.

1.6 Methodology

The design approach requires six steps:

- Generate linear time-invariant (LTI) state-space models of the C-135 for different weights and center of gravity.

1-4

- Implement a Mach-hold, altitude-hold, wing leveler autopilot that operates for all aircraft models.

- Model the disturbances due to wind gusts and refueling.

- Extend QFT design approach for disturbances at the output.

- Design the AFCS using QFT.

- Simulate the design on MATRIX$_x$ and EASY5x to validate the AFCS design.

1.7 Overview of the Thesis

This thesis describes the research performed in the development of the AFCS. Chapter *II* discusses QFT and the expansion of the QFT equations to include external output disturbance. The air-to-air refueling AFCS concept is discussed in Chapter *III*. Chapter *IV* presents the aircraft and disturbance models. The AFCS design process is shown in Chapter *V* followed by linear and nonlinear simulations in Chapter *VI*. Finally, Chapter *VII* presents the thesis conclusions and recommendations.

1.8 Summary

Future USAF cargo/transport requirements may very well involve long flights with many air-to-air refuelings. An AFCS to automatically pilot the aircraft during air-to-air refueling will greatly reduce the pilot workload and reduce fatigue. MIMO QFT design techniques are ideally suited for the design of such a flight control system with its wide range of parameter uncertainty. This thesis takes on the challenge of validating MIMO QFT for design of regulator AFCSs. And demonstrating automatic air-to-air refueling flight control systems are technically achievable. The next chapter briefly reviews the QFT process and the development of the output disturbance QFT design technique.

II. QFT and Output Disturbance Rejection

2.1 Introduction

The essence of QFT designed compensators is the ability to accommodate plant parameter structured uncertainty and reject disturbances [2]. This Chapter outlines the QFT method and how nonlinear plants can be modeled as linear-time-invariant (LTI) plants with uncertainty. First a brief description of QFT is presented, followed by the development of the QFT output disturbance model.

2.2 Overview of QFT

Quantitative Feedback Theory is a powerful design method for synthesizing fixed parameter compensation capable of controlling a system in the realities of large plant uncertainties, disturbance (rejection), nonlinear plant models, time variations of plant parameters, and stringent performance specifications. Included in QFT is the ability to design a compensator to cause the system to produce outputs that meet required specifications based on particular inputs and disturbance rejection requirements. The general QFT design process is based on the diagram presented in Figure 2.1, which represents either a multiple-input single-output (MISO) or a MIMO system [2] [3]. U represents the commanded input and D_1, D_2 are disturbance inputs. G(s) is a cascade compensator and F(s) is a prefilter. In QFT, $\mathcal{P}$(s) represents a set of J LTI transfer functions, representing the plant at different operating conditions. The designer chooses the individual transfer
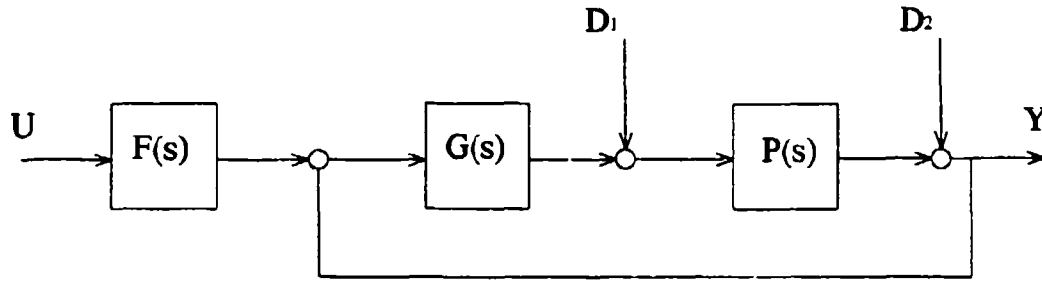
Figure 2.1 QFT Controller Design

functions, $P_j(s) \in \mathcal{P}(s)$, where j=1,2,...,J, so that the entire operational envelope or the structured uncertainty of the plant is adequately covered. The prefilter, F(s), is designed so that the system meets the tracking requirements of the output Y to the input U. For a regulator control system (as opposed to tracking) the commanded input is zero, thus, no prefilter is required.

The objective in designing the G(s) compensator is to ensure that the set of control ratios (when applicable):

$$T_R(s) = \frac{Y(s)}{U_{cmd}(s)} = \frac{F(s)G(s)P(s)}{1 + G(s)P(s)} \qquad (2.1)$$

and the disturbance ratios:

$$T_D(s) = \frac{Y(s)}{D_1(s)} = \frac{P(s)}{1 + G(s)P(s)} \qquad \text{when } D_2 = 0 \qquad (2.2)$$

$$T_D(s) = \frac{Y(s)}{D_2(s)} = \frac{P(s)}{1 + G(s)P(s)} \qquad \text{when } D_1 = 0 \qquad)$$

meet the desired performance and disturbance rejection specification for all $P_j(s) \in \mathcal{P}(s)$.

The nominal loop transmission is L_o, expressed as

2-2

$$L_o = GP_o \qquad\qquad (2.4)$$

where P_o represents the nominal plant. The designer selects $P_o \in \mathcal{P}(s)$ based on his/her preference on the placement of the templates' boundaries. To form the stability bounds, templates are derived based on the $\mathcal{P}$ information. The templates are plots of the dB magnitude versus phase, for a fixed frequency ω_i for each P_j contained within $\mathcal{P} = \{P_j\}$. L_o is shaped to meet the tracking $B_R(s)$ and/or disturbance rejection $B_D(s)$ bounds derived from the templates on the Nichols chart. Combining $B_R(s)$ and $B_D(s)$ yields the optimal boundary $B_o(j\omega)$, which along with the stability contour (U-contour), constrain L_o such that for each frequency ω_i, the Lm $L_o(j\omega_i)$ point must lie on or above $B_o(j\omega_i)$, and not intersect the U-contour. Once L_o is formed, $G(s)$ is directly derived from Eq. (2.4).

After $G(s)$ is formed, whenever applicable, the prefilter $F(s)$ is shaped to guarantee that the closed loop frequency response lies within the desired tracking specifications.

In the case where $U_{cmd} = 0$ (regulator), the prefilter is not required and the problem becomes a pure disturbance rejection problem . In this thesis, the rejection of the input disturbance D_2 at the system output is the desired performance specification.

2.3 MIMO QFT

Multiple-input multiple-output QFT design method requires transforming the system into equivalent multiple-input single-output (MISO) loops as shown in Figure 2.2 for the 3x3 case. The Schauder fixed point Theorem justifies the sequential design process, where each loop is individually "closed" [2]. Equation (2.5) represents the control ratio r_{ij} which relates the ith output to the jth input of the i,j MISO loop, where i = 1,2,...,m, and
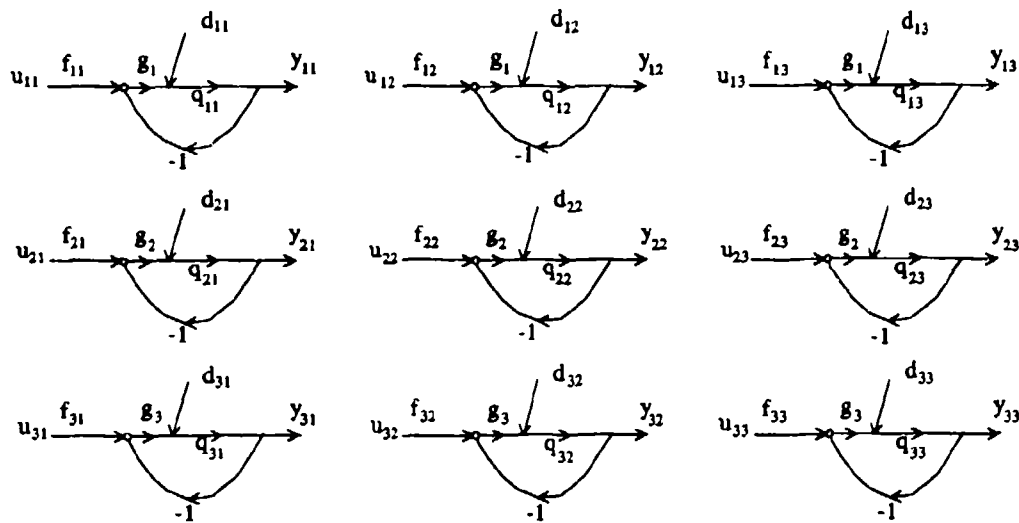
Figure 2.2 3x3 MISO Equivalent Loops

$j = 1,2,...,m, f_{ij}$ is the prefilter of the i,j MISO loop, l_i is the ith loop transmission, and d_{ij} represents the disturbance input in the i,j loop. The q_{ij} are the reciprocal of the terms contained in the inverse of the square plant matrix $P = [p_{ij}]$. That is, $P^* = [p^*_{ij}] = P^{-1}$, where $[p^*_{ij}] = [1/q_{ij}]$, and $Q = [q_{ij}]$. The disturbance d_{ij} given by Eq. (2.6) represents the cross-coupling between loops. The disturbance bounds B_D, are calculated to satisfy Eq (2.7).

$$l_{ij} = \frac{f_{ij}l_i + d_{ij}q_{ii}}{1 + l_i} \qquad (2.5)$$

$$d_{ij} = -\sum_{k \neq i}^{m}\left[\frac{t_{kj}}{q_{ik}}\right] \qquad k = 1, 2, ..., m \qquad (2.6)$$

2-4

$$\left| 1 + l_i \right| \geq \left| -\sum_{k \neq i}^{m} \frac{B_{D_k}}{q_{ik}} \right| \frac{\left| q_{ii} \right|}{t_{ij}} \qquad k = 1, 2, ..., m \qquad (2.7)$$

Note, external disturbances are not accounted for in this development. Only cross-coupling loop to loop interaction type disturbances are considered. A separate MIMO QFT development including external disturbances is presented in the following section.

According to the original QFT method each loop is designed independently, but this leads to extreme overdesign. A better approach, called the improved method, is to utilize the known structure of g_i and f_{ij} of the loop that is designed first. The improved method uses the known structure of the designed loop to provide a more accurate estimate of the cross-coupled disturbance from the designed loop to the other uncompensated loops. Based on the new estimate of the cross-coupled disturbance, new disturbance rejection bounds for the uncompensated loops are calculated. The improved method is applied after each loop is compensated. The normal QFT loop shaping process is performed for a given uncompensated loop using the new disturbance bounds. The improved method reduces the overdesign of the original method by taking into account that compensated loop will have less cross-coupling disturbance into the uncompensated loops. [3]

2.4 MIMO QFT with External Output Disturbance

Output disturbance rejection is the primary design criterion in this thesis. The previous discussion of MIMO QFT did not consider external disturbance in the calculation of disturbance rejection bounds. Therefore, equations including the external disturbance are developed in this thesis. The following discussion outlines this development.

The following development quantifies external uncertain disturbances. Figure 2.3 represents an mxm MIMO closed-loop system in which F(s), G(s), P(s), and $P_d(s)$ are mxm matrices. $\mathcal{P}(s) = \{P(s)\}$ and $\mathcal{P}_d(s) = \{P_d(s)\}$ are sets of matrices due to plant and disturbance uncertainties respectively. The objective is to find a suitable mapping that permits the analysis and synthesis of a MIMO control system by a set of equivalent MISO control systems.
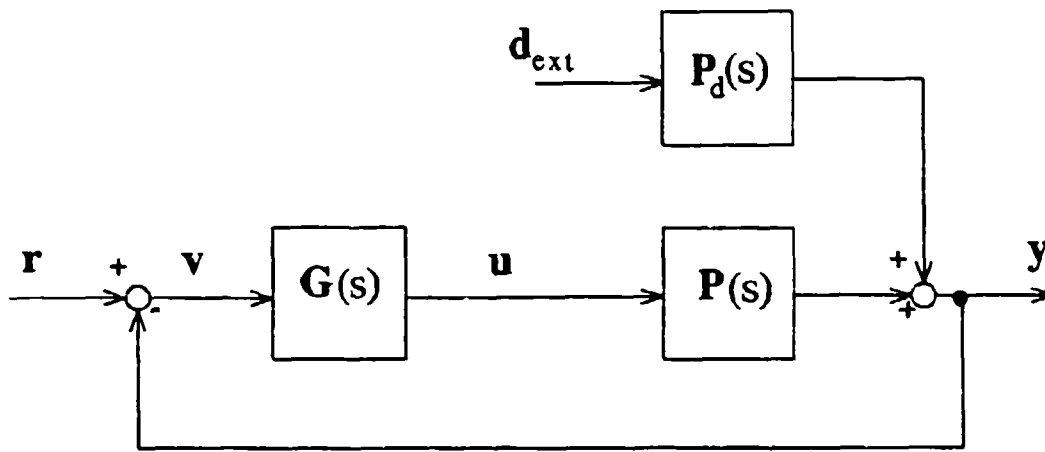
Figure 2.3 QFT Controller with Output External Disturbance

From Figure 2.3, the following equations are written

$$y = P(s)u + P_d(s)d_{ext} \qquad u = G(s)v \qquad v = r - y \qquad (2.8)$$

For the regulator case with zero tracking input

$$r = [0, \ 0, \ 0]^T \qquad (2.9)$$

From Eqs. (2.8) and (2.9) where henceforth the (s) is dropped in the continuing development

$$v = -y \qquad u = -Gy \qquad (2.10)$$

which yields

$$y = -PGy + P_d d_{ext} \qquad (2.11)$$

Equation (2.11) is rearranged to yield

$$y = \left[I + PG \right]^{-1} P_d d_{ext} \qquad (2.12)$$

Based upon unit impulse disturbance inputs for d_{ext}, the system control ratio relating d_{ext} to y is

$$T_d = \left[I + PG \right]^{-1} P_d \qquad (2.13)$$

Premultiply Eq. (2.13) by $[I + PG]$ yields

$$\left[I + PG \right] T_d = P_d \qquad (2.14)$$

when P is nonsingular. Premultiplying both sides of Eq. (2.14) by P^{-1} results in

$$\left[P^{-1} + G \right] T_d = P^{-1} P_d \qquad (2.15)$$

Let

$$P^{-1} = \begin{bmatrix} p^{*}_{11} & p^{*}_{12} & \cdots & p^{*}_{1m} \\ p^{*}_{21} & p^{*}_{22} & \cdots & p^{*}_{2m} \\ \vdots & \vdots & & \vdots \\ p^{*}_{m1} & p^{*}_{m2} & \cdots & p^{*}_{mm} \end{bmatrix} \qquad (2.16)$$

2-7

The m^2 effective plant transfer functions are formed as

$$q_{ij} \equiv \frac{1}{p^{*}_{ij}} = \frac{\det \mathbf{P}}{\text{adj } \mathbf{P}_{ij}} \qquad (2.17)$$

the Q matrix is then formed as

$$\mathbf{Q} = \begin{bmatrix} q_{11} & q_{12} & \cdots & q_{1m} \\ q_{21} & q_{22} & \cdots & q_{2m} \\ \vdots & \vdots & & \vdots \\ q_{m1} & q_{m2} & \cdots & q_{mm} \end{bmatrix} = \begin{bmatrix} 1/p^{*}_{11} & 1/p^{*}_{12} & \cdots & 1/p^{*}_{1m} \\ 1/p^{*}_{21} & 1/p^{*}_{22} & \cdots & 1/p^{*}_{2m} \\ \vdots & \vdots & & \vdots \\ 1/p^{*}_{m1} & 1/p^{*}_{m2} & \cdots & 1/p^{*}_{mm} \end{bmatrix} \qquad (2.18)$$

where $\mathbf{P} = [p_{ij}]$, $\mathbf{P}^{-1} = [p^{*}_{ij}] = [1/q_{ij}]$, and $\mathbf{Q} = [q_{ij}] = [1/p^{*}_{ij}]$. Partition the $\mathbf{P}^{-1}$ matrix as follows;

$$\mathbf{P}^{-1} = [p^{*}_{ij}] = [1/q_{ij}] = \Lambda + \mathbf{B} \qquad (2.19)$$

where Λ is the diagonal part of $\mathbf{P}^{-1}$ and $\mathbf{B}$ is the balance of $\mathbf{P}^{-1}$. Thus $\lambda_{ii} = 1/q_{ii} = p^{*}_{ii}$, $b_{ii} = 0$, and $b_{ij} = 1/q_{ij} = p^{*}_{ij}$ for $i \neq j$. Substituting Eq. (2.19) into Eq. (2.15) with G diagonal, results in

$$[\Lambda + \mathbf{B} + \mathbf{G}]\mathbf{T}_d = [\Lambda + \mathbf{B}]\mathbf{P}_d \qquad (2.20)$$

Rearranging Eq. (2.20) produces

$$\mathbf{T}_d = [\Lambda + \mathbf{G}]^{-1}[\Lambda\mathbf{P}_d + \mathbf{B}\mathbf{P}_d - \mathbf{B}\mathbf{T}_d] \qquad (2.21)$$

This equation defines the desired fixed point mapping, where each of the m^2 matrix elements on the right side of Eq. (2.21) are interpreted as MISO problems. Proof of the fact that the design of each MISO system yields a satisfactory MIMO design is based on

2-8
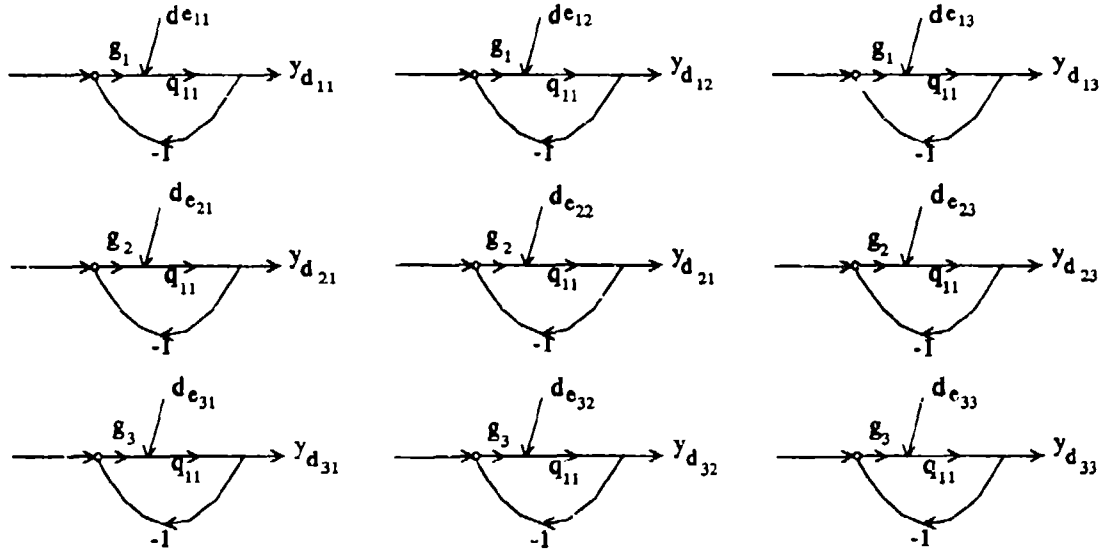
Figure 2.4 3x3 MISO Equivalent Loops for External Output Disturbance

the Schauder fixed point theorem. [2] The theorem defines a mapping $Y(T_d)$

$$Y(T_d) = [\ \Lambda + G \ ]^{-1}[\ \Lambda P_d + BP_d - BT_d \ ] \qquad (2.22)$$

where each member of T_d is from the acceptable set $\mathfrak{S}_d$. If this mapping has a fixed point, i.e., $T_d \in \mathfrak{S}_d$, then this T_d is a solution of Eq. (2.21).

Figure 2.4 shows the effective MISO loops resulting from a 3x3 system. Since Λ and G in Eq. (2.21) are diagonal, the (1,1) element on the right side of Eq. (2.22) for the 3x3 case, for a *unit impulse* input, provides the output

$$y_{d_{11}} = \frac{q_{11}}{1 + g_1 q_{11}} \left[\frac{P_{d_{11}}}{q_{11}} + \frac{P_{d_{21}}}{q_{12}} + \frac{P_{d_{31}}}{q_{13}} - \left(\frac{t_{d_{21}}}{q_{12}} + \frac{t_{d_{31}}}{q_{13}} \right) \right] \qquad (2.23)$$

Equation (2.23) corresponds precisely to the first structure in Figure 2.4. Similarly, each of the nine structures in Figure 2.4 corresponds to one of the elements of $\mathbf{Y}(\mathbf{T}_d)$ of Eq. (2.22). The control ratios for the external disturbance inputs d_{ex} and the corresponding outputs y_i for each feedback loop of Eq. (2.22) have the form

$$y_{ii} = w'_{ii}(d_{e_i}) \qquad (2.24)$$

where $w_{ii} = q_{ii}/(1 + g_i q_{ii})$ and

$$d_{e_i} = \sum_{k=1}^{x} \frac{P_{d_k}}{q_{ik}} - \sum_{k \neq i}^{m} \frac{t_{d_k}}{q_{ik}} \qquad \begin{array}{l} x = \text{number of disturbance inputs} \\ m = \text{dimension of square MIMO system} \end{array} \qquad (2.25)$$

Thus Eq (2.25) not only contains the loop interaction but also the external disturbances.

Additional equations, quantifying the internal cross-coupling due to external disturbances, are derived to utilize the improved method QFT design technique. These equations are used to define the disturbance bounds for subsequent loops based on the completed design of a single loop. For this development, the equations for the case of a 2x2 MIMO system are presented.

From Eq. (2.24) and for the 1-2 loop case, which is the output of loop 1 due to disturbance input 2, including the cross-coupling terms from loop 2, yields, for unit impulse inputs, the following control ratio

$$t_{d_{12}} = y_{12} = w_{i1}(d_{e_{12}}) = \frac{q_{11}}{1 + L_1}\left[\frac{P_{d_{12}}}{q_{11}} + \frac{P_{d_{22}}}{q_{12}} - \frac{t_{d_{22}}}{q_{12}}\right] \tag{2.26}$$

Substituting in for $t_{d_{22}}$

$$t_{d_{12}} = \frac{q_{11}}{1 + L_1}\left[\frac{P_{d_{12}}}{q_{11}} + \frac{P_{d_{22}}}{q_{12}} - \frac{q_{22}d_{e_{22}}}{(1 + L_2)q_{12}}\right] \tag{2.27}$$

$$t_{d_{12}} = \frac{q_{11}}{1 + L_1}\left[\frac{P_{d_{12}}(1 + L_2)q_{12} + P_{d_{22}}(1 + L_2)q_{11} - q_{22}q_{11}d_{e_{22}}}{(1 + L_2)q_{11}q_{12}}\right] \tag{2.28}$$

rearranging, and substituting in for $d_{e_{22}}$ yields

$$t_{d_{12}} = \frac{(1 + L_2)(P_{d_{12}}q_{12} + P_{d_{22}}q_{11}) - q_{22}q_{11}\left(\dfrac{P_{d_{12}}}{q_{21}} + \dfrac{P_{d_{22}}}{q_{22}} - \dfrac{t_{d_{12}}}{q_{21}}\right)}{(1 + L_1)(1 + L_2)q_{12}} \tag{2.29}$$

$$t_{d_{12}} = \frac{(1 + L_2)(P_{d_{12}}q_{12} + P_{d_{22}}q_{11}) - \dfrac{q_{22}q_{11}P_{d_{12}}}{q_{21}} - q_{11}P_{d_{22}} + \dfrac{q_{22}q_{11}t_{d_{12}}}{q_{21}}}{(1 + L_1)(1 + L_2)q_{12}} \tag{2.30}$$

$$t_{d_{12}} = \frac{(1 + L_2)(P_{d_{12}}q_{12} + P_{d_{22}}q_{11})q_{21} - q_{22}q_{11}P_{d_{12}} - q_{11}q_{21}P_{d_{22}} + q_{22}q_{11}t_{d_{12}}}{(1 + L_1)(1 + L_2)q_{12}q_{2i}} \tag{2.31}$$

where $\gamma_{12} = q_{11}q_{22}/q_{21}q_{12}$. Solving for $t_{d_{12}}$ yields

$$t_{d_{12}}((1+L_1)(1+L_2)) = \frac{(1+L_2)(P_{d_{12}}q_{12} + P_{d_{22}}q_{11})}{q_{12}}$$
$$- \frac{q_{11}P_{d_{22}}}{q_{12}} - \gamma_{12}P_{d_{12}} + \gamma_{12}t_{d_{12}} \tag{3.32}$$

$$t_{d_{12}}((1+L_1)(1+L_2) - \gamma_{12}) =$$
$$(1+L_2)\frac{q_{11}}{q_{12}}P_{d_{22}} + (1+L_2)P_{d_{12}} - \frac{q_{11}}{q_{12}}P_{d_{22}} - \gamma_{12}P_{d_{12}} \tag{3.33}$$

$$t_{d_{12}} = \frac{L_2\dfrac{q_{11}}{q_{12}}P_{d_{22}} + (1+L_2-\gamma_{12})P_{d_{12}}}{L_1(1+L_2) + 1 + L_2 - \gamma_{12}} \tag{3.34}$$

Equation (3.34) is rearranged as follows:

$$t_{d_{12}} = \frac{\dfrac{L_2\dfrac{q_{11}}{q_{12}}P_{d_{22}}}{1+L_2-\gamma_{12}} + P_{d_{12}}}{1 + \dfrac{L_1(1+L_2)}{1+L_2-\gamma_{12}}} \tag{3.35}$$

From Eq. (3.35) the effective plant is defined as

$$q_{11_e} = \frac{q_{11}(1+L_2)}{1+L_2-\gamma_{12}} \tag{3.36}$$

Substituting Eq. (3.36) into Eq. (3.35), yields

Thus, in general, for the 2x2 case, the improved method control ratio of the jth external disturbance input to the ith system output is

2-12

$$t_{d_{11}} = \frac{\dfrac{L_2 P_{d_{21}} q_{11_*}}{q_{12}(1 + L_2)} + P_{d_{11}}}{1 + g_1 q_{11_*}} \tag{3.37}$$

$$t_{d_*} = \frac{\dfrac{L_k P_{d_*} q_{ii_*}}{q_{ik}(1 + L_k)} + P_{d_*}}{1 + g_i q_{ii_*}} \quad \text{where } i = 1, 2 \text{ and } k \neq i \tag{3.38}$$

The new disturbance bounds are calculated at a given frequency to satisfy

$$B_{D_*} \geq \left| t_{d_*} \right| = \left| \frac{\dfrac{L_k P_{d_*} q_{ii_*}}{q_{ik}(1 + L_k)} + P_{d_*}}{1 + g_i q_{ii_*}} \right| \quad \text{where } i = 1, 2 \text{ and } k \neq i \tag{3.39}$$

or

$$\left| 1 + g_i q_{ii_*} \right| \geq \frac{1}{B_{D_*}} \left| \frac{L_k P_{d_*} q_{ii_*}}{q_{ik}(1 + L_k)} + P_{d_*} \right| \quad \text{where } i = 1, 2 \text{ and } k \neq i \tag{3.40}$$

The improved QFT method uses these equations to reduce overdesign inherent in the original design process. The order in which loops are designed is important. Any order can be used, but some orders produce less overdesign (less bandwidth) than others. The last loop designed has the least amount of overdesign, therefore the most constrained loop is done first by the original method. Then the design is continued through the remaining loop by the second method. The first loop is then redesigned using the improved method.

At this point it is important to point out that when the disturbance rejection specification is considered, the designer must decide how much disturbance rejection is

for cross-coupling and how much is for external disturbances. In other words the designer can "tune" the disturbance rejection specification depending on the nature of the disturbance for a particular loop. For example, if one loop is only effected by external distrubance, the disturbance rejection specification would consider external disturbance only. But if the loop disturbance was a mix of cross-coupling and external disturbance, the designer would have to "tune" the disturbance rejection specification accordingly. Since each loop may not exhibit the same disturbance characterisitics, disturbance rejection specification tuning provides flexibilty in the QFT design process .

2.5 Summary

This chapter presented the basic improved QFT method and its extension to MIMO systems. The development to include the effects of external output disturbances is detailed. Equations to calculate the new disturbance bounds for the improved method are discussed. The next chapter covers modeling the aircraft and the external disturbances.

III. Air-to-Air Refueling FCS Design Concept

3.1 Introduction

The aircraft modeled in this thesis is the cargo variant of the 135 class aircraft, the C-135B. This aircraft is chosen because of the availability of the aerodynamic data [1]. This chapter describes the modeling of the C-135B. A Mach-hold, altitude hold, and wing-leveler autopilot is included in the C-135B model [6]. Wind gusts and fuel transfer disturbance models are developed in this chapter, as well as the AFCS concept.

3.2 C-135B Modeling

EASY5x is used to develop the state-space six-degrees-of-freedom bare (uncontrolled) aircraft model. EASY5x is a computer aided design (CAD) tool, written by Boeing Computer Services, used to model, simulate, and analyze dynamic systems [5]. EASY5x's graphical interface expedites modeling and analysis. Generic pre-written air vehicle modules further simplify modeling in EASY5x. The user need only provide aircraft stability derivatives, flight conditions, and desired input/outputs.

The basic aircraft model is illustrated in Figure 3.1. The LO block calculates the longitudinal forces and moments, while LD does the same for the lateral-directional axes. The AV block includes the aerodynamic variables and calculates changes in speed and rates due to wind gusts. Also, it computes dynamic pressure and angle-of-attack (AOA). The SD block contains the six-degrees-of-freedom equations of motion. It calculates

3-1
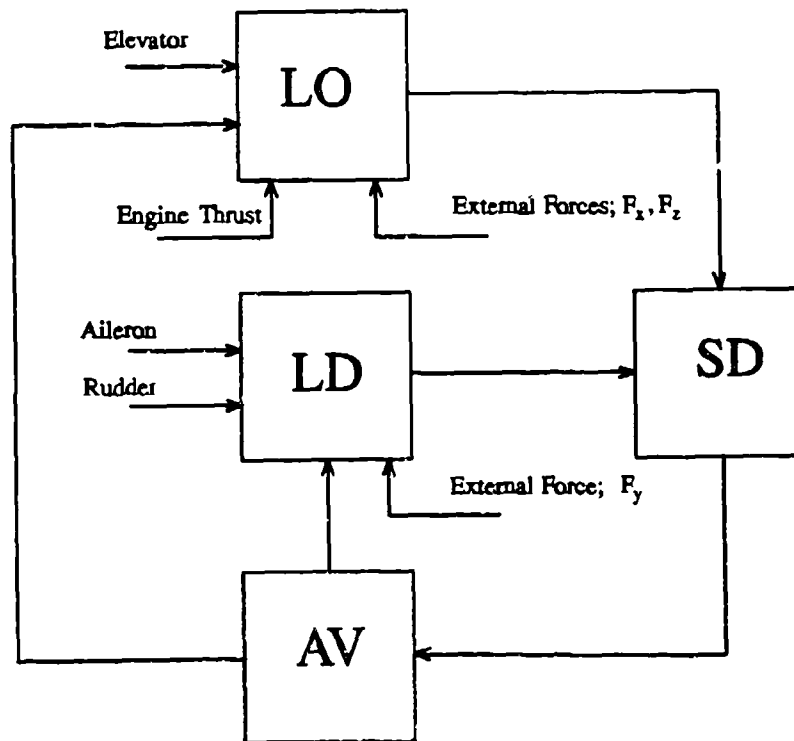
Figure 3.1. Bare Aircraft Plant

attitude, body axes rates, Euler angles, and body axes angular rates based on data supplied

by the LO and LD blocks. Further information can be obtained from the EASY5x user

manual [5].

Sixteen bare aircraft plants are developed to account for the uncertainty of the C-

135B during air-to-air refueling. The 16 models are based on two different coefficients

of lift, C_L = 0.2, 0.6, for eight different aircraft weights, each flying Mach 0.69 at 28,500

feet. These discrete values are selected based on the availability of data, normal refueling

speed and altitude, and represent weights ranging from empty/low fuel to loaded/full fuel

aircraft. Typically, during air-to-air refueling, the C-135B will have a C_L between 0.27

and 0.45 [1]. Therefore, the 16 plant models envelop the structured uncertainty of the C-

135B during air-to-air refueling. Tables containing the aerodynamic stability derivatives for all 16 plant models are provided in Appendix A.

The six-degrees-of-freedom state-space models, generated by EASY5x, are loaded into MATRIX$_x$. MATRIX$_x$ is a programmable, matrix calculator with graphics. MATRIX$_x$ was designed by control engineers to aid in the design of complex control problems. It is ideally suited to manipulate matrices and apply both input/output (classical) control and state-space (modern) control [7].

MATRIX$_x$ is used to design the autopilot using root-locus design techniques. The autopilot is designed to control all 16 plant cases. The bare aircraft and autopilot are shown in Figure 3.2. An autopilot is used for two reasons: (1) autopilots reduce the high frequency cutoff of the aircraft (2) all aircraft have autopilots. Lowering the cutoff of the aircraft reduces high frequency parameter uncertainty. Since autopilots are available, using it in the QFT design eliminates duplication of a control system to provide input to the bare aircraft, reducing cost and overhead. The inputs to the autopilot are thrust, elevator, aileron, and rudder commands. The outputs are z-position (altitude), x-position, and y-position in a local inertial reference frame where x is positive out the nose of the aircraft, y out the right wing, and altitude is positive up. The three outputs frame of reference is translated from the aircraft center of gravity (cg) to the approximate location of the air-to-air refueling receptacle on the top of the aircraft.

In order to have a square plant, 3x3, one of the autopilot inputs is not used. The Mach hold command input is used to control the x position, altitude hold controls altitude, and the rudder command is used to control the y position. Mach and altitude are self

3-3

Figure 3.2 C-135B Bare Aircraft with Autopilot

evident, rudder is chosen over aileron because the rudder does not roll the aircraft as much as the ailerons. By using the rudder for the QFT controller, good performance is obtained while leaving the aileron controller to handle wing leveling. See Appendix C for aircraft response to step input commands on all four autopilot command inputs.

3.3 Disturbance Modeling

Disturbance models are generated by developing augmented state-space models of the aircraft in the presence of wind gusts and fuel transfer inputs. This development starts by examining the aerodynamic moments and forces.

3.3.1 Pitch Plane Wind Induced Disturbance

In the pitch plane, the total aircraft airspeed is a combination of wind velocity and aircraft velocity in the x and z stability axis directions.

$$\text{Airspeed} - \begin{bmatrix} U_A \\ W_A \end{bmatrix} - \begin{bmatrix} \bar{U} + u + u_w \\ w + w_w \end{bmatrix} \qquad (3.1)$$

Where $\bar{U}$ is the steady-state aircraft speed, u & w are the perturbation speed in the x and z directions respectively, and u_w & w_w are the aircraft speeds due to wind in the respective x and z directions.

The pitch plane aerodynamic moments and forces are in the form of the following functions

$$M = \frac{\bar{q}Sc}{I_{yy}} C_m(\alpha, q, \delta)(\frac{180}{\pi})$$

$$F_x = \frac{\bar{q}S}{m} C_x(\alpha, \delta) \qquad (3.2)$$

$$F_z = \frac{\bar{q}S}{m\bar{U}} C_z(\alpha, q, \delta)(\frac{180}{\pi})$$

where

$$\bar{q} = \frac{1}{2}\rho(U_A^2 + W_A^2)$$

$$\alpha = \arctan\left(\frac{W_A}{U_A}\right) \approx \frac{W_A}{U_A} \qquad (3.3)$$

and the $\dot{\alpha}$ effects in the M and F_z equations are neglected.

It is important to note that the following equations of motion are written with respect to the inertial kinematic variables q, U, and W. However, the perturbations in U and W are $u + u_w$ and $w + w_w$ respectively. The q perturbation is $q + q_w$.

3-5

The $\dot{q}$ equation of motion is

$$\dot{q} = M_\alpha \alpha + M_q q + M_q q_w + M_\delta \delta$$

$$+ \frac{180}{\pi} \frac{\rho S c}{I_{yy}} C_m \big[U_A (u + u_w) + W_A (w + w_w) \big] + M_\alpha \frac{1}{\bar{U}} w_w$$

$$= M_\alpha \alpha + M_q q + M_q q_w + M_\delta \delta$$

$$+ \frac{180}{\pi} \frac{\rho S c}{I_{yy}} C_m \Big[(\bar{U} + u + u_w)(u + u_w) + (w + w_w)^2 \Big] + M_\alpha \frac{1}{\bar{U}} w_w$$

(3.4)

assuming u, w, u_w, and $w_w \ll \bar{U}$ Eq. (3.4) reduces to

$$\dot{q} = M_\alpha \alpha + M_q q + M_q q_w + M_\delta \delta + M_u [u + u_w] + M_\alpha \frac{1}{\bar{U}} w_w$$

(3.5)

grouping the wind terms results in

$$\dot{q} = M_\alpha \alpha + M_q q + M_\delta \delta + M_u u + [M_q q_w + M_u u_w + M_\alpha \frac{1}{\bar{U}} w_w]$$

(3.6)

A similar derivation for the $\dot{\alpha}$ and $\dot{u}$ equations of motion yield

$$\dot{\alpha} = Z_\alpha \alpha + Z_q q + Z_u u + Z_\delta \delta + [Z_u u_w + (Z_q - 1) q_w + \frac{1}{\bar{U}} \frac{d w_w}{dt} + \frac{1}{\bar{U}} Z_\alpha w_w]$$

$$\dot{u} = X_\alpha \alpha + X_q q + X_u u + X_\delta \delta + [X_u w_w + X_q q_w + \frac{1}{\bar{U}} X_\alpha w_w]$$

(3.7)

Hence, the effect of a moving airmass is akin to "process noise", i.e., if the state is

$$x = (\theta, u, \alpha, q)$$

(3.8)

3-6

the state-space equation

$$\dot{x} = A x + B u \qquad (3.9)$$

is augmented to yield

$$\dot{x} = A x + B u + \Gamma_{pitch}' d_{pitch} \qquad (3.10)$$

where

$$\Gamma_{pitch} = \begin{bmatrix} 0 & 0 & 0 \\ X_u & X_q & \dfrac{1}{U}X_\alpha \\ Z_u & Z_q - 1 & \dfrac{1}{U}Z_\alpha \\ M_u & M_q & \dfrac{1}{U}M_\alpha \end{bmatrix} \qquad (3.11)$$

and the disturbance vector is

$$d_{pitch} = \begin{bmatrix} u_w \\ q_w \\ w_w \end{bmatrix} \qquad (3.12)$$

Note, $\dfrac{1}{U}\dfrac{dw_w}{dt}$, which is an angle-of-attack rate, is neglected. This simplification is in

line with discarding of the $\dot{\alpha}$ effects. Further simplification is achieved by neglecting

q_w . Hence, Γ_{pitch} and d_{pitch} in the pitch channel are reduced to

3-7

$$\Gamma_{pitch} = \begin{bmatrix} 0 & 0 \\ X_u & \dfrac{1}{U}X_\alpha \\ Z_u & \dfrac{1}{U}Z_\alpha \\ M_u & \dfrac{1}{U}M_\alpha \end{bmatrix} \qquad d_{pitch} = \begin{bmatrix} u_w \\ w_w \end{bmatrix} \qquad (3.13)$$

3.3.2 Lateral Channel Wind Induced Disturbance

For the lateral channel, arguments similar to the pitch channel development are made to generate the augmented state-space equation for the effects of wind. In conformity with the level of modeling in the pitch channel, if the state is

$$x = (\psi, \ p, \ r, \ \beta) \qquad (3.14)$$

Γ_{lat} and d_{lat} are derived to be

$$\Gamma_{lat} = \begin{bmatrix} 0 \\ \dfrac{1}{U}L_\beta \\ \dfrac{1}{U}N_\beta \\ \dfrac{1}{U}Y_\beta \end{bmatrix} \qquad d_{lat} = \begin{bmatrix} v_w \end{bmatrix} \qquad (3.15)$$

3.3.3 Disturbance Due to Refueling

As the aircraft is taking on fuel, the moments of inertia and cg are changing. These variations alter the flying behavior of the aircraft. This change in aircraft behavior

is modeled as a disturbance. Based on first order approximation, refueling (rf) caused disturbance is confined to the pitch channel. Again, paralleling the pitch channel development, the state-space model is augmented. Γ_{rf} and d_{rf} are found to be

$$\Gamma_{rf} = \begin{bmatrix} 0 \\ 0 \\ \dfrac{12}{100} * c * \dfrac{32.2}{I_{yy}} \\ \dfrac{1}{U} * \dfrac{32.2}{m} \end{bmatrix} \qquad d_{rf} = \begin{bmatrix} \text{fuel transfer rate (lbs/min)} \end{bmatrix} \qquad (3.16)$$

Where 12/100 is the percentage of the mean aerodynamic cord the cg is allowed to shift during refueling and m is the mass of the aircraft.

3.3.4 Total Disturbance

The total modeled disturbance is

$$\Gamma d = \Gamma_{pitch} d_{pitch} + \Gamma_{lat} d_{lat} + \Gamma_{rf} d_{rf} \qquad (3.17)$$

where Γ_{pitch} and Γ_{rf} augment the state-space equation containing the states that identify pitch plane flight behavior. In the same manner, Γ_{lat} augments the lateral channel states. The result of the disturbance summation for the augmented disturbed states (θ, u, α, q, ψ, p, r, β) is shown in Eq. (3.18).

$$\Gamma = \begin{bmatrix} 0 & 0 & 0 & 0 \\ X_u & \dfrac{1}{U}X_\alpha & 0 & 0 \\ Z_u & \dfrac{1}{U}Z_\alpha & 0 & \dfrac{12}{100}*c*\dfrac{32.2}{I_{yy}} \\ M_u & \dfrac{1}{U}M_\alpha & 0 & \dfrac{1}{U}*\dfrac{32.2}{m} \\ 0 & 0 & 0 & 0 \\ 0 & 0 & \dfrac{1}{U}L_\beta & 0 \\ 0 & 0 & \dfrac{1}{U}N_\beta & 0 \\ 0 & 0 & \dfrac{1}{Y}L_\beta & 0 \end{bmatrix} \qquad d = \begin{bmatrix} u_w \\ w_w \\ v_w \\ lbs/min \end{bmatrix} \qquad (3.18)$$

The state-space equation now takes on the form

$$\dot{x} = A\,x + B\,u + \Gamma d$$
$$y = C\,x \qquad\qquad (3.19)$$

Note as the disturbances are applied to the bare aircraft, they enter into the inner most loop, around which the autopilots, and later, the QFT loops are closed.

3.4 Plant and Disturbance Matrices

Based on zero initial conditions, then from Eqs (3.19)

$$s\,x = A\,x + B\,u + \Gamma d \qquad (3.20)$$

$$x = \left[s\,I - A\right]^{-1} B\,u + \left[s\,I - A\right]^{-1} \Gamma d \qquad (3.21)$$

$$y = Cx = C[sI - A]^{-1}Bu + C[sI - A]^{-1}\Gamma d$$

$$= P(s)u + P_d(s)d \tag{3.22}$$

where

$$P(s) = C[sI - A]^{-1}B$$

$$P_d(s) = C[sI - A]^{-1}\Gamma \tag{3.23}$$

Equation (3.22) is represented in Figure 2.3. Thus the QFT formulation of Section 2.4 is applicable for this problem.

3.5 Control Problem Approach

The tanker's position ia assumed fixed and hence the receiver aircraft's position is measured from this frame of reference. In this approach the control problem can be viewed as a formation flying problem. The receiver maintains the total obligation of regulating its position. The tanker is free to change course, altitude, and velocity while the receiver compensates for these changes and maintains position.

Equations are developed that identify perturbations from the set position. These perturbations are viewed as disturbances by the receiver. The perturbations are caused by wind gusts and disturbances due to refueling. Other, unmodeled, disturbances may include the tanker changing course. The control problem's goal is to minimize the perturbations to be within a specified volume of space where the refueling boom can operate. Normal boom operating position and length defines this volume.

The KC-135 tanker refueling boom has the following operational constraints, (1) nominal boom operation position is 30 degrees down from horizontal, (2) the boom can move as much as four degrees up and down from normal position and continue delivering fuel, (3) it can move as much as ten degrees up and down from normal position and maintain its connection to the receiver, but cannot deliver fuel, (4) horizontal movement is limited to 10 degrees left and right while maintaining fuel flow, (5) the disconnect limit horizontally is 15 degrees left and right, (6) nominal boom length is 477.5 inches (39.8 ft), (7) it can expand or constrict 13.5 inches and maintain refueling, (8) it can expand or constrict as much as 73.5 inches and maintain contact but not refueling. [1]

These dimensions provide a maximum perturbation from nominal boom position of approximately 2.85 feet up or down, 7 feet left or right, in order to maintain fuel flow. In order to maintain connection, the maximum perturbation can be 7.5 feet up or down, and 11.5 feet left or right.

Using the tanker as the point of reference, the relationship in Figure 3.3 can be used to develop the equations required to define the regulation control problem. R is the nominal boom length measure from the boom hinge point on the tanker. Z is the vertical distance between the boom hinge point and receiver aircraft's refueling receptacle. X is the horizontal distance between these same points. Y measures the distance between the center line of the boom hinge point and receiver receptacle.

The following equations are derived

$$R^2 = X^2 + Y^2 + Z^2 \qquad\qquad (3.24)$$

where

$$R = \bar{R} + r$$
$$X = \bar{X} + x$$
$$Y = \bar{Y} + y \qquad (3.25)$$
$$Z = \bar{Z} + z$$

which are the sums of the nominal positions (overbar terms) and perturbations (lower case

terms). Substituting Eq. (3.25) into Eq. (3.24) and squaring the terms, yields

$$\bar{R}^2 + 2r\bar{R} + r^2 = \bar{X}^2 + 2x\bar{X} + x^2 + \bar{Y}^2 + 2y\bar{Y} + y^2 + \bar{Z}^2 + 2z\bar{Z} + z^2 \qquad (3.26)$$
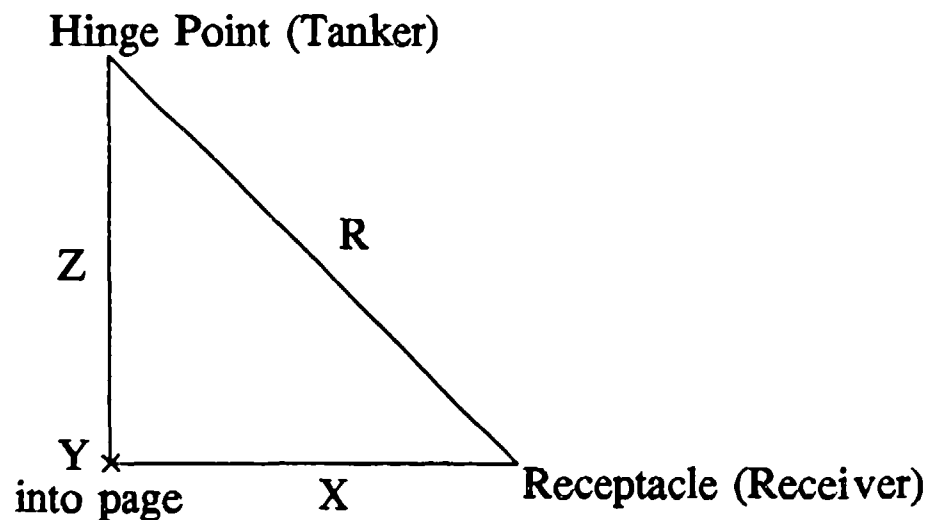
Hinge Point (Tanker)

Figure 3.3 Control Problem Geometry

Since r, x, y, z $\ll$ $\bar{R}$, $\bar{X}$, $\bar{Y}$, $\bar{Z}$ respectively, Eq. (3.26) is approximated as

$$\bar{R}^2 + 2r\bar{R} = \bar{X}^2 + 2x\bar{X} + \bar{Y}^2 + 2y\bar{Y} + \bar{Z}^2 + 2z\bar{Z} \qquad (3.27)$$

Taking the derivative with respect to time where the overbar terms are constant yields

$$\bar{R}\frac{dr}{dt} = \bar{X}\frac{dx}{dt} + \bar{Y}\frac{dy}{dt} + \bar{Z}\frac{dz}{dt} \qquad (3.28)$$

Integrating, rearranging, and setting $r = 0$

$$r = \frac{\bar{X}}{\bar{R}}x + \frac{\bar{Y}}{\bar{R}}y + \frac{\bar{Z}}{\bar{R}}z = 0 \qquad (3.29)$$

defining

$$
\begin{aligned}
x &= x_T - x_R \\
y &= y_T - y_R \\
z &= z_T - z_R
\end{aligned}
\qquad
\begin{aligned}
&\text{T - Tanker} \\
&\text{R - Receiver}
\end{aligned}
\qquad (3.30)
$$

Thus, $r = 0$ if and only if, $x = y = z = 0$. Therefore, the control problem is to design the compensator, G, of Figure 3.4 that will satisfy Eqs. (3.29) and (3.30).
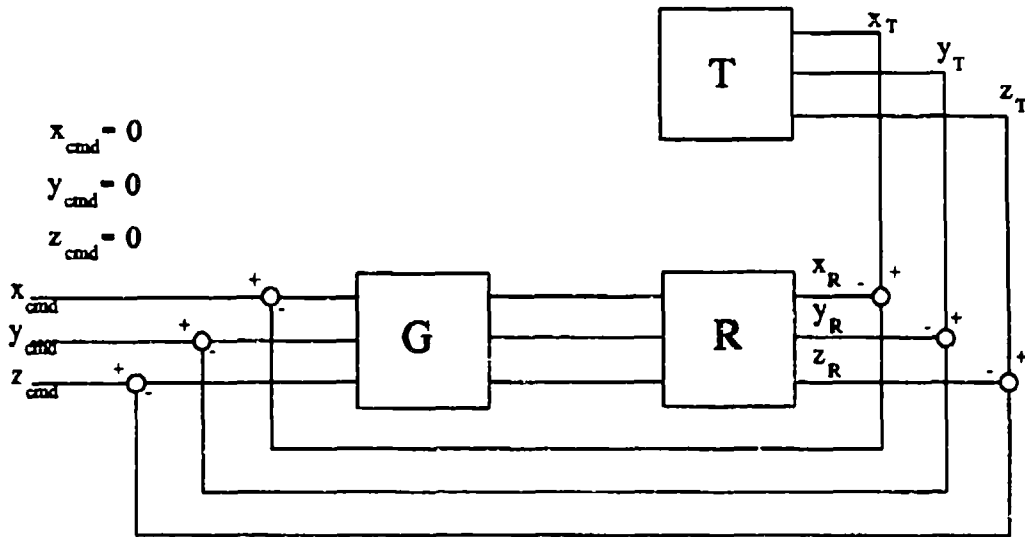
Figure 3.4. Control Problem

3.6 Summary

The C-135B model is developed using the CAD program EASY5x. An autopilot is designed for the bare aircraft model. The QFT plants are the 16 aircraft models with autopilot. External disturbances enter the plant, the aircraft state-space model is augmented to model the disturbance. The regulation control problem is identified. The next chapter is devoted to the generation of the LTI plants and disturbances.

IV. LTI Plant and Disturbance Model Generation

4.1 Introduction

Before QFT output disturbance rejection is applied to the design of an AFCS, the LTI

plant matrix, P(s), and disturbance matrix, $P_d(s)$ must be generated. This chapter presents

the results of applying the methods of chapters *II* and *III* in forming the plant *q*'s. First,

the state-space models are generated and transformed into LTI transfer functions

representing the 16 plants. Next, the q's are formed by applying the plant inversion

process. Finally, disturbance transfer functions are generated for all 16 plants. The

results represent the uncertainty in the plants as well as the disturbance.

4.2 Plant Transfer Function Generation

First the bare aircraft state-space model is generated in EASY5x. This model is

loaded into MATRIX$_x$ where the state-space model with autopilot is formed. The plant

matrix P(s) of Eq. (3.23) is calculated in the MIMO/QFT CAD package from the state-

space model.

$$\dot{x} = A\,x + B\,u$$
$$y = C\,x \tag{4.1}$$

The transfer functions are calculated, as shown in Sec. 3.4, from the following relationship

$$y = C(sI - A)^{-1}Bu$$
$$y(s) = P(s)u(s) \qquad (4.2)$$

Therefore

$$P(s) = C(sI - A)^{-1}B \qquad (4.3)$$

For the 3x3 MIMO system, P(s), is a matrix of nine transfer functions. The transfer functions along the matrix diagonal, $P_{11}(s)$, $P_{22}(s)$, and $P_{33}(s)$, represent the respective output response to the given input, e.g., output 1 to input 1. Off-diagonal terms represent the cross-coupling between channels, e.g., output 1 to input 2. The columns indicate input, column 1/input 1, and the rows are the outputs, row 2/output 2. Hence, the MISO loop {2,1} is the output channel 2 due to input channel 1. As seen in Figure 4.1, Figure 4.2, the dominant input for output 1 is input 2, see MISO loop {1,2}. This indicates a strong correlation between channels 1 and 2.

This correlation is expected. Channel 1 is the altitude hold autopilot and channel 2 is the Mach hold. The altitude is controlled by using the thrust. To increase altitude the throttle is advanced, which increases the speed and hence lift, therefore increasing the altitude. The reverse is true for decreasing altitude. The speed is controlled with the elevator that controls the pitch angle of the aircraft. To increase speed the aircraft is pitched down, decreasing the drag, resulting in an increase of aircraft airspeed. The opposite is true to decrease airspeed. Lift and drag are inversely related, and thus highly coupled. An increase in drag decreases lift. Therefore a decrease in airspeed (increased drag), also results in a decrease in altitude (reduced lift). As the Mach hold autopilot controls airspeed it adjusts pitch angle, increasing or decreasing drag. This results in
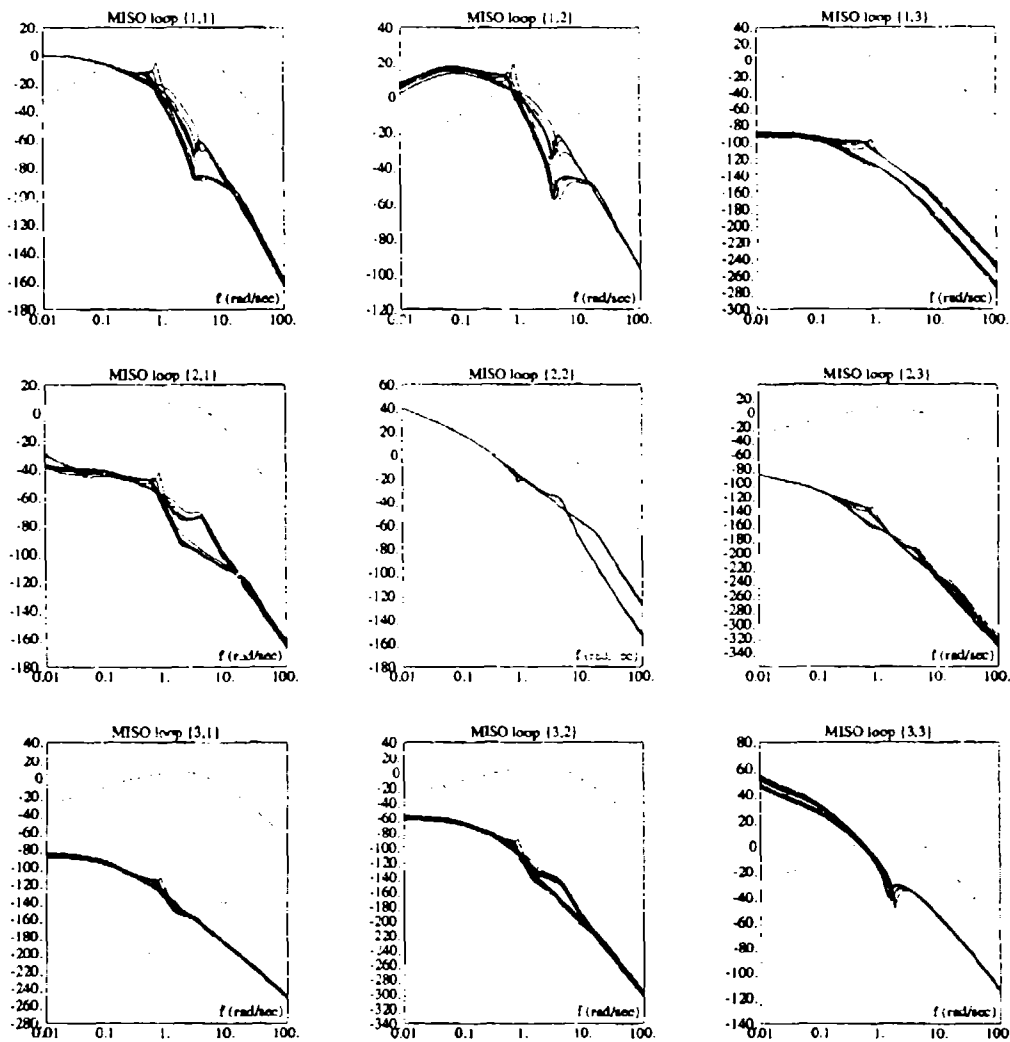
Figure 4.1 P(s) Log Magnitude Plot

changes of altitude, which is controlled by the thrust. The thrust is adjusted using the engines which have a longer lag time (longer reaction time) than the elevators. This causes a delay between when the altitude hold senses change in altitude and the altitude correction. Thus, the correlation of input 2 to output 1.

4-3

Notice next that channel 3 (y position) is essentially decoupled from channels 1 and 2. MISO loops {1,3}, {2,3}, {3,1}, and {3,2}. Again this is expected. Channel 3 is the lateral channel, derived separately from channels 1 and 2, longitudinal (pitch) channel. Decoupling channel 3 allows the 3x3 MISO system to be broken down to two design problems, a 2x2 MISO system and a 1x1 SISO system. Thus the QFT improved method is applied only to channels 1 and 2.

The single dotted line in the MISO loops of Figure 4.1 is the log magnitude plot of the disturbance rejection specification. Log magnitude of P's above this line indicates that the output due to cross-coupling disturbance exceeds the disturbance rejection specification for the frequencies that lie above the line. Note that P(s) MISO loops {1,3}, {2,3}, {3,1}, and {3,2} are below the disturbance rejection line, reinforcing replacement of the 3x3 system by the 2x2 and 1x1 systems as discussed previously.

Finally notice in Figure 4.1 the tight grouping of the 16 plants over the frequency range plotted. This indicates little uncertainty in magnitude for the 16 plants. This is an added robustification benefit due to the "inner loop" autopilots.

The QFT Q(s) matrix is formed in the MIMO/QFT CAD program by matrix inverting the transfer functions of the P(s) matrix. The q_{ij} transfer functions for the 16 plants are shown in Appendix B. Figure 4.2 shows the log magnitude (Lm) plots of the q_{ij} transfer functions for all plant cases. As mentioned above, channel 3 is consider completely decoupled from channels 1 and 2. Thus, for design purposes q_{13}, q_{23}, q_{31}, and q_{32} are set to zero since their cross-coupling contribution is essentially zero.
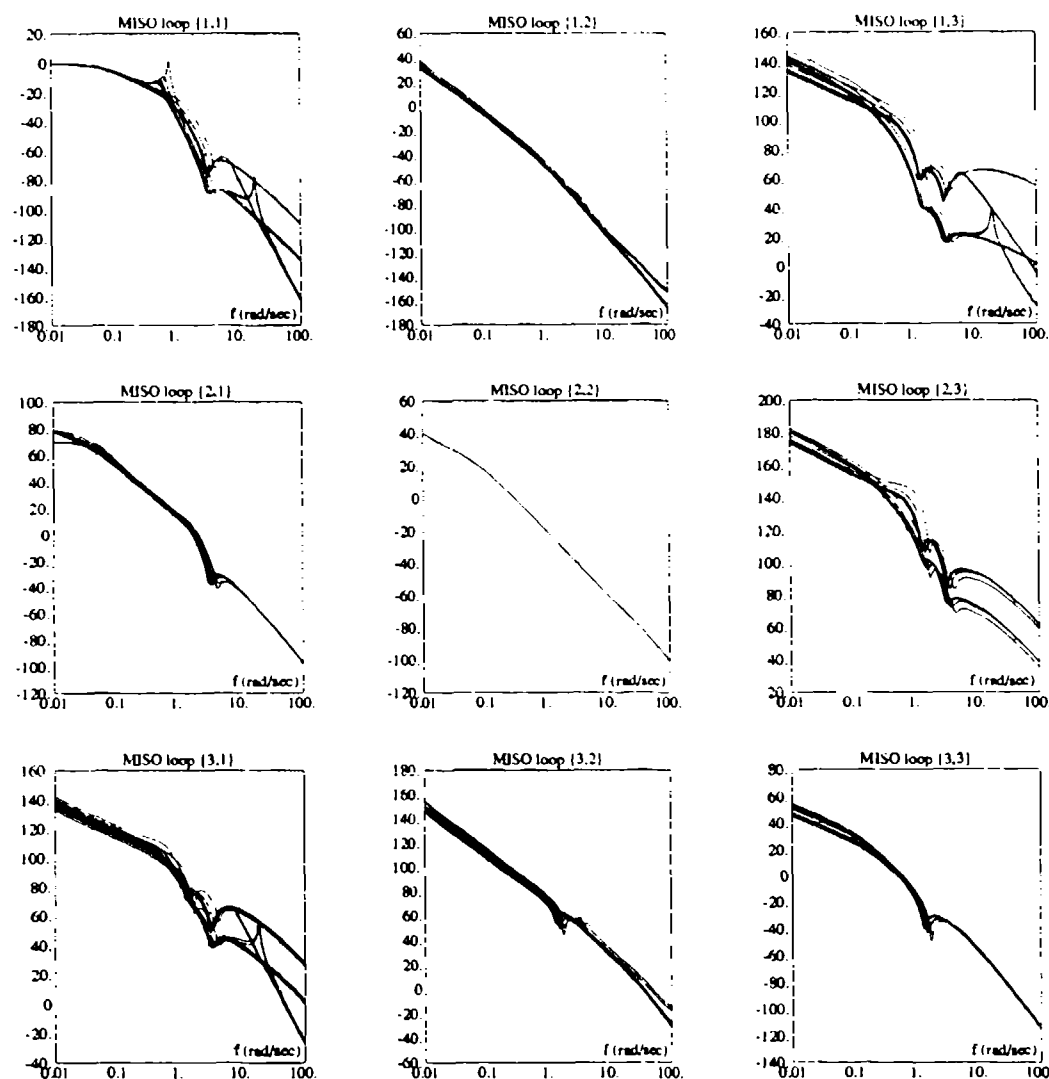
Figure 4.2 Q(s) Log Magnitude Plots

4.3 Disturbance Transfer Function Generation

The disturbance models $P_d(s)$ of Eq (3.23) are calculated similar to P(s). The disturbance augmented state-space model is developed, as detailed in Chapter *III*.

$$\dot{x} = A x + B u + \Gamma d$$
$$y = C x \qquad\qquad\qquad (4.4)$$

The disturbance matrix $P_d(s)$ is given by

$$P_d(s) = C(sI - A)^{-1}\Gamma \qquad\qquad (4.5)$$

$P_d(s)$'s are calculated for all 16 plants. Like $P(s)$, $P_d(s)$ is a matrix of transfer functions with the same matrix diagonal, off-diagonal characteristics.

The disturbance driving functions are: wind gusts in the vertical up direction, horizontal left to right, and fuel flow rate. The magnitude of the wind gusts, horizontal and vertical, are 10 feet/sec, applied in a step function. The fuel flow rate is 10,000 pounds per minute (maximum fuel delivery rate of the KC-135 tanker), applied in a ramp function.

Figure 4.3 presents the Lm $P_d(s)$ plots for all plant cases. It is important to keep in mind that the wind and fuel disturbances enter the bare aircraft but the $P_d(s)$ models include the autopilots. Therefore the $P_d(s)$ output will not only exhibit the effects of the disturbance input but also the cross-coupling nature of the autopilot discussed previously.

In Figure 4.3 column 1 maps disturbance input 1 (refueling) to the three system outputs, altitude, x position, and y position respectively. Column 1 shows very little effect from refueling on the outputs (MISO Loops {1,1}, {2,1} and {3,1}). Column 2 demonstrates that disturbance input 2 (vertical wind) has a strong effect on both altitude and x position. Column 3, input 3 (horizontal wind) effects only y position.

In Figure 4.3 notice that MISO loops {*,1} and {*,2} show two distinct groupings of $P_d(s)$ log magnitude plots. Each grouping represents the plant differences based on C_L.

Figure 4.3 $P_d(s)$ Log Magnitude Plots
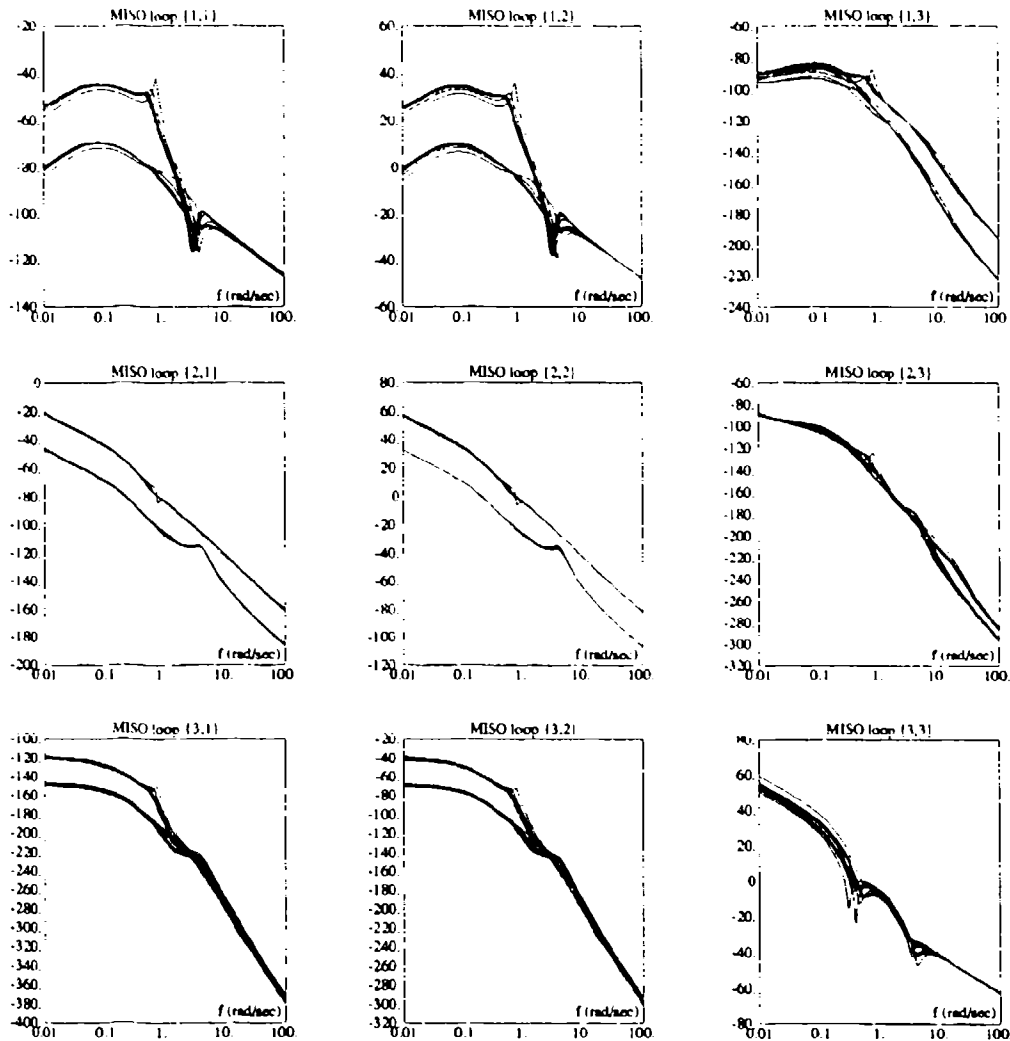
The distinct groupings indicate that the external disturbances effect the $C_L = 0.6$ plants more than the $C_L = 0.2$ This is also evident in the P_d time response plots presented in Appendix D.

The single dotted line in the MISO loops of Figure 4.3 is the log magnitude plot of the disturbance rejection specification. Log magnitude of P_d's above this line indicates

that the output due to disturbance exceeds the disturbance rejection specification for the frequencies that lie above the line. $P_d(s)$ MISO loops {1,3}, {2,3}, {3,1}, and {3,2} are below the disturbance rejection line, thus, further justifying the break down of this 3x3 system into 2 systems, 2x2 and 1x1.

4.4 Summary

In this chapter, LTI models and Bode plots for $P(s)$ and $P_d(s)$ are generated. The calculation of the $Q(s)$ matrix is discussed as well as the significance of channel 3 being uncoupled from channels 1 and 2. The next chapter describes the AFCS QFT design.

V. QFT AFCS Design

5.1 Introduction

This chapter details the QFT AFCS design. First the disturbance rejection specification is identified. Next, design of the loop transmissions for all three channels is described. This chapter, nor this thesis, is a detailed step-by-step guide for the QFT design process. The reader is assumed to have at least a basic understanding of the QFT method.

5.2 Disturbance Rejection Specification

The primary goal in designing the AFCS system is to regulate the position of the aircraft receiving fuel relative to the tanker. As discussed in Section 2.4, any deviation from the nominal set position is considered a disturbance. Hence a disturbance rejection specification is determined based on modeled disturbance inputs and the basic QFT design pretense of unit impulse inputs.

Since the most severe disturbance is due to wind, see Appendix D, the disturbance specification is "tuned" to the wind input of 10 ft/sec. Section 3.4 indicates a maximum deviation from the nominal set position of 2 feet in any direction will confine the receiving aircraft to a volume that will permit continued fuel delivery. Therefore the following disturbance specification is derived. Given an impulse input of magnitude 10 feet/sec, the system response will deviate no more than 2 ft. Additionally, the system

will attenuate to half the maximum deviation in less than 1 second. Equation (5.1) identifies the transfer function for the disturbance rejection specification, and Figure 5.1 shows the disturbance rejection model response to an 10 ft/sec impulse input.

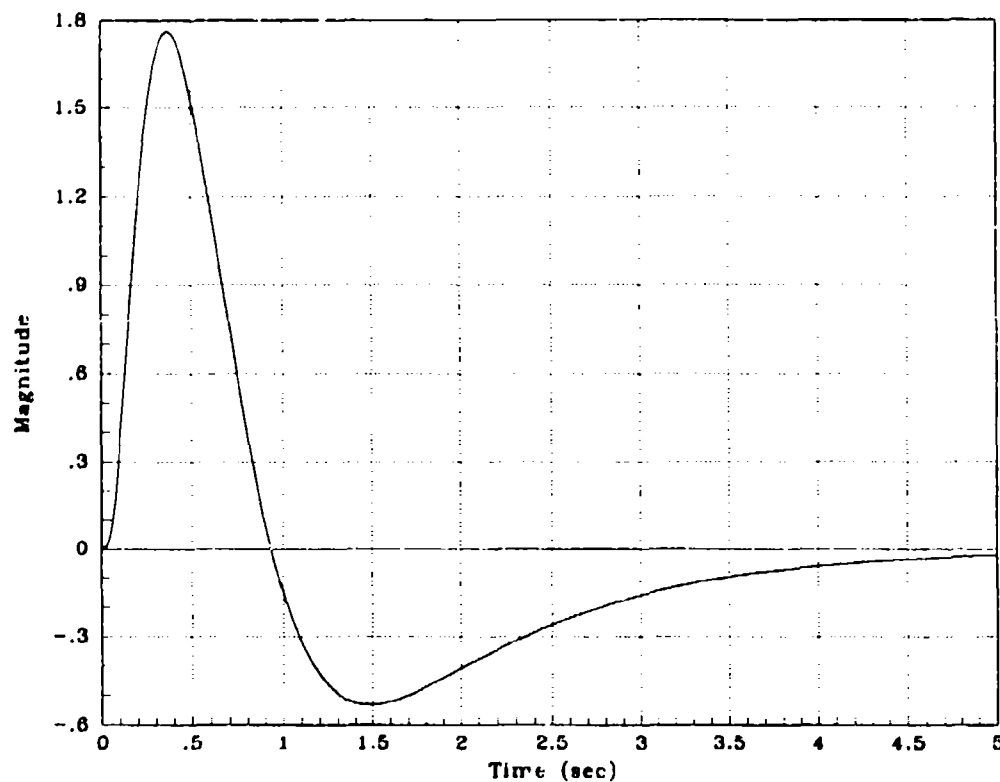$$\text{Disturbance rejection model} = \frac{400s}{(s+1)(s+5)^3} \qquad (5.1)$$

Figure 5.1 Disturbance Rejection Model Response to 10 ft/sec Impulse

In Figure 4.1 the Lm of the disturbance rejection specification is superimposed over the Lm P(s) MISO loop plots. Notice that MISO loops {2,1}, {3,1}, {3,2}, {1,3}, and {2,3} are below the disturbance specification before compensation is applied.

5-2

5.3 Loop Shaping

The order of loop shaping is determined by the amount of cross coupling each MISO loop exerts on each other. As discussed in Section 4.2, channel 2 couples strongly into channel 1. Therefore, channel 2 is designed first, the improved method is applied to utilize the known g_2 to recalculate the disturbance bounds for channel 1. Channel 1 is then designed. Channel 3 is designed last since it is completely decouple and considered a 1x1 SISO system.

The bandpass of the plants are relatively low, a benefit of the autopilot, in shaping the loops the overall system bandpass is designed to remain approximately equal to the plant bandpass. This requirement may require tradeoffs on meeting certain higher frequency bounds.

5.3.1 Channel 2 Loop Design

For channel 2 plant case 2 is chosen to be the nominal loop. Plant 2 is chosen because through initial design attempts it proved to be the most difficult to shape around the stability contour. A successful shaping of plant case 2 guarantees stability for all plant cases. Templates, stability and disturbance boundaries are calculated, see Appendix E. Composite bounds are formed in the MIMO QFT CAD Package. The channel 2 plants are 360 degrees out of phase between the plants derived from aircraft with $C_L = 0.2$ and $C_L = 0.6$. This is evident from the 360 degree wide templates and the stretching of the bounds over 360 degrees. The phase difference did not present a problem as the MIMO CAD Package was able to accommodate this scenario. Compensator g_2 poles and

zeros are added to shape the loop. Channel 2 is relatively easy to shape and proved to have the lowest order compensator, g_2. shown in Appendix F.

Shown in Figure 5.2 the channel 2 loop easily satisfies all QFT loop shaping requirements for composite bound and stability contours, guaranteeing a stable design satisfying the disturbance rejection specification. Figure 5.3 shows the Nichols plot for all 16 plants. From this figure the 360 degree phase difference in the plant is evident. Though there is a phase difference, each plant correctly goes around the stability contour indicating a stable design for all plant cases. The following compensator is designed for channel 2.

$$g_2 = \frac{(s+0.25)(s+0.75)(s+1.2)(s+1.3)}{s(s+0.98\pm 1)(s+10)(s+20)(s+120)} \tag{5.2}$$

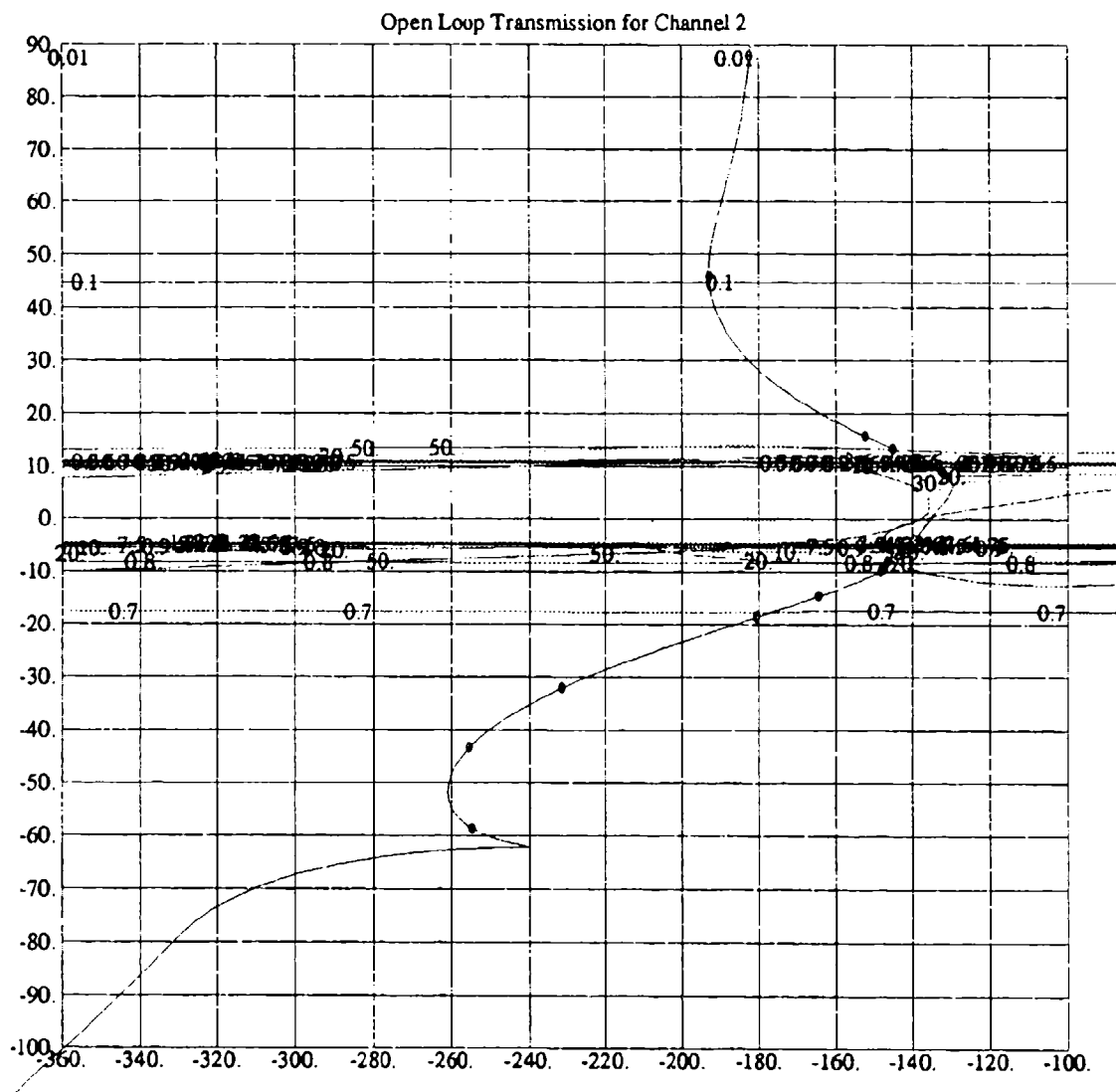Figure 5.2   Channel 2 Loop Shaping P_o = Plant Case 2

5-5

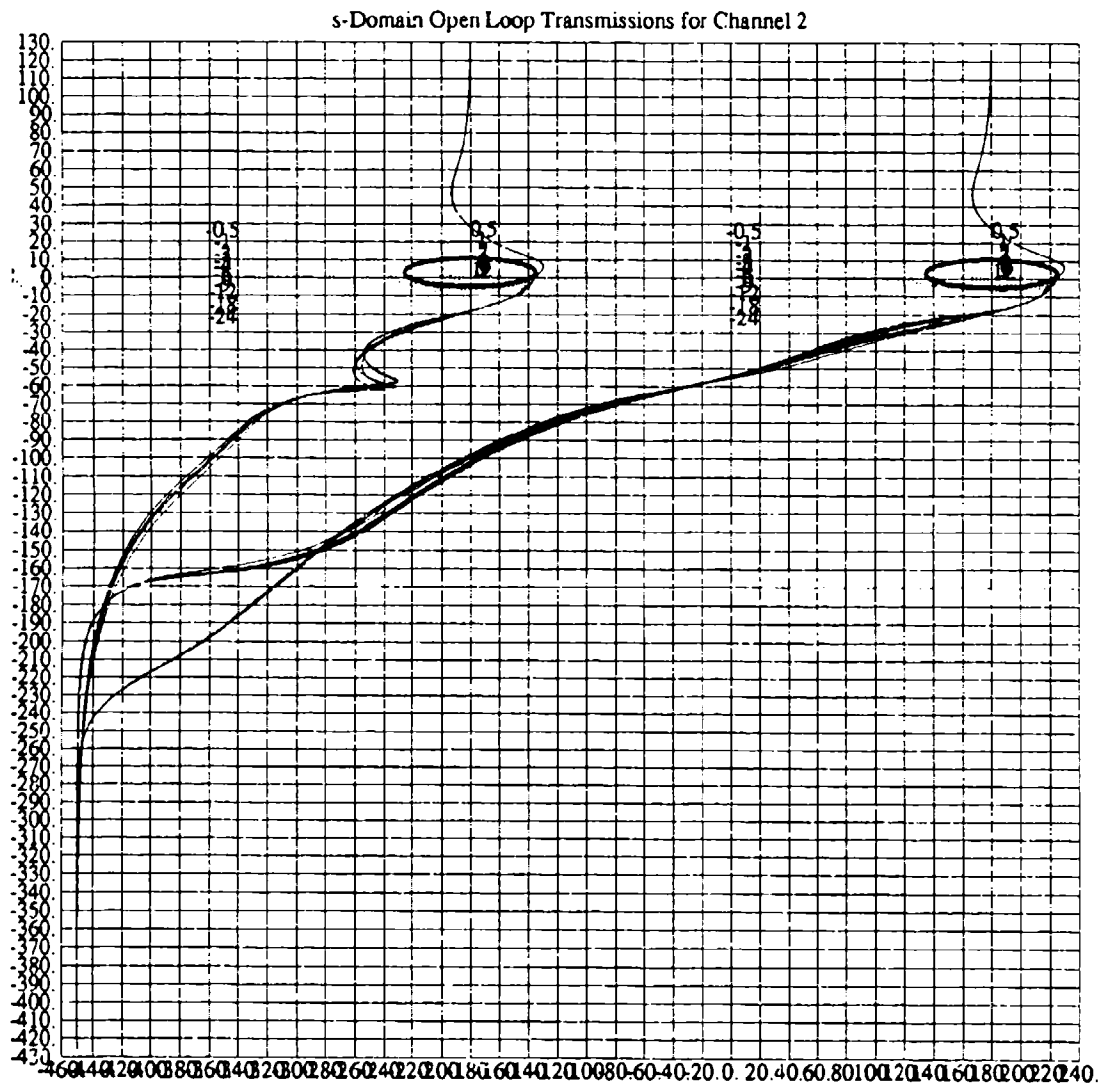s-Domain Open Loop Transmissions for Channel 2

Figure 5.3 Channel 2 Nichols Plot all Plant Cases

5-6

5.3.2 Channel 1 Loop Design

After g_2 is designed the improved method is applied using the equations derived in Section 2.4. Utilizing the known structure of g_2 a more accurate calculation of the cross-coupled disturbance from the compensated channel 2 to the uncompensated channel 1 is achieved. New disturbance and hence composite bounds are generated, shown in Appendix E. The new bounds have smaller magnitude, thus, overdesign is reduced.

For the same reason as channel 2, the nominal loop for channel 1 is plant case 2. Again, as in channel 2 the templates show a 360 degree phase difference between the two plant cases of $C_L = 0.2$ and 0.6. But unlike channel 2 there is a magnitude uncertainty evident in the channel 1 templates, see Appendix E. The magnitude uncertainty arises due to the strong coupling from channel 2 into channel 1, and also from the difference in the effect of wind disturbance between the 2 classes of aircraft plants based on C_L. The plants of $C_L = 0.6$ have a larger wind induced disturbance as shown in Appendix D. Therefore these plants have not only more external disturbance, but also larger cross coupling disturbance.

The loop shaping is more difficult for channel 1. The loop tends to curl at certain frequencies as shown in Figure 5.4. The curling causes a large change in phase with little or no change in magnitude. This type of behavior makes it difficult to shape a loop that is stable, satisfies the composite bound criteria, and maintains a low system bandpass. The loop for channel 1 is shaped with a compromise on the bandpass. A lag-lead compensator is used to "stretch" the low frequency curl. Additional lag-lead compensators are tried to further "stretch" the curl but caused the loop to increase in magnitude as the

frequency increased. A loop shape is finally achieved that satisfies the lower frequency bounds, stability, and slightly increases the system bandpass. The channel 1 compensator, g_1, has a higher order than the channel 2 compensator, see Appendix F. This is an indicator of the difficulties in achieving a loop shape that satisfies design criteria.

The Nichols plot of all 16 plants in Figure 5.5 shows the uncertainty in the low frequency range of the plants. Though there is large phase and magnitude differences between the plants the QFT method is able to achieve a design that satisfies stability and disturbance rejection for all plant cases. The following compensator is designed for channel 1.

$$g_1 = \frac{(s+0.3)(s+0.25\pm 0.433)(s+3)(s+9)(s+1.14\pm 3.747)(s+200)}{s(s+2)(s+0.32\pm 3.184)(s+90\pm 4.02D{-6})(s+135\pm 65.38)(s+1100)} \quad (5.3)$$

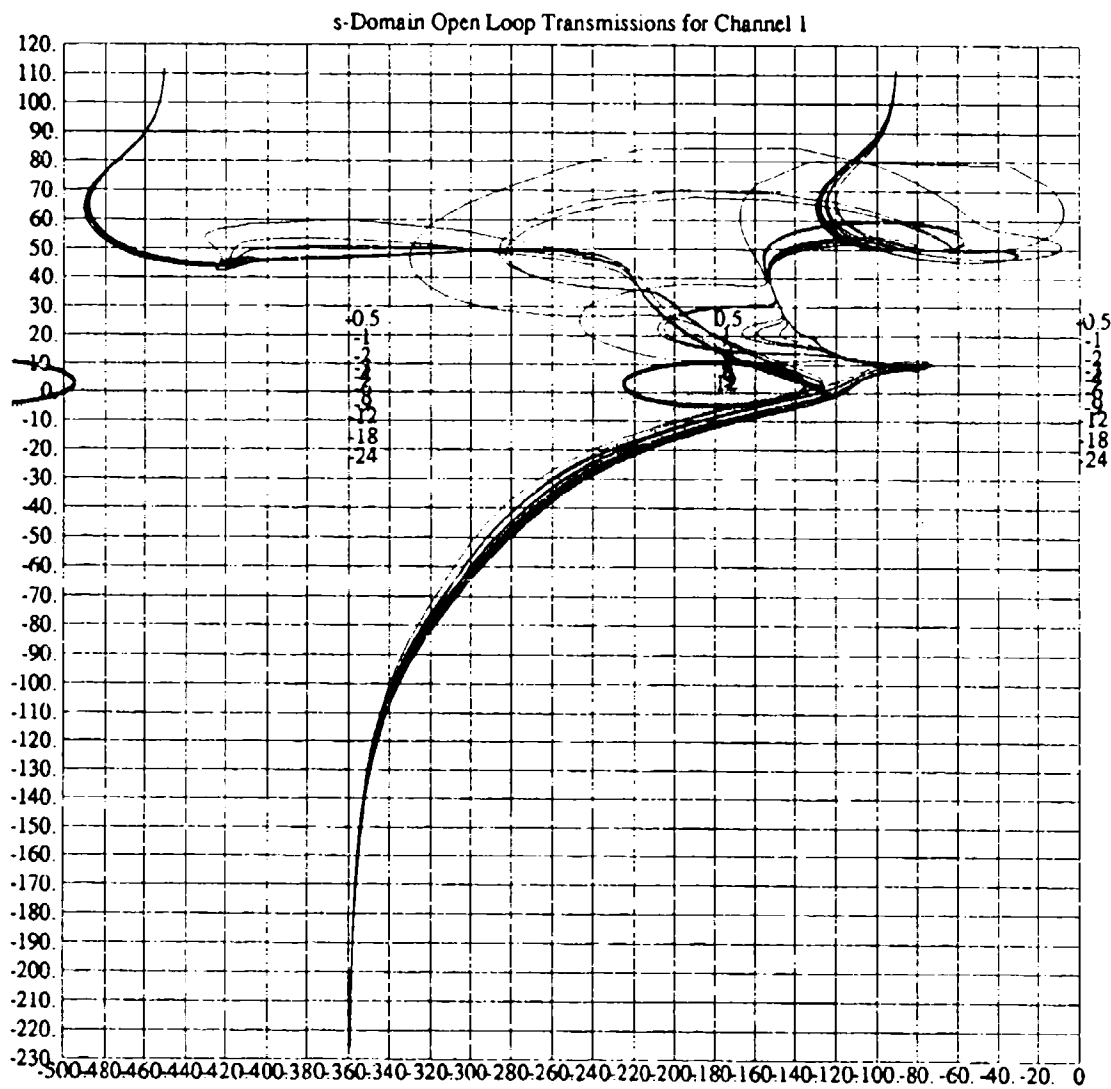Figure 5.4 Channel 1 Loop Shaping P_o = Plant Case 2

Figure 5.5 Channel 1 Nichols Plot all Plant Cases

5-10

5.3.3 Channel 3 Loop Design

Channel 3 exhibits none of the channel 1 or channel 2 characteristics. The channel 3 templates have relatively small phase and magnitude uncertainty. There is no coupling from channels 1 or 2 into channel 3. The external disturbances have similar effects on channel 3 for all plant cases.

The lack of cross coupling disturbance and relatively certain external disturbance is evident in Figure 5.6 where the bounds collapse around the stability contour. The channel 3 loop has a tendency to curl up as the frequency increases. The main difficulty is to add compensation to shape the loop around the bounds and stability contour at +180 degrees and then add further compensation to keep the loop from penetrating the stability region at -180 degrees. To achieve stability the very low frequency bounds are penetrated. This tradeoff is considered acceptable since channel 3, y position has the largest margin of disturbance allowed, 7.5 feet, as detailed in Section 3.4.

The Nichols plot of Figure 5.7 shows a very tight grouping of all plant cases. Again, further evidence of relatively small uncertainty in channel 3. Notice the large change in phase with no decrease in magnitude. This is deemed acceptable since it occurs below the zero dB line at frequencies below the cutoff. The following compensator is designed for channel 3.

$$g_3 = \frac{(s + 0.05)(s + 0.1)(s + 0.2)(s + 0.6)(s + 1.5 \pm 2.6)(s + 5)(s + 30)}{s(s + 2.5D - 4)(s + 0.6 \pm 1.91)(s + 10)(s + 35 \pm 35.707)(s + 37.5 \pm 64.95)} \qquad (5.4)$$
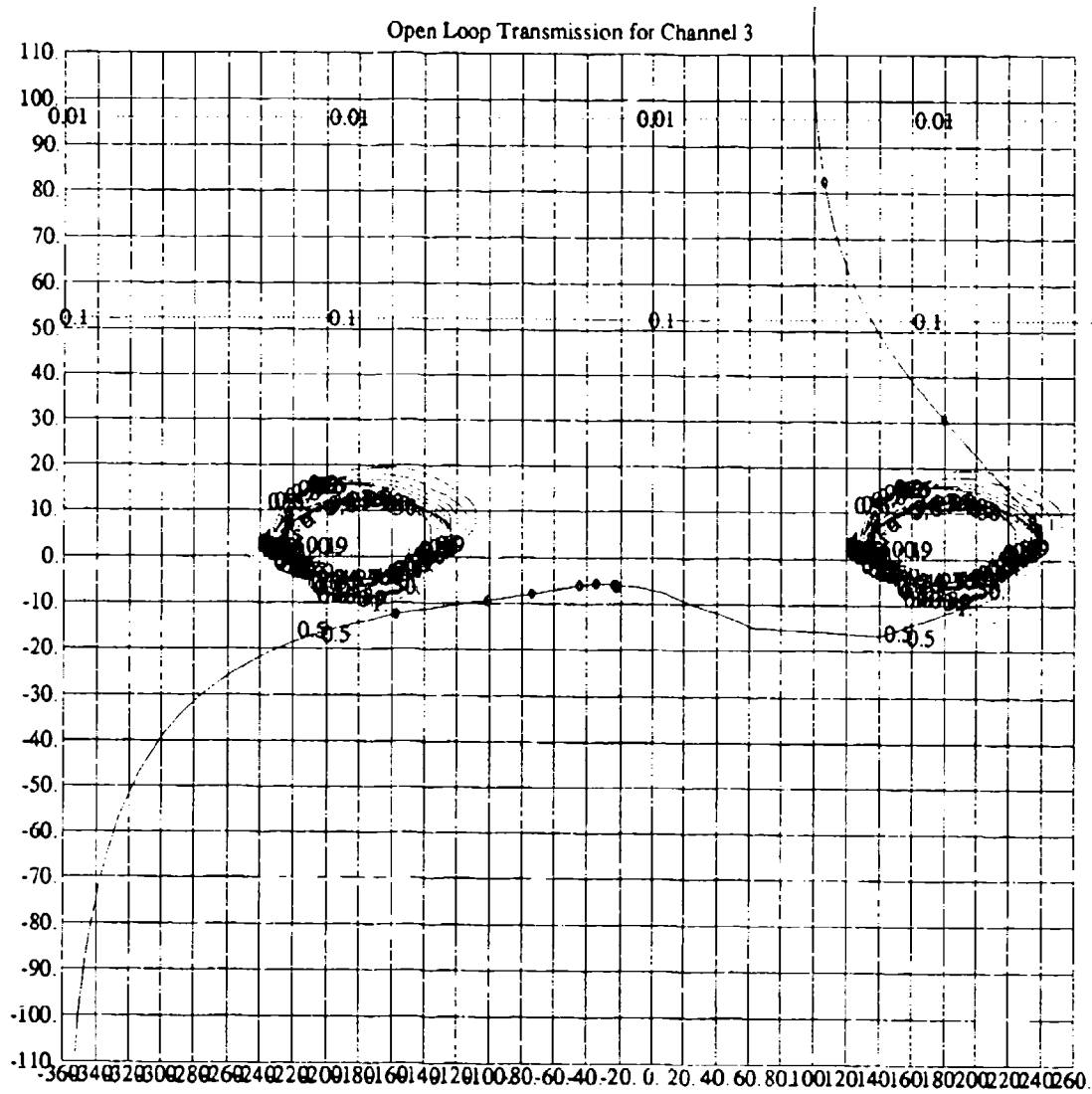
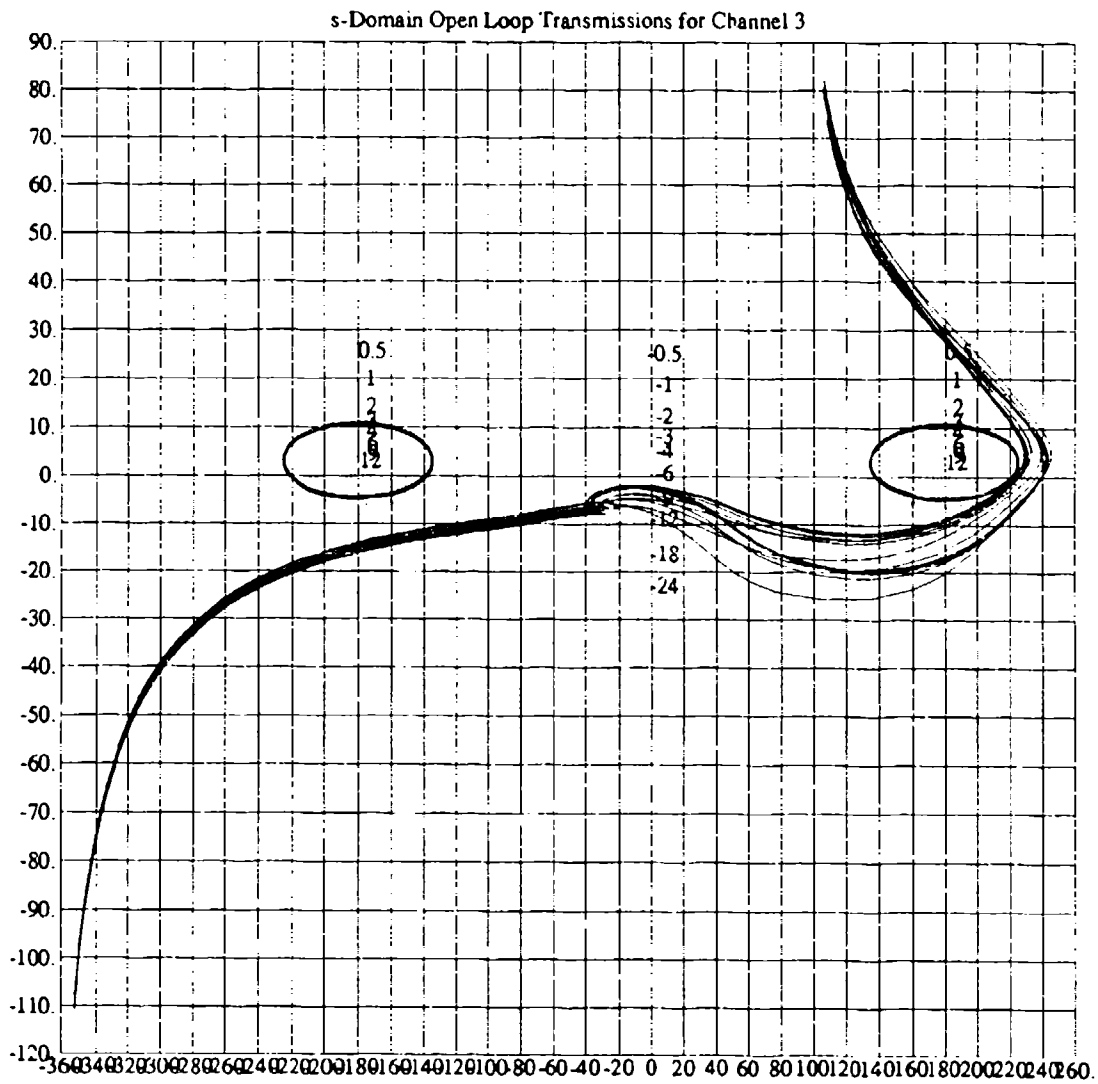Figure 5.6 Channel 3 Loop Shaping P_o = Plant Case 2

Figure 5.7 Channel 3 Nichols Plot all Plant Cases

5-13

5.4 Closed Loop Lm Plots

The overall equivalent MISO system closed loop Lm plots are shown in Figure 5.8.

From these plots you can easily see that disturbance rejection specification is met for all

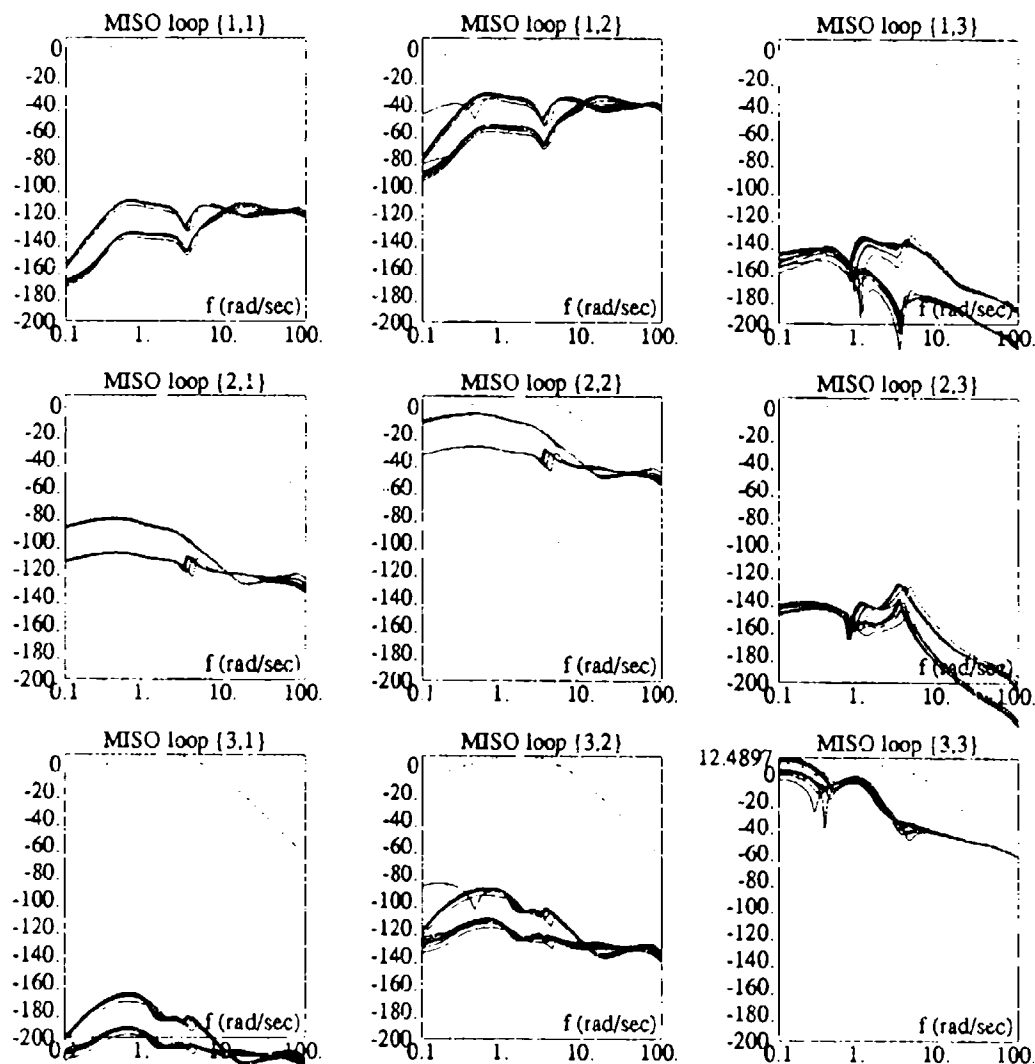MISO loops except fo: as noted in the low frequency portion of the MISO loop {3,3}.

Figure 5.8 MISO Equivalent System Lm Plots

The closed loop MISO plots of Figure 5.8 are an excellent indicator of success in meeting the design specification.

5.5 Summary

In this chapter the AFCS is designed. Each loop shaping is detailed, covering the particular difficulties in shaping the loops for each channel. Also the inherent nature of QFT's ability in handling large plant uncertainties is discussed. Finally the Lm of closed loop MISO system is shown, indicating a successful design given the tradeoffs made. The next chapter discusses the linear and nonlinear simulations.

VI. Air-to-Air Refueling Simulations

6.1 Introduction

In this chapter the compensators designed in the previous chapter are installed in the AFCS and simulations are run to analyze their performance. Linear simulations are run for all plant cases in MATRIX$_X$. Nonlinear simulations are for two plant cases, one for each $C_L = 0.2$ and 0.6, are performed in EASY5x.

6.2 Linear Simulations

Linear simulation are performed in MATRIX$_X$ with the modeled external disturbances forcing the system to deflect from the set point. The simulations are executed in the presence of all external disturbances simultaneously.

The results of the linear separation for channel 1 (Z separation) demonstrate excellent results with very little perturbation from the set point. Figure 6.1 presents the channel 1 response. The plots demonstrate two distinct responses corresponding to aircraft C_L. The aircraft with $C_L = 0.2$ show a maximum perturbation of approximately 0.0025 feet. Also the response dampens faster for the aircraft modeled with $C_L = 0.2$. The aircraft with $C_L = 0.6$ deflected to a maximum value of approximately 0.008 feet with slower dampening.

The channel 2 (X separation) linear simulation demonstrates similar characteristics for response based on C_L. Again, excellent rejection of external disturbance is achieved as shown in Figure 6.2. $C_L = 0.2$ aircraft have a maximum deflection of approximately

0.025 feet, while $C_L = 0.6$ aircraft deflect approximately 0.425 feet from the set point. Recall that the aircraft with $C_L = 0.6$ have a larger uncompensated perturbation due to external wind disturbance.

Channel 3 (Y separation) has the largest perturbation from the set point in the linear simulation, see Figure 6.3. The maximum perturbation in channel 3 is approximately 1.9 feet. Though considerably larger than channels 1 and 2, the channel 3 perturbation remains within the design specification.

6.3 Nonlinear Simulations

The nonlinear simulation are performed in EASY5x. EASY5x has a Dryden wind gust model preprogrammed in the CAD package. The Dryden wind gust model is used in the nonlinear simulations verses the disturbance model developed in Chapter *III*. Two nonlinear simulations are run. One representing an aircraft with $C_L = 0.2$ and the second for $C_L = 0.6$. The nonlinear simulations require considerable time to setup and perform, therefore, time limitation prevented performing a nonlinear simulating for each plant case.

The nonlinear simulations demonstrate the same excellent results that are achieved in the linear simulation. The nonlinear results are consistent with the linear results, very small perturbations for channels 1 and 2 with a larger deflection in channel 3, shown in Figure 6.4 and Figure 6.6. As in the linear simulations, the nonlinear simulations are within the design specifications.

Also presented in the nonlinear simulation plots, Figure 6.5 and Figure 6.7, are the control surface and thrust response of the autopilot. The aileron, rudder, and elevator responses are well within the physical capability of these devices. On the other hand the

6-2

thrust requirements are probably beyond engine response capability. The engine response is most likely due to the autopilot design. The autopilot is a "text book" design and is not very sophisticated. A QFT design using the actual C-135B autopilot can probably achieve similar results without extreme engine response requirements.

6.4 Summary

The compensators designed in Chapter *V* are integrated into the air-to-air refueling AFCS. Linear and nonlinear simulations are performed with excellent results. The system response is within design specification. The QFT design process worked extremely well in designing the AFCS in the presence of external output disturbance. The next chapter contains the conclusion and recommendations for this thesis.
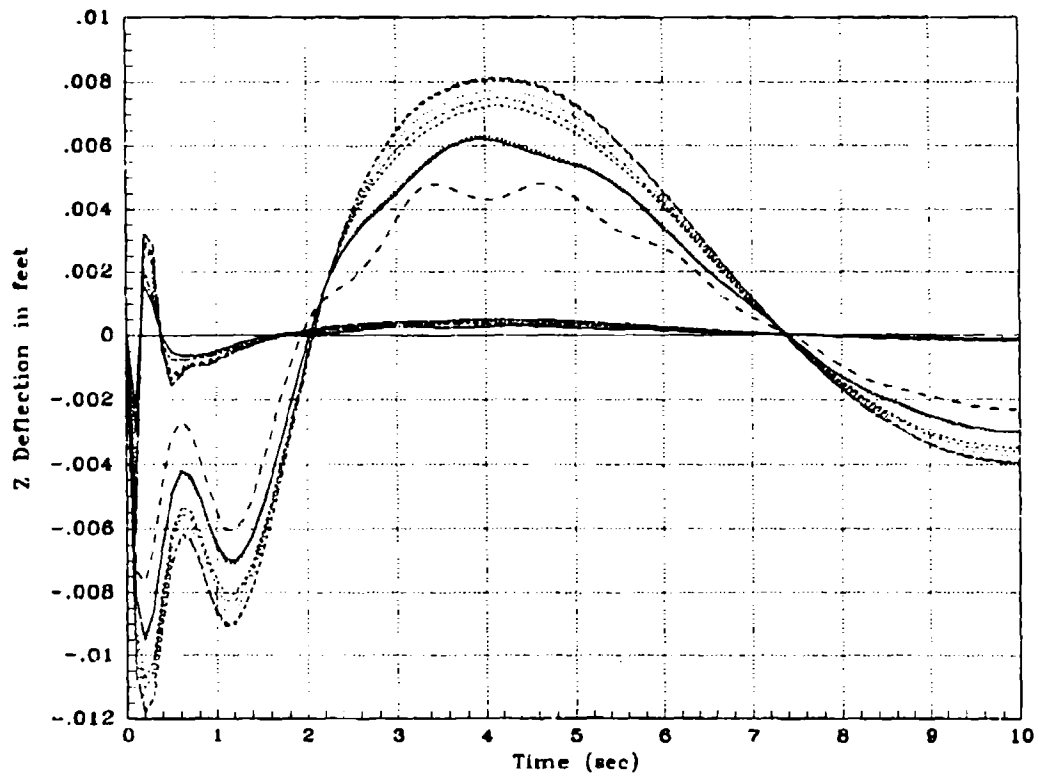
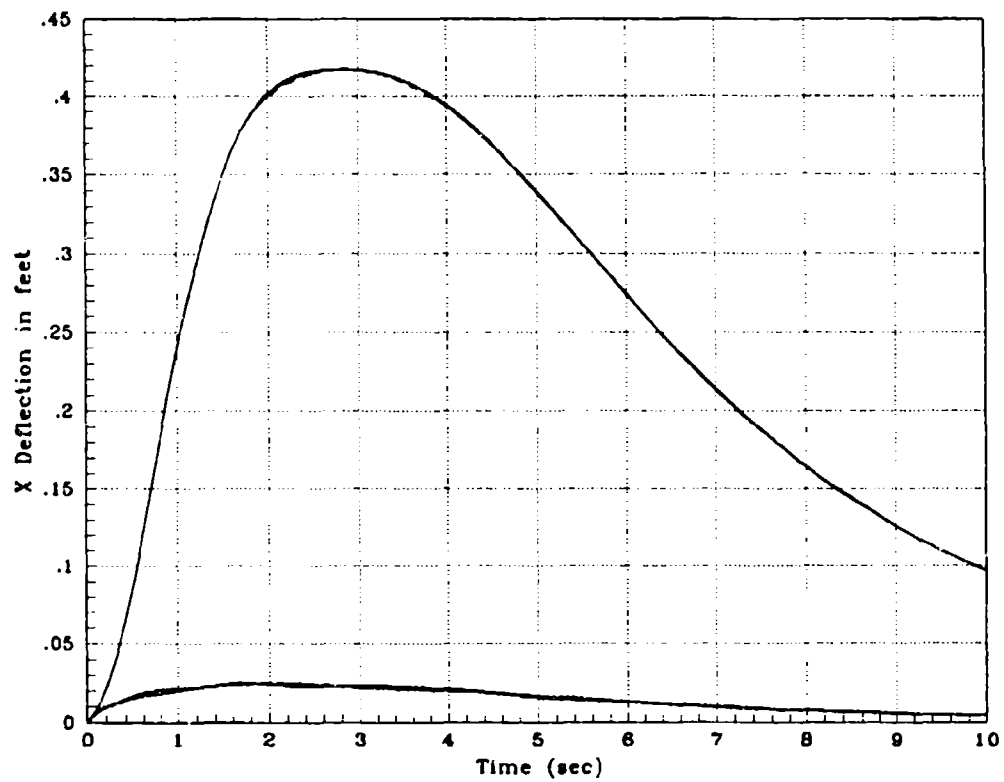Figure 6.1 Linear Simulation - Z Separation Deflection all Plant Cases

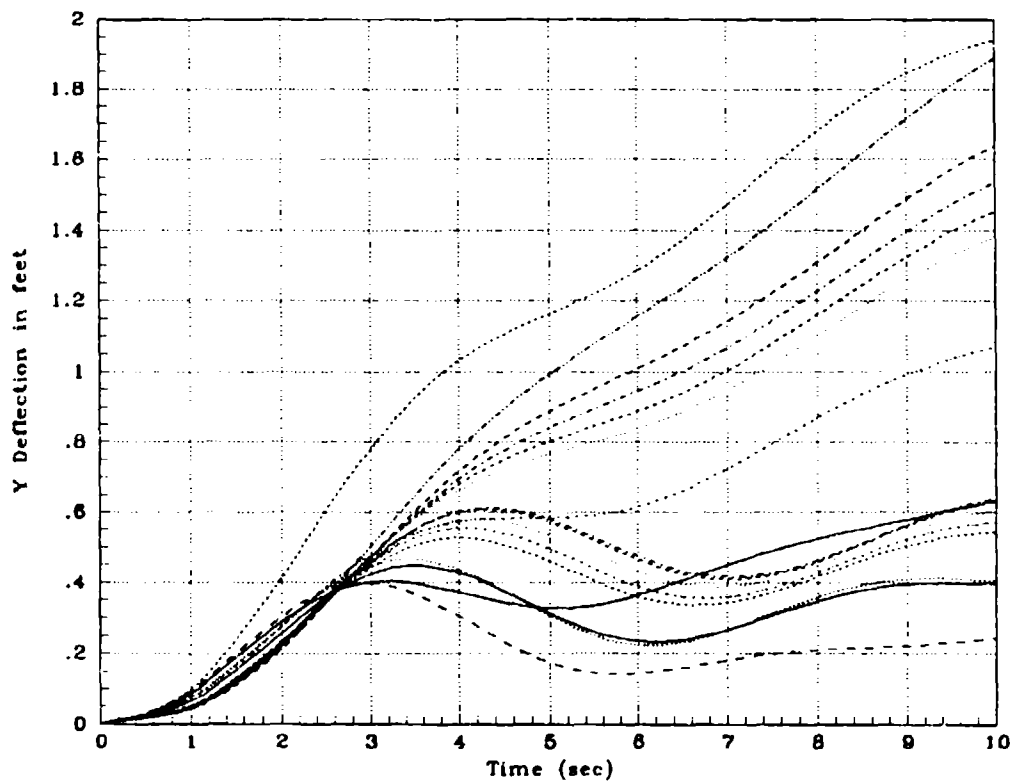Figure 6.2 Linear Simulation - X Position Deflection all Plant Cases

Figure 6.3 Linear Simulation - Y Position Deflection all Plant Cases

Figure 6.4 Nonlinear Simulation - X, Y, Z Position Defection, Plant 1 $C_L = 0.2$

6-7

Figure 6.5 Nonlinear Simulation - Control Surface and Throttle Response, Plant 1
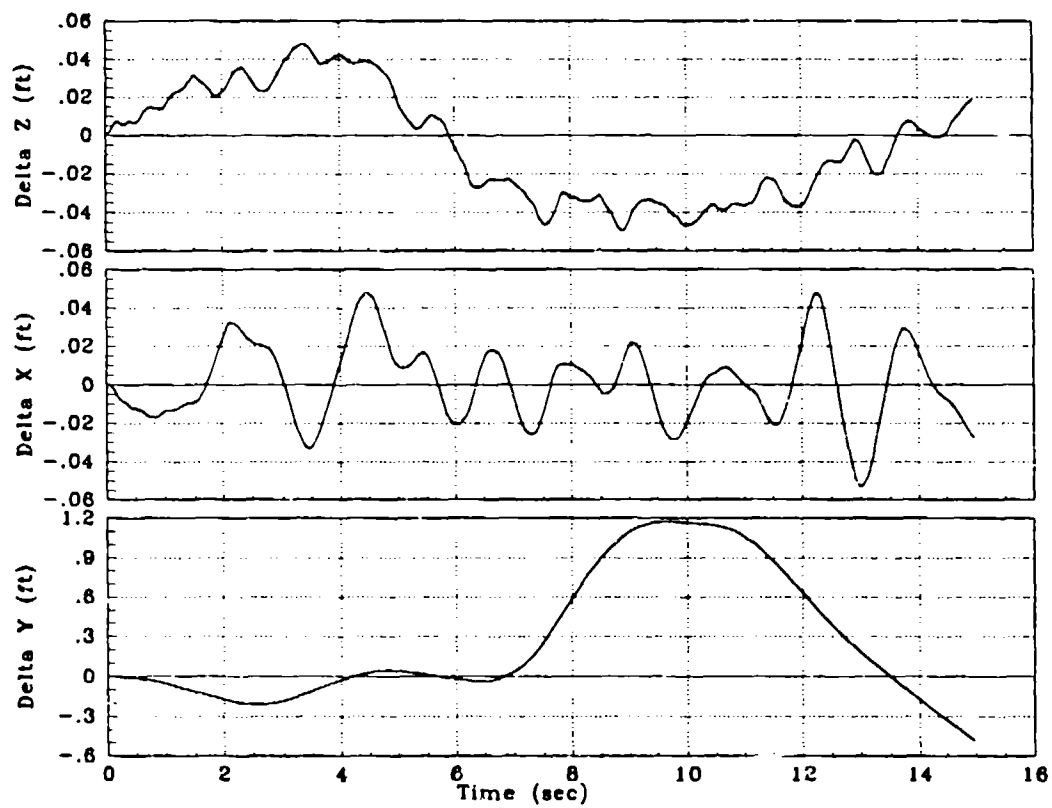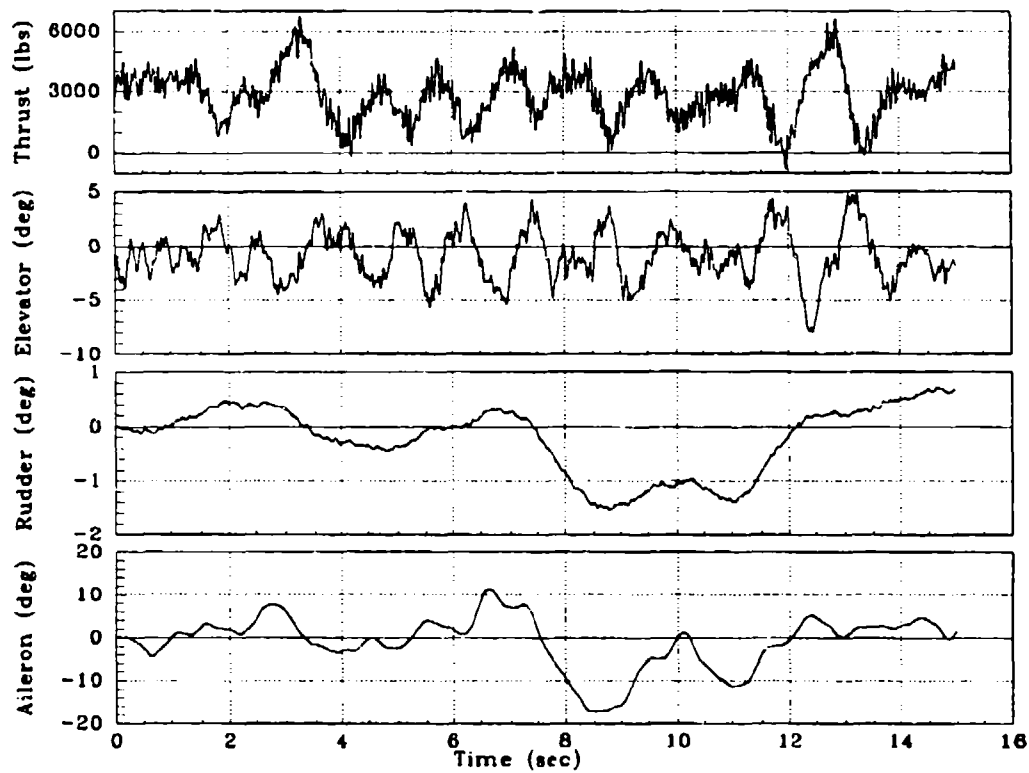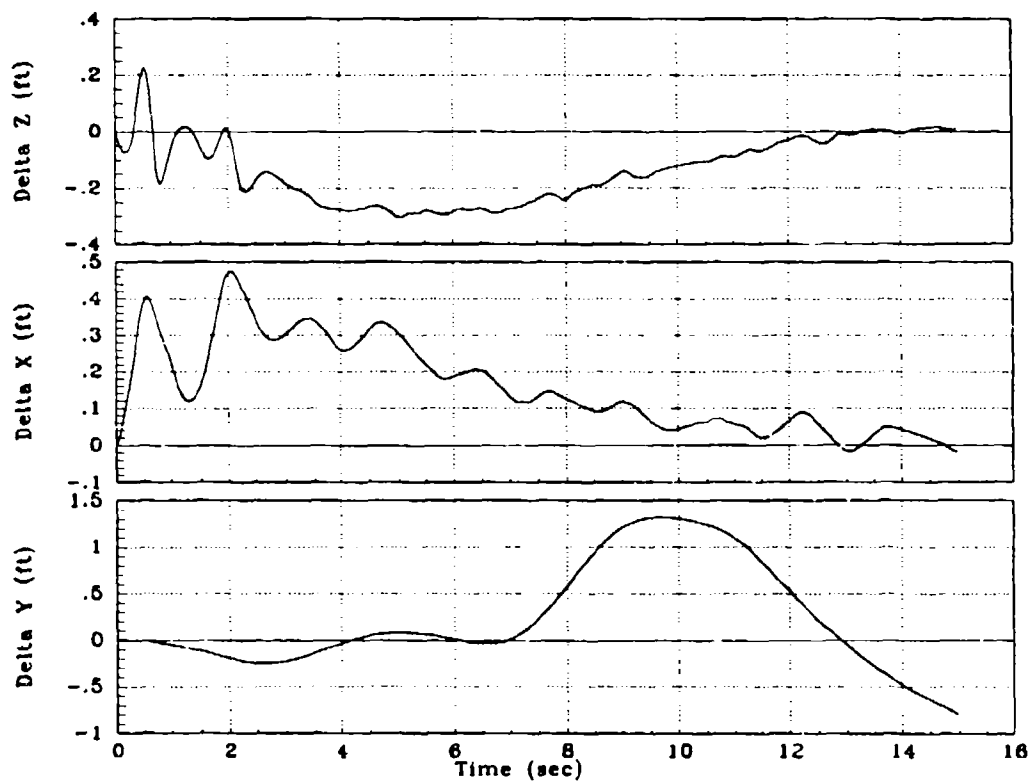
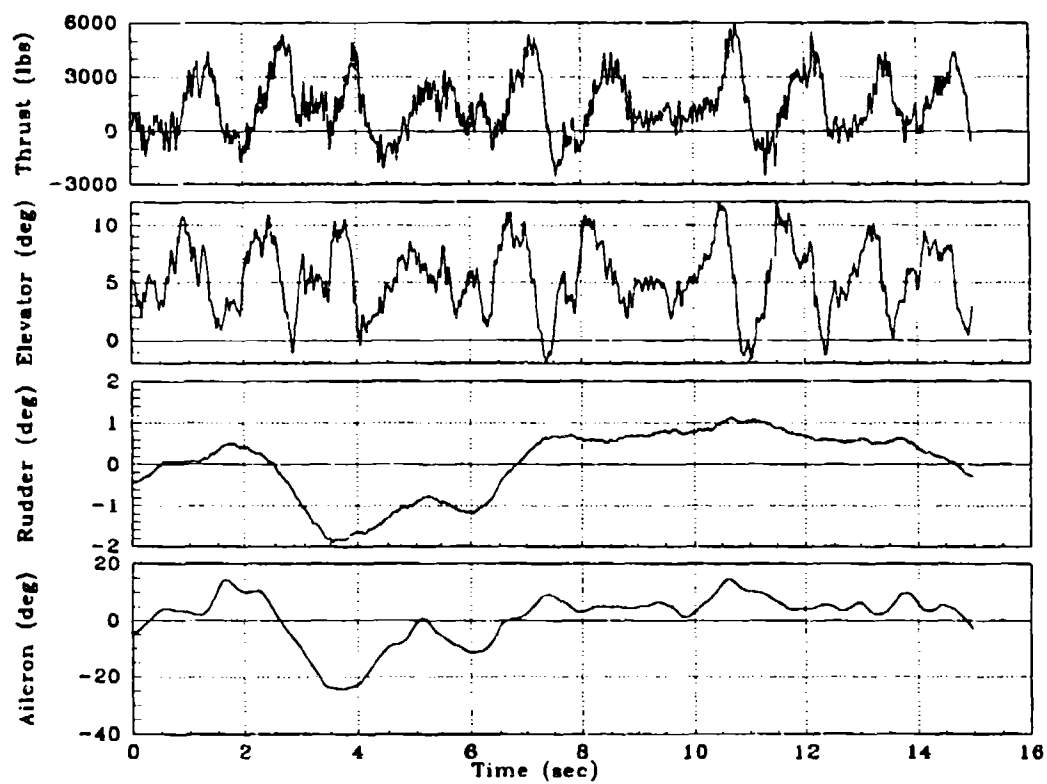Figure 6.6 Nonlinear Simulation - X, Y, Z Position Deflection, Plant 2 $C_L = 0.6$

Figure 6.7 Nonlinear Simulation - Control Surface and Throttle Response, Plant 2

VII. Conclusions and Recommendation

7.1 Discussion

The purpose of this thesis is to develop an AFCS to regulate the position of a cargo/transport aircraft relative to the tanker during air-to-air refueling using QFT. To do this aircraft models are developed that envelop the structured uncertainty of the fuel receiving aircraft. The uncertainties are based on dynamic changes in the aircraft due to taking on fuel and the varying C_L. Once the aircraft models are developed, an autopilot is designed to control altitude, speed, and heading. The autopilot ensures a stable minimum-phase plant with a low frequency cutoff. Disturbance models are developed to identify the effects of wind and refueling disturbances on the plant. The disturbances enter the system at the plant output, therefore, the QFT equations are redeveloped to include the effect of external output disturbance. Since the MISO equivalent is not diagonal dominant, the improved method QFT equations are rederived to include the external disturbance. The MIMO QFT CAD package, developed by Mr Richard Sating is used to design the compensators for the control system. After the loops are shaped the QFT designed compensator are included in the control system where linear and nonlinear simulations are performed. The linear simulation uses the disturbance model to generate the external output disturbance. The Dryden wind gust model is used in the nonlinear simulations.

7.2 Conclusions

MIMO QFT CAD Package An outstanding QFT design tool. The CAD package greatly enhanced the design process. Though problems were initially encountered, they were quickly solved and the package proved to be very robust and easy to use.

QFT External Output Disturbance Equations The successful design of compensators based on these equations and the subsequent simulations validate that the equations are correct. These equation are now part of the MIMO QFT CAD Package and should prove to be valuable in future QFT design work.

Air-to-Air Refueling AFCS The excellent results from the linear and nonlinear simulations demonstrate the very real possibility of being able to implement this system on Air Force aircraft.

7.3 Recommendations

The successful simulations the QFT designed air-to-air refueling prove the technology exists to develop this AFCS. Further research should be accomplished using more modern aircraft with actual inservice autopilot. Upon successful conclusion of this research , the Air Force should give serious consideration to implementing this system.

Appendix A. C-135 Nondimensional Stability Derivatives

This apperdix contains the nondimesioanl stability derivatives used to generate the

C-135B bare aircraft model.

A.1 Nondimensional Stability Derivative Definitions

A.1.1 Lonitudinai

C_D - Aircraft drag co......ient

C_L - Aircraft lift coefficient

$C_{L\alpha}$ - Lift curve slope

$C_{L\delta e}$ - "Change" in lift due to a change in elevator deflection

$C_{m\alpha}$ - "Change" in pitching moment due to a change in alpha

$C_{m\dot\alpha}$ - "Change" in pitching moment due to a change in alpha rate

C_{mq} - "Change" in pitching moment due to a change in pitch rate

$C_{m\delta e}$ - "Change" in pitching moment due to a change in elevator deflection

A.1.2 Lonitudinal

$C'_{y\beta}$ - "Change" in side force due to a change in beta

C_{yp} - "Change" in side force due to a change in roll rate

C_{yr} - "Change" in side force due to a change in yaw rate

$C_{y\delta r}$ - 'Change" in side force due to a change in rudder deflection

$C_{y\delta a}$ - "Change" in side force due to a change in aileron deflection

$C_{l\beta}$ - "Change" in rolling moment due to a change in beta

C_{lp} - "Change" in rolling moment due to a change in roll rate

C_{lr} - "Change" in rolling moment due to a change in yaw rate

$C_{l\delta r}$ - "Change" in rolling moment due to a change in rudder deflection

$C_{l\delta a}$ - "Change" in rolling moment due to a change in aileron deflection

$C_{n\beta}$ - "Change" in yawing moment due to a change in beta

C_{np} - "Change" in yawing moment due to a change in roll rate

C_{nr} - "Change" in yawing moment due to a change in yaw rate

$C_{n\delta r}$ - "Change" in yawing moment due to a change in rudder deflection

$C_{n\delta a}$ - "Change" in yawing moment due to a change in aileron deflection

Stability Derivative	Value
$C_{y\beta}$	-0.74485
C_{yr}	0.410
$C_{y\delta r}$	0.253
$C_{y\delta a}$	-0.0074
C_{lp}	-0.3550
$C_{l\delta a}$	0.0160
$C_{n\delta r}$	-0.109
$C_{n\delta a}$	0.00160
$C_{l\alpha}$	-4.641
$C_{l\delta e}$	-0.1977
$C_{m\alpha}$	-0.8309
$C_{m\delta e}$	-0.67609

Table A.1 Constant Stability Derivatives for all Plant Cases

A-2

Stability Derivative		Value	
	C_L	0.2	0.6
C_{yp}		-0.237	-0.196
$C_{l\beta}$		-0.17762	-0.22059
C_{lr}		0.108	0.192
$C_{l\delta r}$		0.03724	0.0258
$C_{n\beta}$		0.15183	0.16043
C_{np}		0.0	-0.006
C_{nr}		-0.183	-0.187
C_D		-0.014	-0.03

Table A.2 Stability Derivatives that Change with C_L

	Gross Weight ($\times 10^3$ lbs)	Center of Gravity (% MAC)	$C_{m\dot{\alpha}}$	C_{mq}	I_{xx} ($\times 10^6$)	I_{yy} ($\times 10^6$)	I_{zz} ($\times 10^6$)
1	160.166	28.8	-6.10	-14.25	2.0	2.70	4.575
2	207.316	28.0	-6.13	-14.5	2.725	2.70	5.375
3	210.189	30.1	-6.03	-14.275	3.15	2.75	5.85
4	245.500	22.9	-6.35	-15.025	3.175	2.855	6.0
5	253.500	26.0	-6.22	-14.725	3.1875	3.0	6.1
6	263.500	23.8	-6.30	-14.925	3.2	3.05	6.19
7	275.500	24.1	-6.30	-14.915	3.525	3.10	6.5
8	277.500	24.8	-6.27	-14.835	3.55	3.105	6.51

Table A.3 Stability Derivatives that Change with Weight and Center of Gravity

Appendix B. Plant Transfer Functions

This appendix presents transfer functions for all plants developed with EASY5 and

MATRIX$_x$.

B.1 Plant Case 1 - C_L = 0.2 Gross Weight = 160,666 pounds

$$q_{11} = \frac{2.05D-3(s+0.286\pm4.346)(s+17.223)(s+43.763\pm73.228)(s+159.108)(s+499.104)}{(s-2.068\pm6.221)(s+0.067)(s+0.754\pm1.208)(s+5.394)(s+10.169)(s+70.040\pm71.419)(s+119.979)}$$

$$q_{12} = \frac{2.42D+13(s+17.223)(s+43.763\pm73.228)(s+159.108)(s+249.323\pm433.897)(s+499.104)}{s(s-6.27D+4\pm3.64D+4)(s+0.001)(s+1)(s+50)(s+444.55\pm7.28D+4)(s+6.35D+4\pm3.64D+4)}$$

$$q_{13} = 0$$

$$q_{21} = \frac{-12.732(s+0.289\pm4.346)}{(s-0.023\pm0.013)(s+0.977\pm1.718)(s+10.031)}$$

$$q_{22} = \frac{49.866(s+0.289\pm4.346)}{s(s+0.099)(s+0.289\pm4.336)(s+501.611)}$$

$$q_{23} = 0$$

$$q_{31} = 0$$

$$q_{32} = 0$$

$$q_{33} = \frac{2.296(s-0.037\pm1.739)(s+0.2)(s+0.289)(s+5.620\pm6.110)}{s(s+0.146\pm0.072)(s-0.285)(s+1.115)((s+5.430\pm5.951)(s+7.136))}$$

B.2 Plant Case 2 - C_L = 0.6 Gross Weight = 160,666 pounds

$$q_{11} = \frac{2.78D-3(s+0.471\pm4.346)(s+17.223)(s+43.123\pm72.056)(s+164.600)(s+369.868)}{(s-0.268\pm19.368)(s+0.022\pm0.820)(s+0.067)(s+1.362)(s-14.244)(s+70.799\pm71.556)(s-119.674)}$$

$$q_{12} = \frac{2.183D - 16(s+0.471 \pm 4.364)(s+17.298)(s+43.123 \pm 72.056)(s+1164.599)(s+249.279 \pm 433.591)(s+369.868)}{s(s-0.004)(s+0.286 \pm 4.340)(s+1)(s+50)}$$

$$q_{13} = 0$$

$$q_{21} = \frac{-12.853(s+0.477 \pm 4.364)}{(s-0.025 \pm 0.040)(s+0.759 \pm 1.818)(s+10.029)}$$

$$q_{22} = \frac{37.163(s+0.477 \pm 4.364)}{s(s+0.101)(s+0.473 \pm 4.341)(s+376.574)}$$

$$q_{23} = 0$$

$$q_{31} = 0$$

$$q_{32} = 0$$

$$q_{33} = \frac{2.215(s-0.095 \pm 1.765)(s+0.2)(s+0.498)(s+5.615 \pm 6.391)}{s(s-0.138)(s-0.156)(s+0.344)(s-1.444)(s+1.957)(s+5.392 \pm 5.795)(s+7.019)}$$

B.3 Plant Case 3 - C_L = 0.2 Gross Weight = 207,316 pounds

$$q_{11} = \frac{2.04D - 3(s+0.208 \pm 3.697)(s+17.275)(s+43.356 \pm 72.537)(s+162.161)(s+413.414)}{(s-2.119 \pm 6.292)(s+0.062)(s+0.704 \pm 0.891)(s+5.40)(s+10.176)(s+70.032 \pm 71.430)(s+119.994)}$$

$$q_{12} = \frac{1.508D - 16(s+17.275)(s+43.356 \pm 72.537)(s+162.161)(s+249.277 \pm 433.702)(s+413.414)}{s(s-0.002)(s+1)(s+50)}$$

$$q_{13} = 0$$

$$q_{21} = \frac{-13.62(s+0.209 \pm 3.698)}{(s-0.029)(s-0.019)(s+0.898 \pm 1.701)(s+10.030)}$$

$$q_{22} = \frac{41.405(s+0.209 \pm 3.698)}{s(s+0.099)(s+0.211 \pm 3.690)(s+418.121)}$$

$$q_{23} = 0$$

$$q_{31} = 0$$

$$q_{32} = 0$$

$$q_{33} = \frac{2.113\,(s - 0.060 \pm 1.483)(s + 0.2)(s + 5.445 \pm 4.568)}{s(s + 0.154 \pm 0.069)(s + 1.275 \pm 0.444)(s + 5.270 \pm 4.318)(s + 7.739)}$$

B.4 Plant Case 4 - C_L - 0.6 Gross Weight = 207,316 pounds

$$q_{11} = \frac{2.60D - 3(s + 0.380 \pm 3.718)(s + 17.350)(s + 42.804 \pm 71.411)(s + 168.723)(s + 322.491)}{(s - 0.748 \pm 19.295)(s + 0.062)(s + 0.076 \pm 0.684)(s + 1.263)(s + 14.283)(s + 70.628 \pm 71.744)(s + 119.960)}$$

$$q_{12} = \frac{-549.466(s + 0.381 \pm 3.718)(s + 17.351)(s + 42.805 \pm 71.411)(s + 168.724)(s + 249.302 \pm 433.469)(s + 322.4906)}{s(s - 1.695D + 9)(s - 0.007)(s + 0.207 \pm 3.690)(s + 1)(s + 50)(s + 1.695D + 9)}$$

$$q_{13} = 0$$

$$q_{21} = \frac{-12.738(s + 0.384 \pm 3.718)}{(s - 0.027 \pm 0.032)(s + 0.611 \pm 1.815)(s + 10.029)}$$

$$q_{22} = \frac{32.740(s + 0.384 \pm 3.718)}{s(s + 0.100)(s + 0.383 \pm 3.702)(s + 332.784)}$$

$$q_{23} = 0$$

$$q_{31} = 0$$

$$q_{32} = 0$$

$$q_{33} = \frac{2.052(s - 0.133 \pm 1.530)(s + 0.2)(s + 0.518)(s + 5.422 \pm 4.802)}{s(s + 0.126)(s + 0.176)(s + 0.347)(s + 1.348 \pm 0.625)(s + 5.228 \pm 4.106)(s + 7.636)}$$

B-3

B.5 Plant Case 5 - $C_L = 0.2$ Gross Weight = 210,189 pounds

$$q_{11} = \frac{2.01D-3(s+0.207\pm3.674)(s+17.280)(s+43.321\pm72.474)(s+162.466)(s+407.121)}{(s-2.1223\pm6.252)(s+0.062)(s+0.702\pm0.875)(s+5.368)(s+10.172)(s+70.031\pm71.429)(s+119.994)}$$

$$q_{12} = \frac{8.854D+4(s+17.280)(s+43.321\pm71.474)(s+162.466)(s+249.276\pm433.686)(s+407.121)}{s(s-4.185D+6\pm7.249D+6)(s-0.002)(s+1)(s+50)(s+8.371D+9)}$$

$$q_{13} = 0$$

$$q_{21} = \frac{-13.365(s+0.209\pm3.674)}{(s-0.030)(s-0.018)(s+0.874\pm1.689)(s+10.030)}$$

$$q_{22} = \frac{40.792(s+0.209\pm3.674)}{s(s+0.099)(s+0.210\pm3.567)(s+412.067)}$$

$$q_{23} = 0$$

$$q_{31} = 0$$

$$q_{32} = 0$$

$$q_{33} = \frac{1.833(s-0.079\pm1.512)(s+0.2)(s+5.406\pm3.822)}{s(s+0.155\pm0.069)(s+1.143\pm0.571)(s+5.210\pm3.523)(s+7.981)}$$

B.6 Plant Case 6 - $C_L = 0.6$ Gross Weight = 210,189 pounds

$$q_{11} = \frac{0.298(s+0.384\pm3.695)}{(s+0.062)(s+0.080\pm0.679)(s+1.260)(s+114.471)}$$

$$q_{12} = \frac{6.175D-3(s+0.384\pm3.695)}{s(s-0.007)(s+0.207\pm3.667)(s+1)}$$

$$q_{31} = 0$$

$$q_{21} = \frac{-13.475(s+0.384\pm3.694)}{(s-0.027+0.032)(s+0.589\pm1.799)(s+10.028)}$$

$$q_{22} = \frac{32.229(s + 0.384 \pm 3.695)}{s(s + 0.100)(s + 0.382 \pm 3.678)(s + 327.733)}$$

$$q_{23} = 0$$

$$q_{31} = 0$$

$$q_{32} = 0$$

$$q_{33} = \frac{1.776(s - 0.150 \pm 1.558)(s + 0.2)(s + 0.524)(s + 5.374 \pm 4.070)}{s(s + 0.125)(s + 0.177)(s + 0.349)(s + 1.213 \pm 0.720)(s + 5.169 \pm 3.262)(s + 7.878)}$$

B.7 Plant Case 7 - $C_L = 0.2$ Gross Weight = 245,500 pounds

$$q_{11} = \frac{5.252(s + 0.170 \pm 3.361)}{(s + 0.058)(s + 0.677 \pm 0.710)(s + 8.867)(s + 119.936)}$$

$$q_{12} = \frac{5.244D - 3(s + 0.170 \pm 3.361)}{s(s - 0.003)(s + 0.169 \pm 3.351)(s + 1)}$$

$$q_{31} = 0$$

$$q_{21} = \frac{-13.193(s + 0.170 \pm 3.361)}{(s - 0.037)(s - 0.013)(s + 0.840 \pm 1.639)(s + 10.029)}$$

$$q_{22} = \frac{35.848(s + 0.170 \pm 3.361)}{s(s + 0.098)(s + 0.172 \pm 3.354)(s + 363.322)}$$

$$q_{23} = 0$$

$$q_{31} = 0$$

$$q_{32} = 0$$

$$q_{33} = \frac{1.985(s - 0.071 \pm 1.346)(s + 0.2)(s + 0.266)(s + 5.381 \pm 3.799)}{s(s + 0.158)(s + 0.067)(s + 0.273)(s + 1.099 \pm 0.591)(s + 5.207 \pm 3.486)(s + 8.049)}$$

B8 Plant Case 8 - $C_L = 0.6$, Gross Weight = 245,500 pounds

$$q_{11} = \frac{0.294(s + 0.341 \pm 3.382)}{(s + 0.058)(s + 0.106 \pm 0.606)(s + 1.213)(s + 128.756)}$$

$$q_{12} = \frac{5.285D - 3(s + 0.341 \pm 3.382)}{s(s - 0.008)(s + 0.169 \pm 3.352)(s + 1)}$$

$$q_{13} = 0$$

$$q_{21} = \frac{-13.296(s + 0.341 \pm 3.382)}{(s - 0.027 \pm 0.027)(s + 0.517 \pm 1.575)(s + 10.027)}$$

$$q_{22} = \frac{28.999(s + 0.341 \pm 3.382)}{s(s + 0.100)(s + 0.339 \pm 3.367)(s + 295.845)}$$

$$q_{23} = 0$$

$$q_{31} = 0$$

$$q_{32} = 0$$

$$q_{33} = \frac{1.924(s - 0.141 \pm 1.407)(s + 0.2)(s + 0.530)(s + 5.352 \pm 4.014)}{s(s + 0.123)(s + 0.184)(s + 0.349)(s + 1.163 \pm 0.735)(s + 5.165 \pm 3.233)(s + 7.957)}$$

B.9 Plant Case 9 - $C_L = 0.2$, Gross Weight = 253,500 pounds

$$q_{11} = \frac{4.984(s + 0.168 \pm 3.313)}{(s + 0.058)(s + 0.672 \pm 0.679)(s + 8.896)(s + 117.665)}$$

$$q_{12} = \frac{5.078D - 3(s + 0.168 \pm 3.313)}{s(s - 0.003)(s + 0.167 \pm 3.303)(s + 1)}$$

$$q_{13} = 0$$

$$q_{21} = \frac{-12.519(s + 0.168 \pm 3.313)}{(s - 0.038)(s - 0.012)(s + 0.793 \pm 1.603)(s + 10.027)}$$

B-6

$$q_{22} = \frac{34.607(s + 0.168 \pm 3.313)}{s(s + 0.098)(s + 0.170 \pm 3.306)(s + 351.087)}$$

$$q_{23} = 0$$

$$q_{31} = 0$$

$$q_{32} = 0$$

$$q_{33} = \frac{1.973(s - 0.070 \pm 1.321)(s + 0.2)(s + 0.264)(s + 5.379 \pm 3.780)}{s(s + 0.159 \pm 0.066)(s + 0.272)(s + 1.073 \pm 0.606)(s + 5.205 \pm 3.467)(s + 8.094)}$$

B.10 Plant Case 10 · $C_L = 0.6$, Gross Weight = 253,500 pounds

$$q_{11} = \frac{0.279(s + 0.339 \pm 3.334)}{(s + 0.058)(s + 0.111 \pm 0.591)(s + 1.203)(s + 126.502)}$$

$$q_{12} = \frac{5.118D - 3(s + 0.339 \pm 3.334)}{s(s - 0.008)(s + 0.167 \pm 3.304)(s + 1)}$$

$$q_{13} = 0$$

$$q_{21} = \frac{-12.617(s + 0.339 \pm 3.334)}{(s - 0.028 \pm 0.026)(s + 0.476 \pm 1.713)(s + 10.026)}$$

$$q_{22} = \frac{27.906(s + 0.339 \pm 3.334)}{s(s + 0.100)(s + 0.337 \pm 3.519)(s + 285.044)}$$

$$q_{23} = 0$$

$$q_{31} = 0$$

$$q_{32} = 0$$

$$q_{33} = \frac{1.913(s - 0.155 \pm 1.3^93)(s + 0.2)(s + 0.531)(s + 5.349 \pm 3.992)}{s(s + 0.122)(s + 0.185)(s + 0.349)(s + 1.135 \pm 0.746)(s + 5.164 \pm 3.220)(s + 8.007)}$$

B.11 Plant Case 11 - $C_L = 0.2$, Gross Weight = 263,500 pounds

$$q_{11} = \frac{4.921(s + 0.160 \pm 3.243)}{(s + 0.057)(s + 0.666 \pm 0.642)(s + 8.904)(s + 120.454)}$$

$$q_{12} = \frac{4.885D - 3(s + 0.160 \pm 3.243)}{s(s - 0.003)(s + 0.159 \pm 3.232)(s + 1)}$$

$$q_{13} = 0$$

$$q_{21} = \frac{-12.361(s + 0.160 \pm 3.243)}{(s - 0.039)(s - 0.011)(s + 0.782 \pm 1.585)(s + 10.027)}$$

$$q_{22} = \frac{33.432(s + 0.160 \pm 3.243)}{s(s + 0.098)(s + 0.162 \pm 3.236)(s + 339.502)}$$

$$q_{23} = 0$$

$$q_{31} = 0$$

$$q_{32} = 0$$

$$q_{33} = \frac{1.975(s - 0.067 \pm 1.290)(s + 0.2)(s + 0.261)(s + 5.376 \pm 3.762)}{s(s + 0.160 \pm 0.066)(s + 0.270)(s + 1.051 \pm 0.616)(s + 5.204 \pm 3.450)(s + 8.132)}$$

B.12 Plant Case 12 - $C_L = 0.6$, Gross Weight = 263,500 pounds

$$q_{11} = \frac{0.276(s + 0.330 \pm 3.264)}{(s + 0.057)(s + 0.117 \pm 0.574)(s + 1.193)(s + 129.283)}$$

$$q_{12} = \frac{4.924D - 3(s + 0.330 \pm 3.264)}{s(s - 0.008)(s + 0.158 \pm 3.234)(s + 1)}$$

$$q_{13} = 0$$

$$q_{21} = \frac{-12.458(s + 0.330 \pm 3.264)}{(s - 0.028 \pm 0.025)(s + 0.458 \pm 1.696)(s + 10.025)}$$

$$q_{22} = \frac{27.074(s + 0.330 \pm 3.264)}{s(s + 0.100)(s + 0.328 \pm 3.250)(s + 276.840)}$$

$$q_{23} = 0$$

$$q_{31} = 0$$

$$q_{32} = 0$$

$$q_{33} = \frac{1.916(s - 0.155 \pm 1.356)(s + 0.2)(s + 0.532)(s + 5.346 \pm 3.971)}{s(s + 0.122)(s + 0.187)(s + 0.349)(s + 1.111 \pm 0.754)(s + 5.162 \pm 3.206)(s + 8.050)}$$

B.13 Plant Case 13 - C_L = 0.2, Gross Weight = 275,500 pounds

$$q_{11} = \frac{4.870(s + 0.153 \pm 3.164)}{(s + 0.056)(s + 0.659 \pm 0.601)(s + 8.909)(s + 124.181)}$$

$$q_{12} = \frac{4.672D - 3(s + 0.153 \pm 3.164)}{s(s - 0.003)(s + 0.152 \pm 3.153)(s + 1)}$$

$$q_{13} = 0$$

$$q_{21} = \frac{-12.232(s + 0.153 \pm 3.164)}{(s - 0.040)(s - 0.010)(s + 0.763 \pm 1.569)(s + 10.027)}$$

$$q_{22} = \frac{32.169(s + 0.153 \pm 3.243)}{s(s + 0.098)(s + 0.155 \pm 3.157)(s + 327.051)}$$

$$q_{23} = 0$$

$$q_{31} = 0$$

$$q_{32} = 0$$

$$q_{33} = \frac{1.875(s - 0.072 \pm 1.266)(s + 0.2)(s + 0.258)(s + 5.347 \pm 3.248)}{s(s + 0.162 \pm 0.065)(s + 0.269)(s + 0.990 \pm 0.647)(s + 5.169 \pm 3.871)(s + 8.240)}$$

B-9

B.14 Plant Case 14 - $C_L = 0.6$, Gross Weight = 275,500 pounds

$$q_{11} = \frac{0.273(s + 0.321 \pm 3.185)}{(s + 0.056)(s + 0.123 \pm 0.555)(s + 1.182)(s + 133.002)}$$

$$q_{12} = \frac{4.708D - 3(s + 0.321 \pm 3.185)}{s(s - 0.009)(s + 0.151 \pm 3.154)(s + 1)}$$

$$q_{13} = 0$$

$$q_{21} = \frac{-12.327(s + 0.321 \pm 3.185)}{(s - 0.028 \pm 0.023)(s + 0.429 \pm 1.680)(s + 10.025)}$$

$$q_{22} = \frac{26.194(s + 0.321 \pm 3.185)}{s(s + 0.100)(s + 0.320 \pm 3.171)(s + 268.140)}$$

$$q_{23} = 0$$

$$q_{31} = 0$$

$$q_{32} = 0$$

$$q_{33} = \frac{1.820(s - 0.163 \pm 1.333)(s + 0.2)(s + 0.539)(s + 5.313 \pm 3.762)}{s(s + 0.121)(s + 0.189)(s + 0.351)(s + 1.048 \pm 0.779)(s + 5.128 \pm 2.573)(s + 8.155)}$$

B.15 Plant Case 15 - $C_L = 0.2$, Gross Weight = 277,500 pounds

$$q_{11} = \frac{4.866(s + 0.152 \pm 3.151)}{(s + 0.056)(s + 0.658 \pm 0.594)(s + 8.910)(s + 124.910)}$$

$$q_{12} = \frac{4.639D - 3(s + 0.152 \pm 3.151)}{s(s - 0.003)(s + 0.151 \pm 3.140)(s + 1)}$$

$$q_{13} = 0$$

$$q_{21} = \frac{-12.224(s + 0.152 \pm 3.151)}{(s - 0.041)(s - 0.010)(s + 0.757 \pm 1.568)(s + 10.026)}$$

$$q_{22} = \frac{31.972(s + 0.152 \pm 3.151)}{s(s + 0.098)(s + 0.154 \pm 3.144)(s + 325.094)}$$

$$q_{23} = 0$$

$$q_{31} = 0$$

$$q_{32} = 0$$

$$q_{33} = \frac{1.879(s - 0.071 \pm 1.259)(s + 0.2)(s + 0.257)(s + 5.344 \pm 3.210)}{s(s - 0.162 \pm 0.065)(s + 0.269)(s + 0.988 \pm 0.648)(s + 5.167 \pm 2.826)(s + 8.242)}$$

B.16 Plant Case 16 - $C_L = 0.6$, Gross Weight = 277,500 pounds

$$q_{11} = \frac{0.273(s + 0.321 \pm 3.172)}{(s + 0.056)(s + 0.124 \pm 0.552)(s + 1.180)(s + 133.736)}$$

$$q_{12} = \frac{4.675D - 3(s + 0.321 \pm 3.172)}{s(s - 0.009)(s + 0.151 \pm 3.142)(s + 1)}$$

$$q_{13} = 0$$

$$q_{21} = \frac{-12.319(s + 0.321 \pm 3.172)}{(s - 0.028 \pm 0.023)(s + 0.421 \pm 1.680)(s + 10.025)}$$

$$q_{22} = \frac{26.060(s + 0.321 \pm 3.172)}{s(s + 0.099)(s + 0.319 \pm 3.158)(s + 266.819)}$$

$$q_{23} = 0$$

$$q_{31} = 0$$

$$q_{32} = 0$$

$$q_{33} = \frac{1.824(s - 0.163 \pm 1.327)(s + 0.2)(s + 0.539)(s + 5.310 \pm 3.420)}{s(s + 0.121)(s + 0.189)(s + 0.351)(s + 1.046 \pm 0.780)(s + 5.126 \pm 2.520)(s + 8.157)}$$

B-11

Appendix C. C-135B and Autopilot Input Response

This appendix contains the time response plots for the C-135B and autopilot.
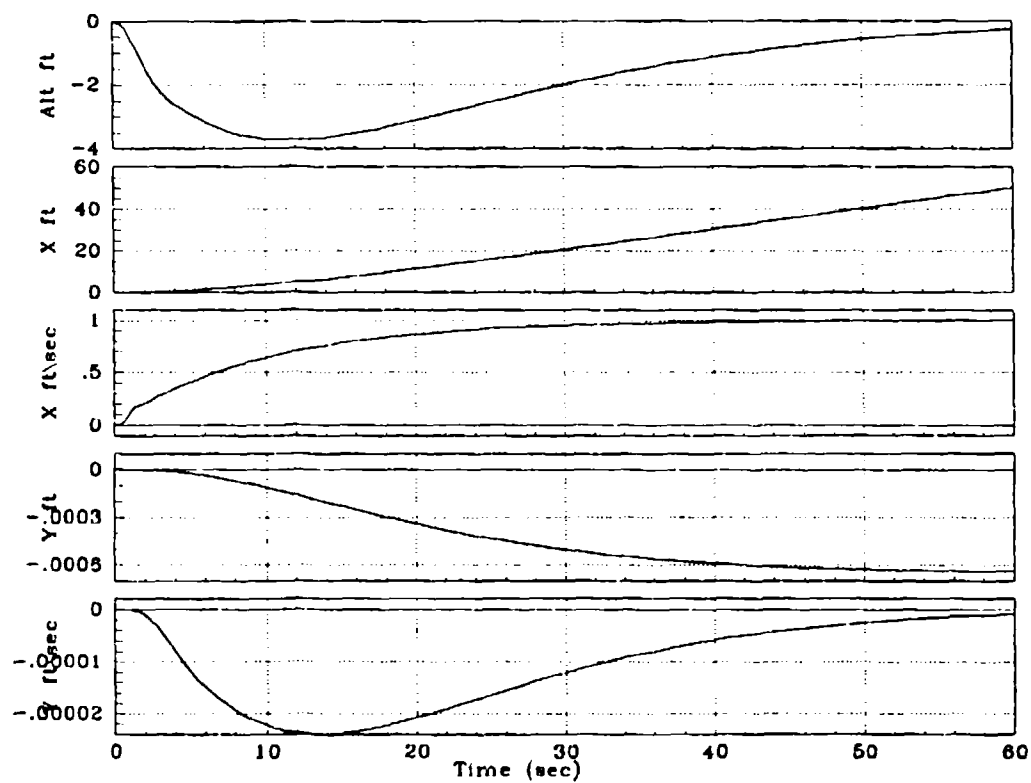
Figure C.1   Mach Hold Response to 1 ft/sec Step Input - $C_L = 0.2$
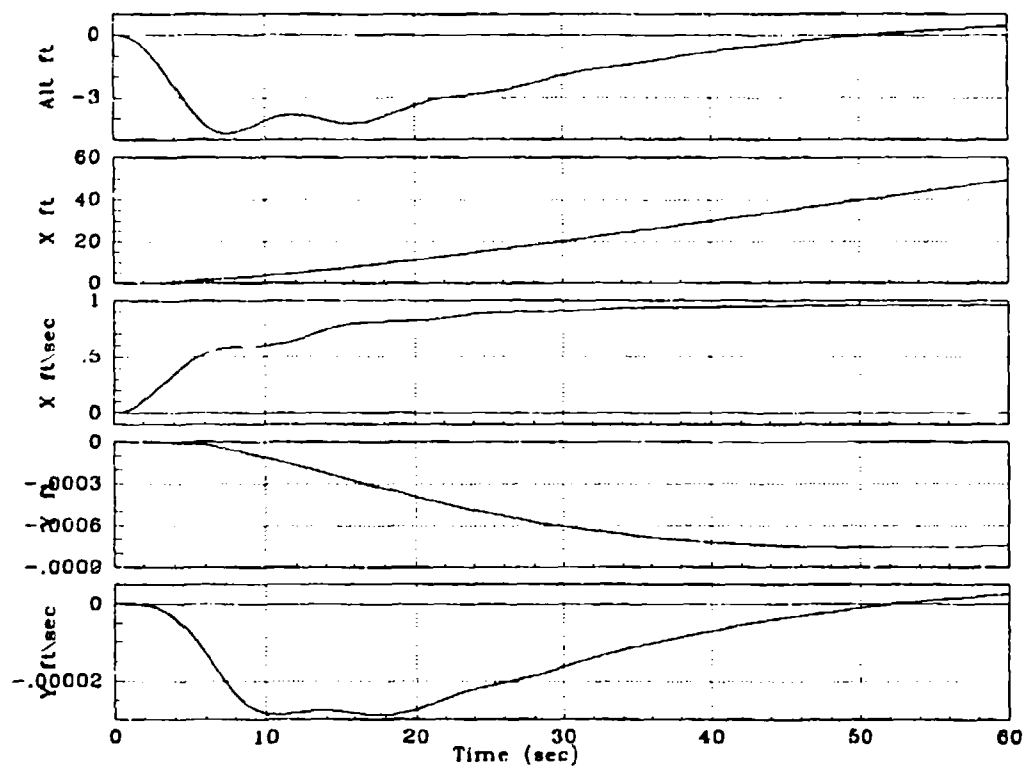
Figure C.2   Mach Hold Response to 1 ft/sec Step Input - C_L = 0.6
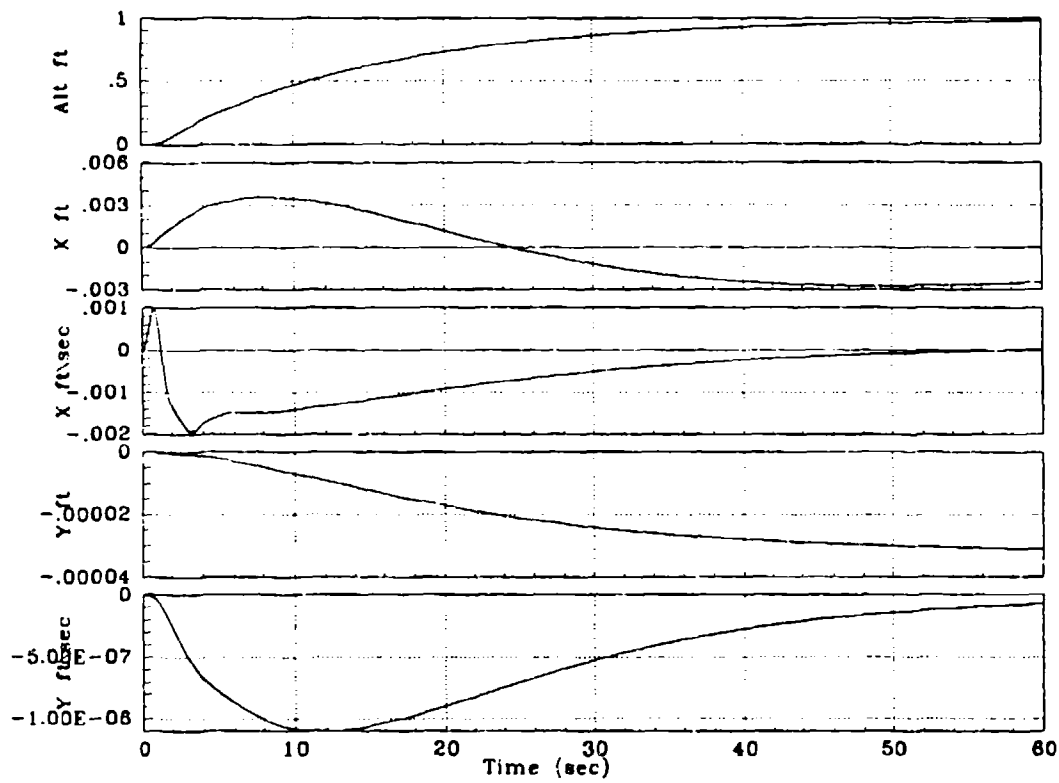
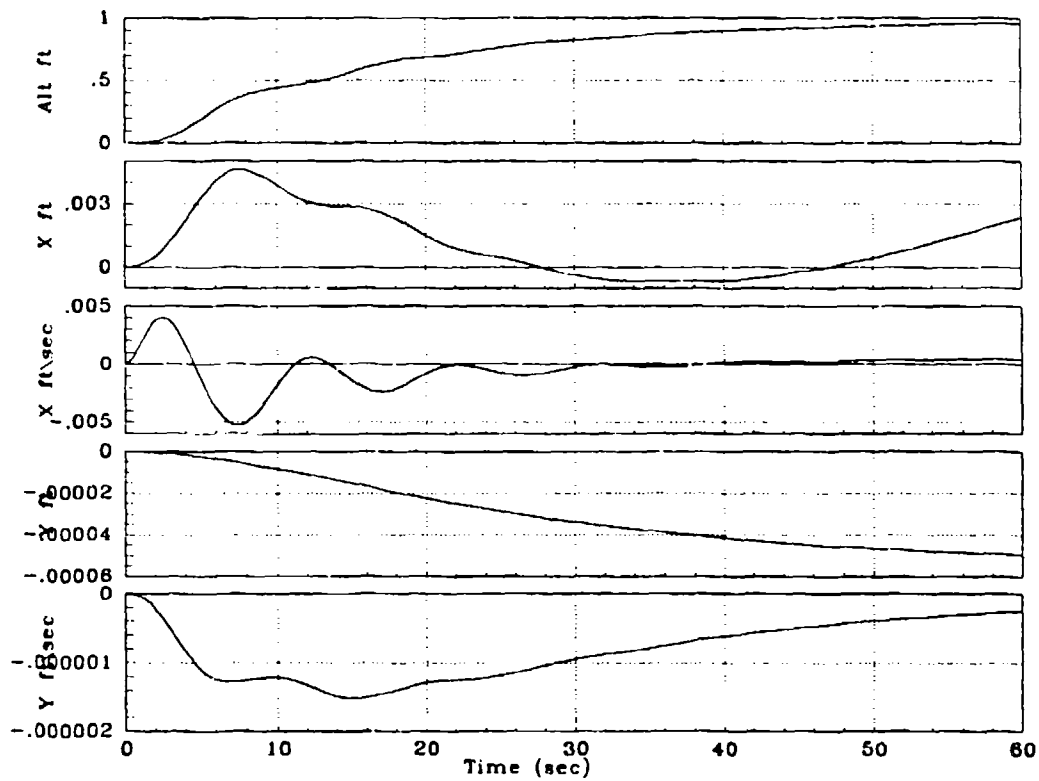Figure C.3 Altitude Hold Response to 1 foot Step input - $C_L = 0.2$

C-4

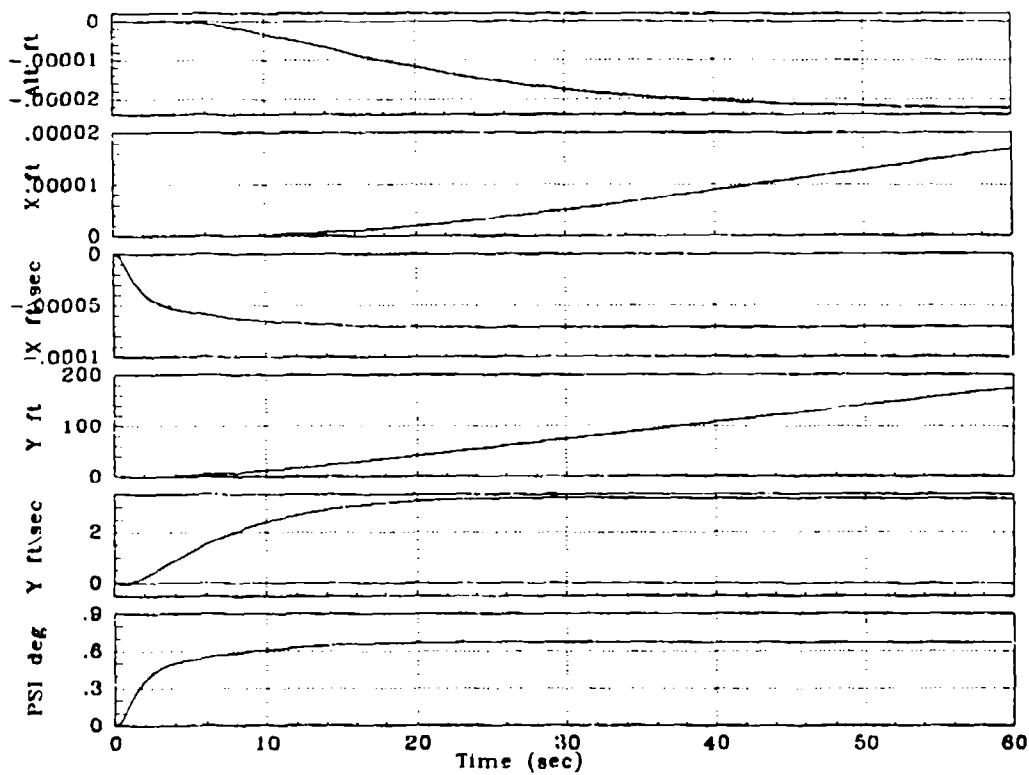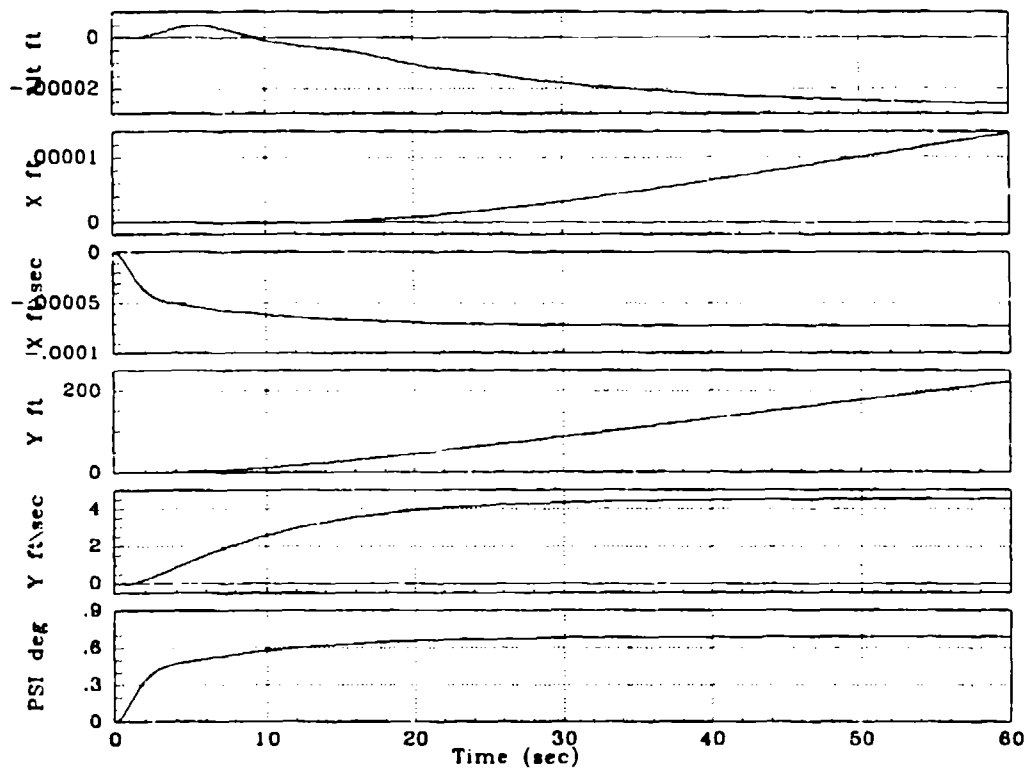Figure C.4   Altitude Hold Response to 1 Foot Step Input - C_L = 0.6

Figure C.5 Rudder Control Response to 1 deg Step Input - $C_L = 0.2$

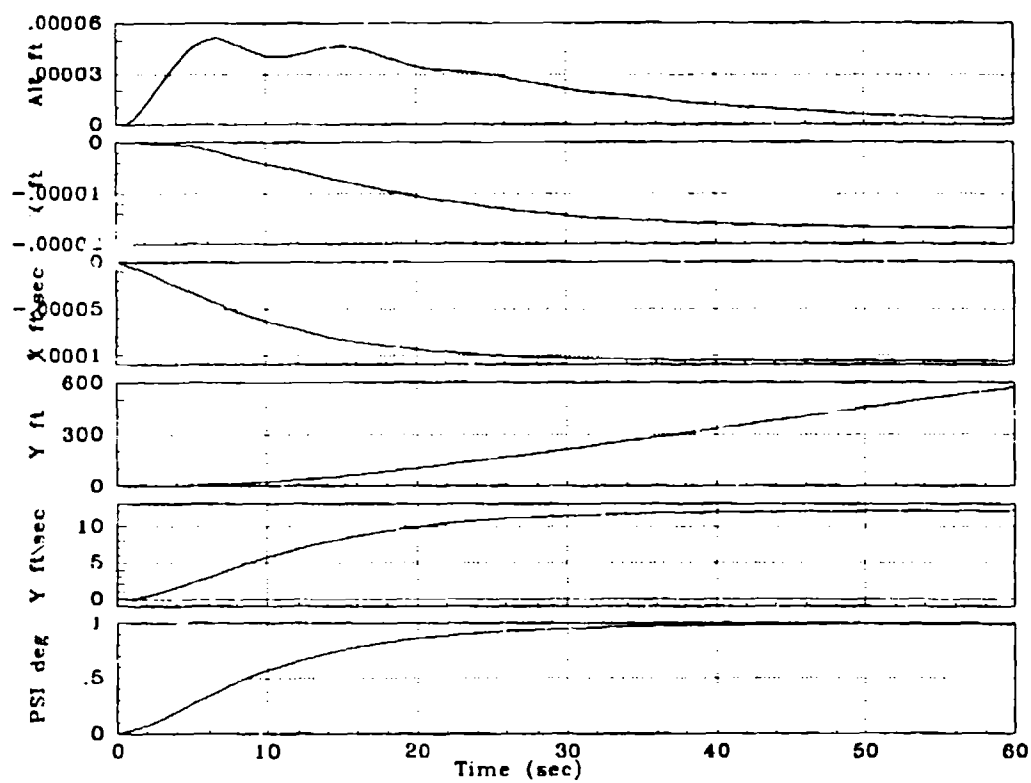Figure C.6 Rudder Control Response to 1 deg Step Input - $C_L = 0.6$
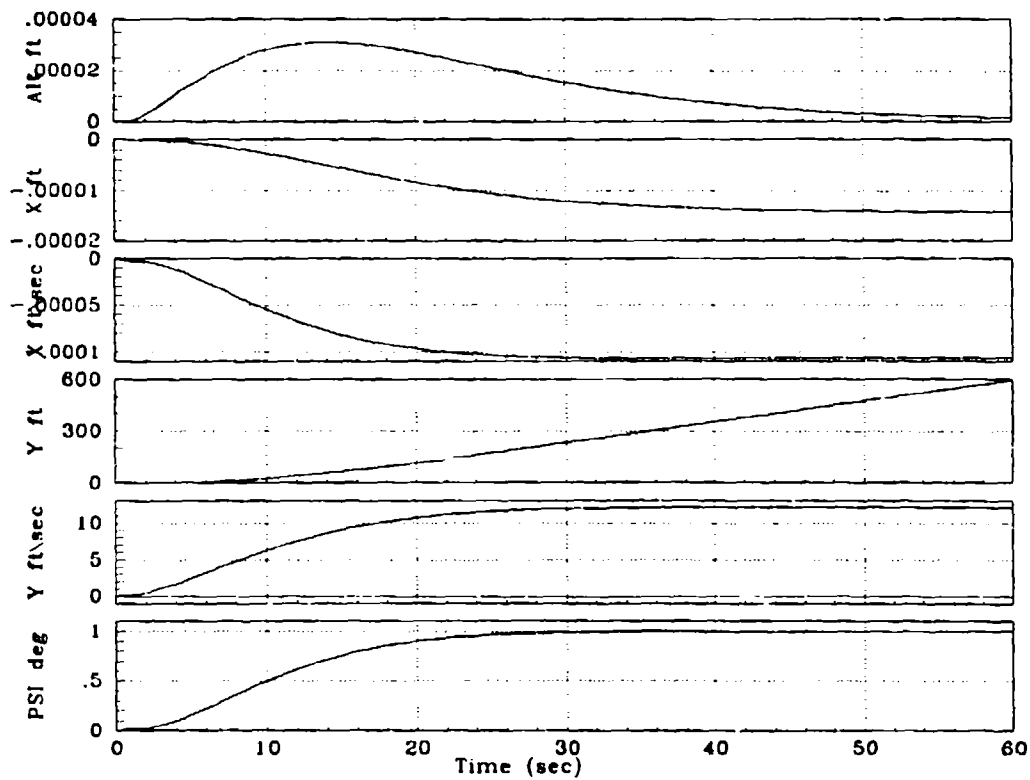
Figure C.7 Aileron Control Response to 1 deg Step Input - $C_L = 0.2$

C-8

Figure C.8 Aileron Control Response to 1 deg Step Input - $C_L = 0.6$

C-9

Appendix D. C-135B and Autopilot Disturbance Response

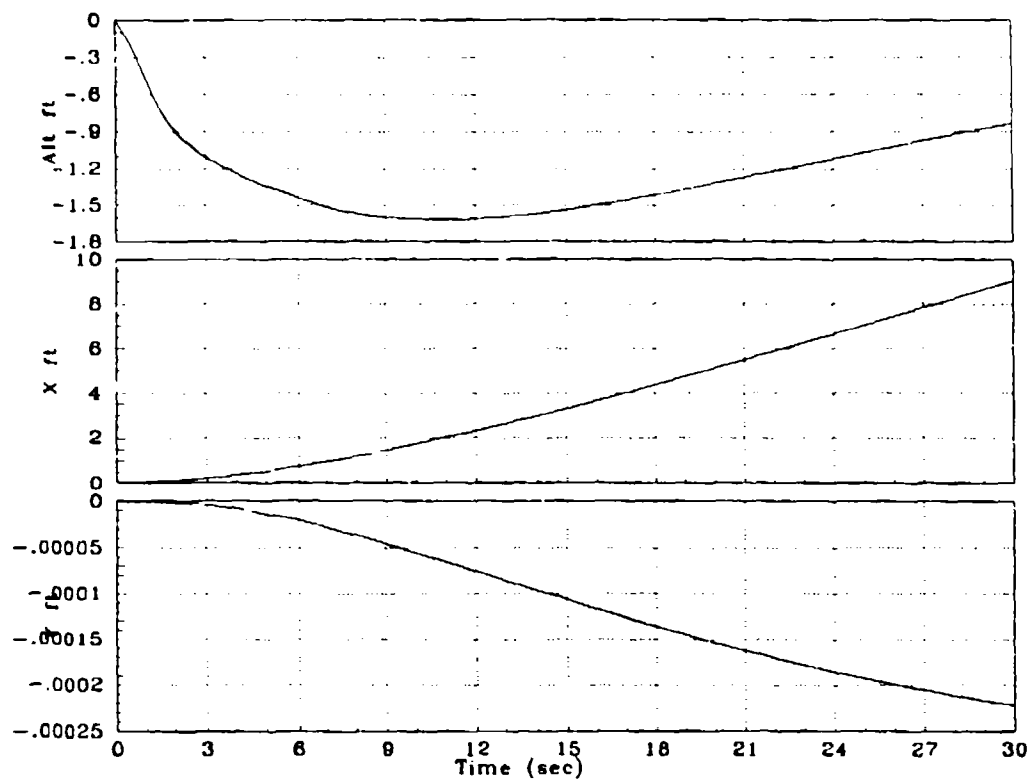This appendix contains the time response plots for the C-135B and autopilot in the presence of external disturbance.

Figure D.1 X, Y, Z Response to Longitudinal Wind Disturbance - $C_L = 0.2$
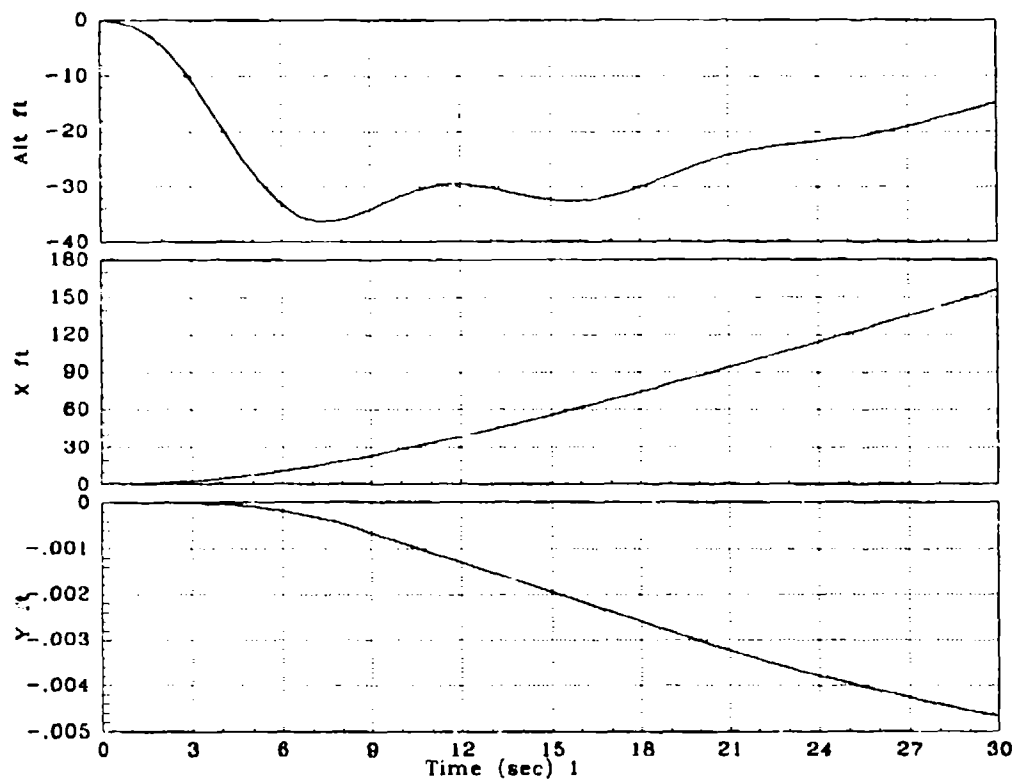
Figure D.2 X, Y, Z Response to Longitudinal Wind Disturbance - $C_L = 0.6$
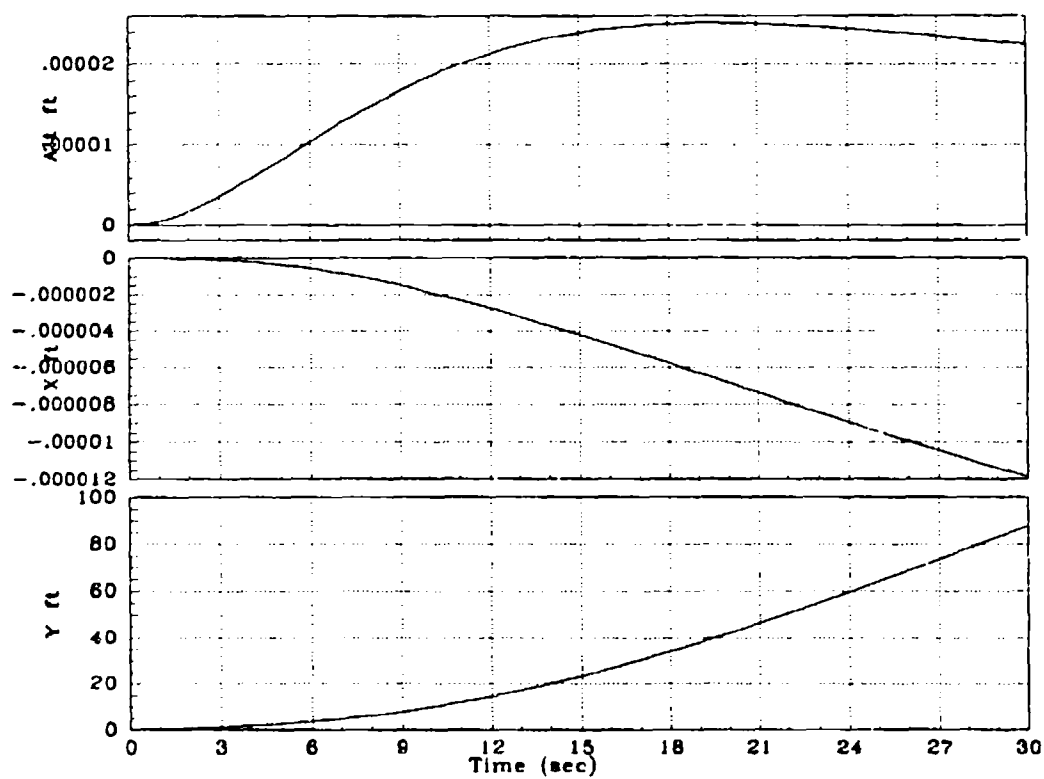
D-3

Figure D.3   X, Y, Z Response to Lateral Wind Disturbance - $C_L = 0.2$
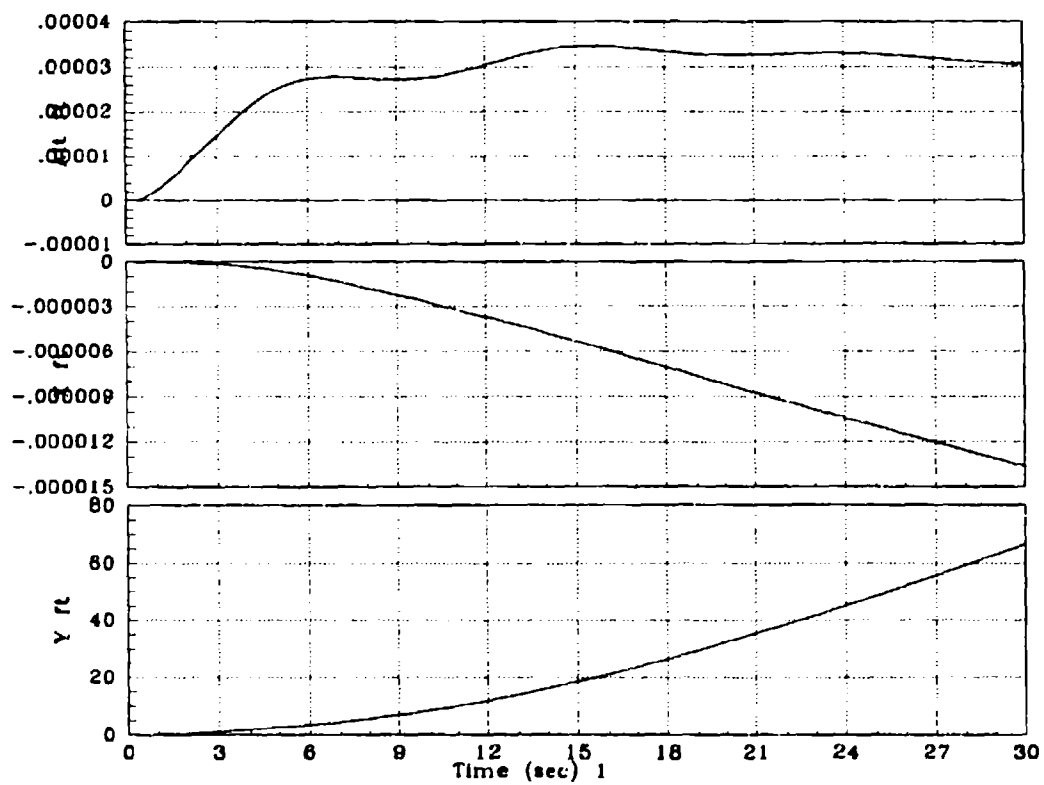
D-4

Figure D.4 X, Y, Z Response to Lateral Wind Disturbance - $C_L = 0.6$
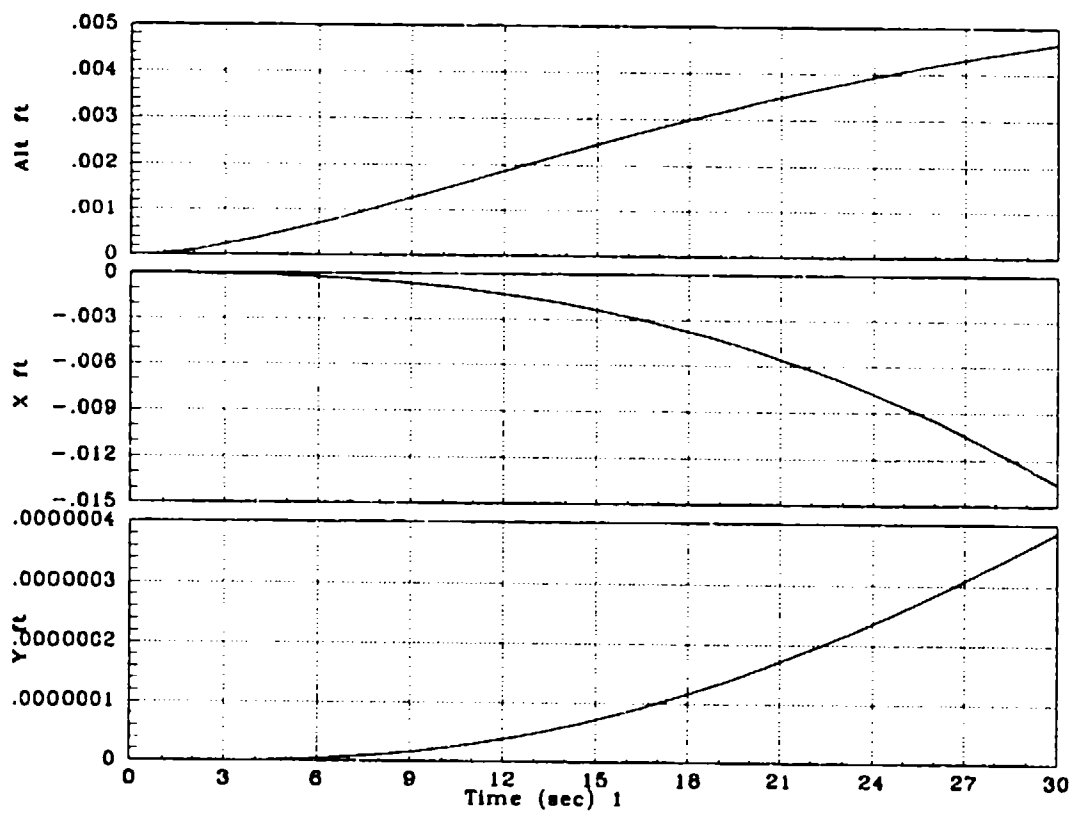
Figure D.5 X, Y, Z Response to Refueling Disturbance - C_L = 0.2
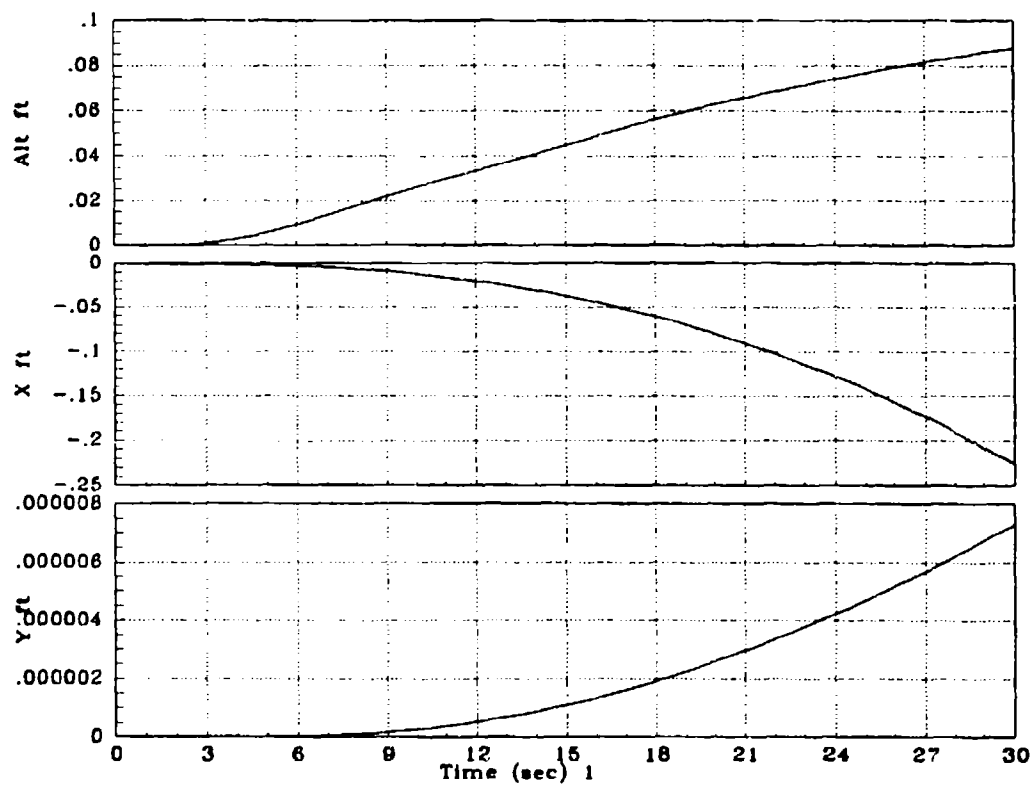
Figure D.6   X, Y, Z Response to Refueling Disturbance - $C_L = 0.6$

Appendix E. Templates and Boundary Plots

This appendix contains the template plots. It also presents the stability and disturbance boundaries used to form the composite bounds.

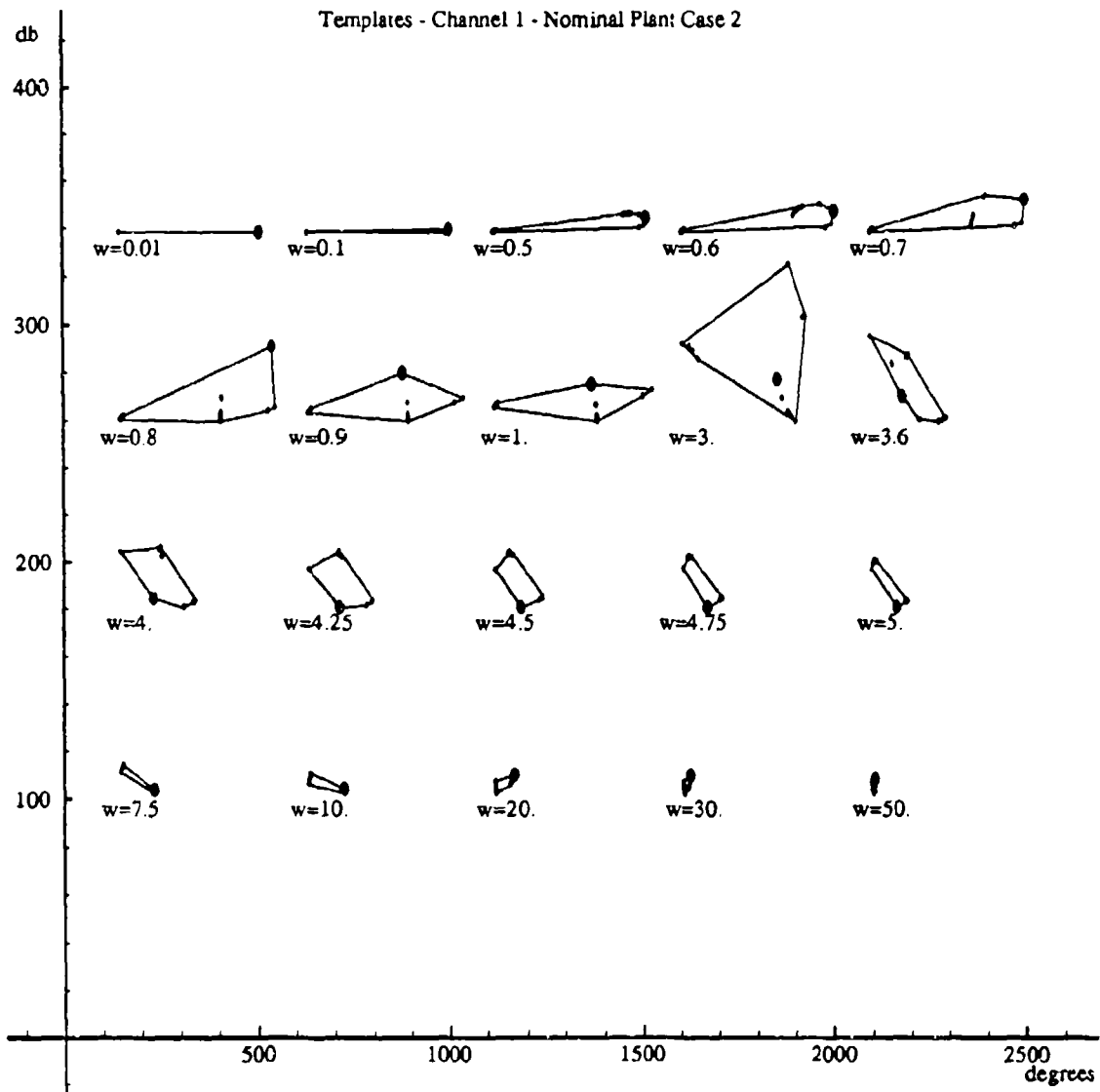Templates - Channel 1 - Nominal Plant Case 2

Figure E.1 Channel 1 Templates

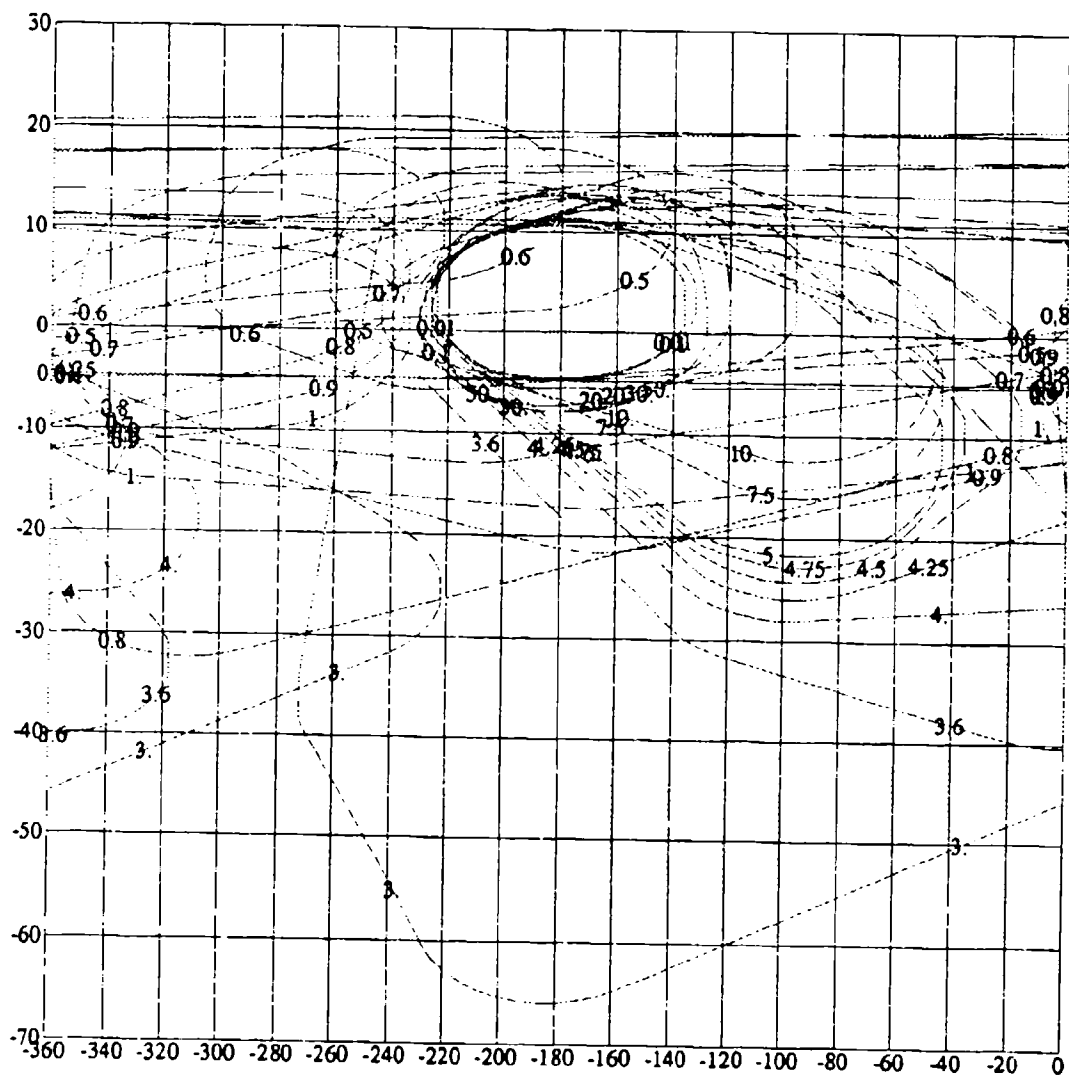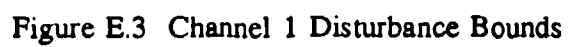Figure E.2 Channel 1 Stability Bounds

E-3

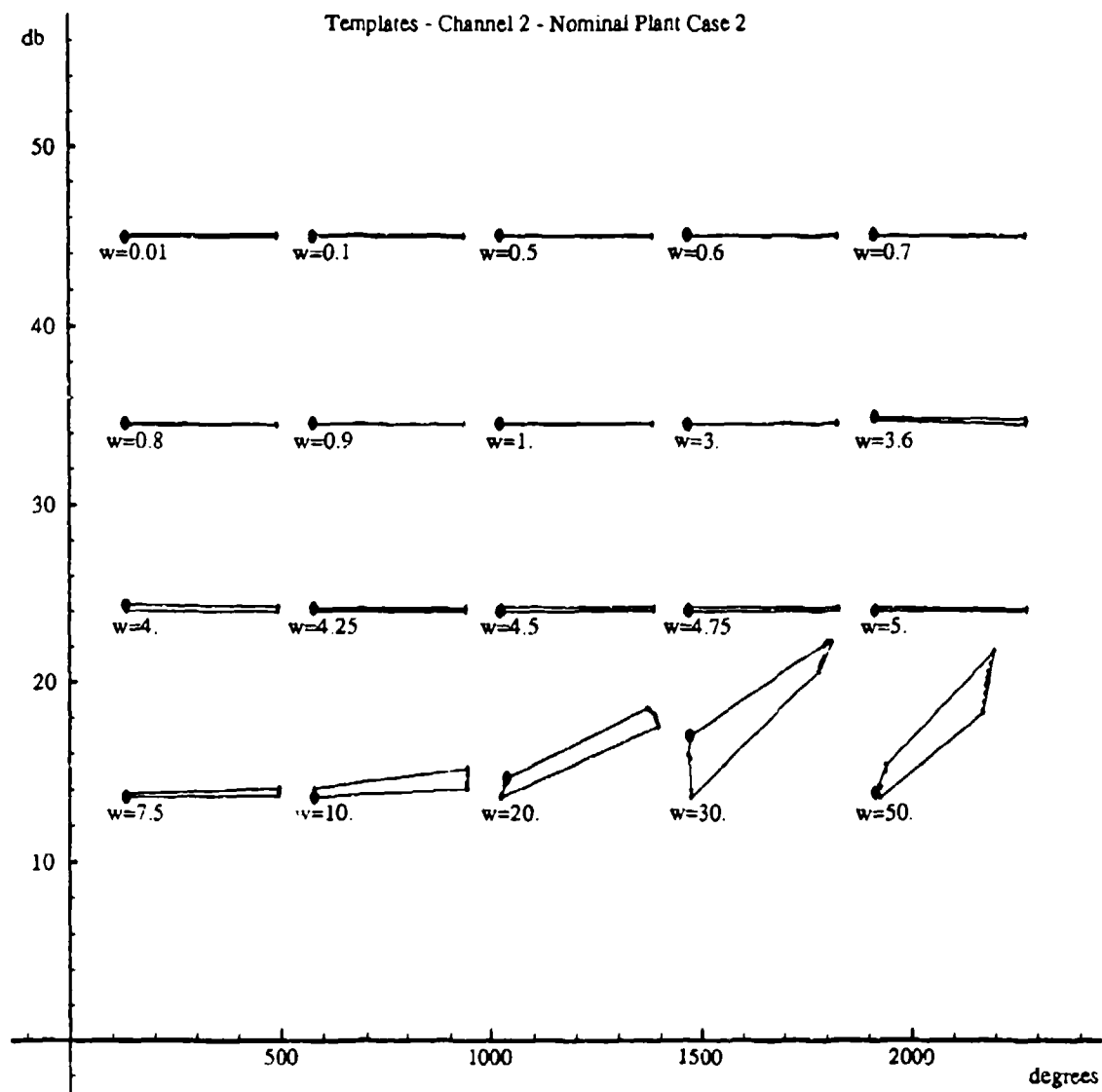Figure E.3 Channel 1 Disturbance Bounds

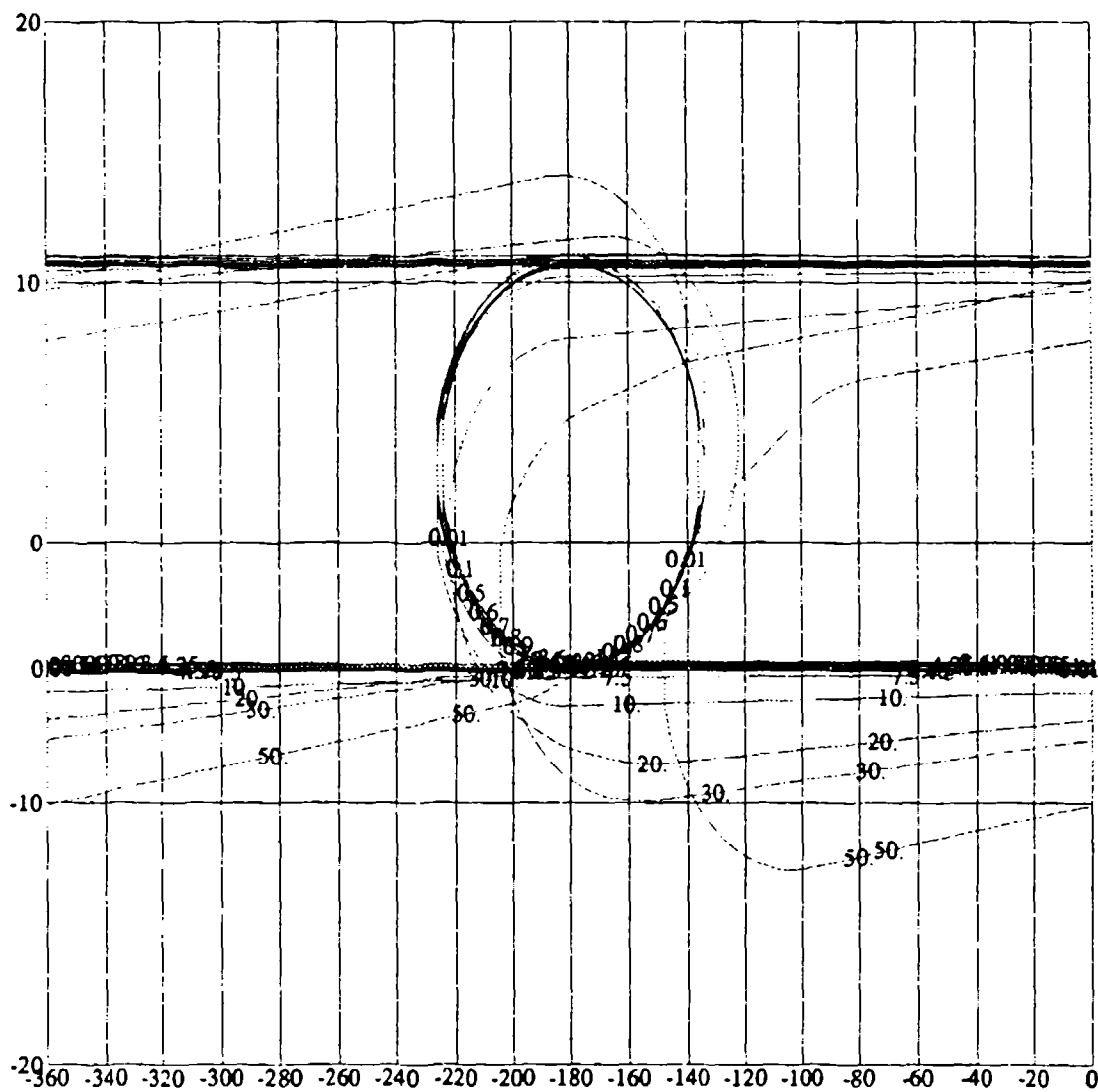Figure E.4   Channel 2 Templates

Figure E.5 Channel 2 Stability Bounds

E-6
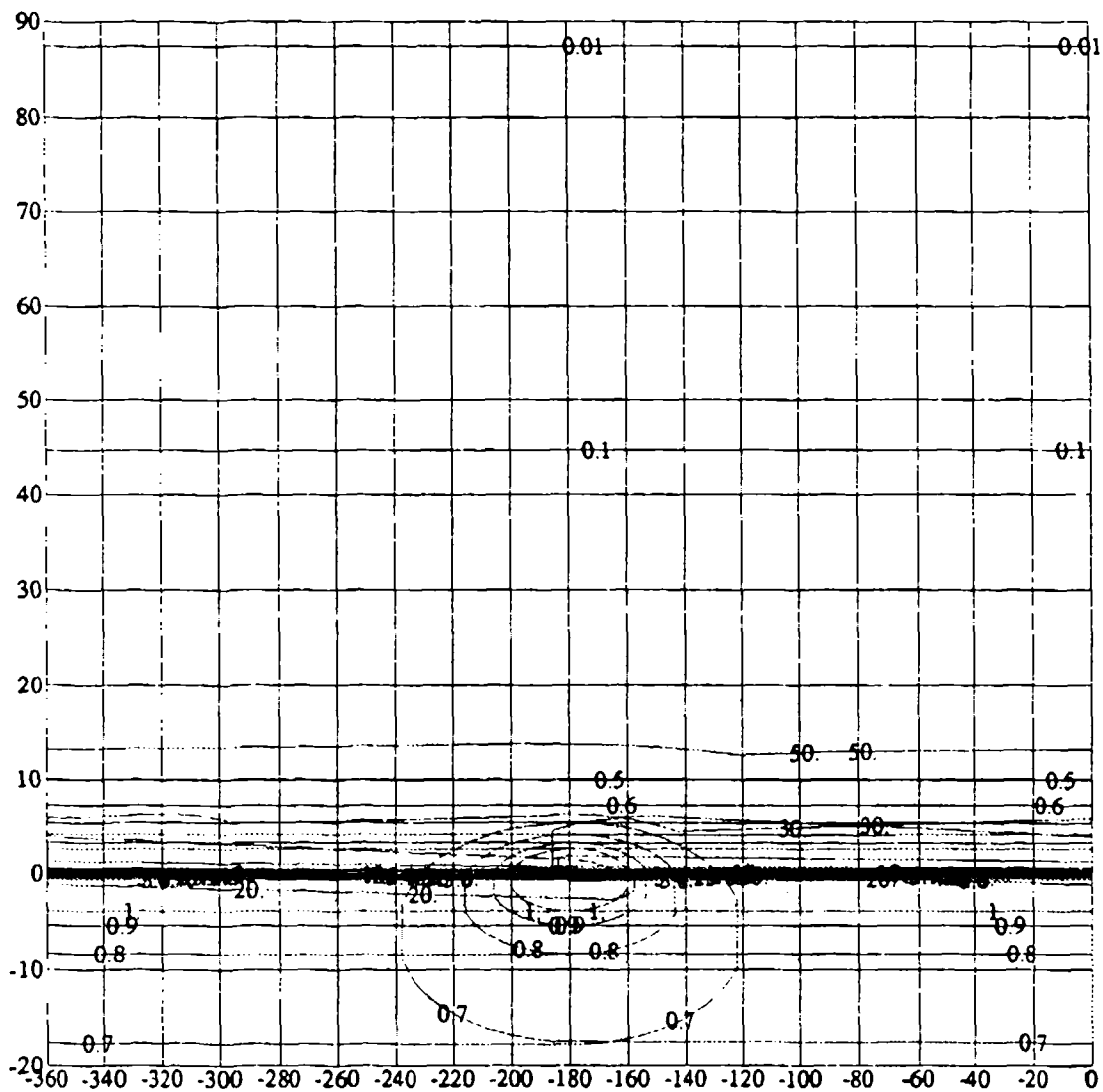
Figure E.6   Channel 2 Disturbance Bounds
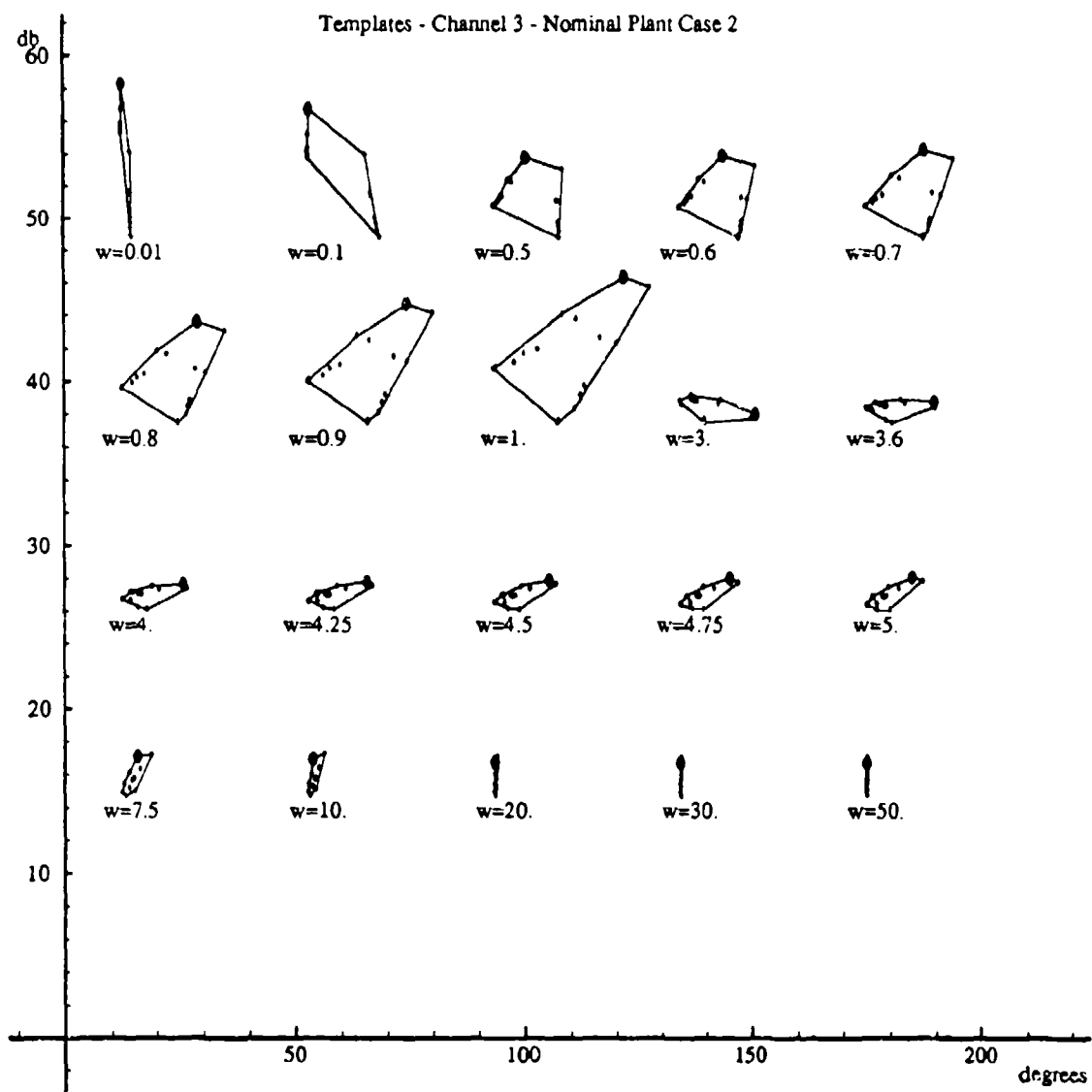
Figure E.7 Channel 3 Templates

E-8

Figure E.8 Channel 3 Stability Bounds

E-9
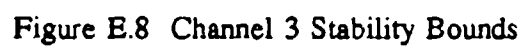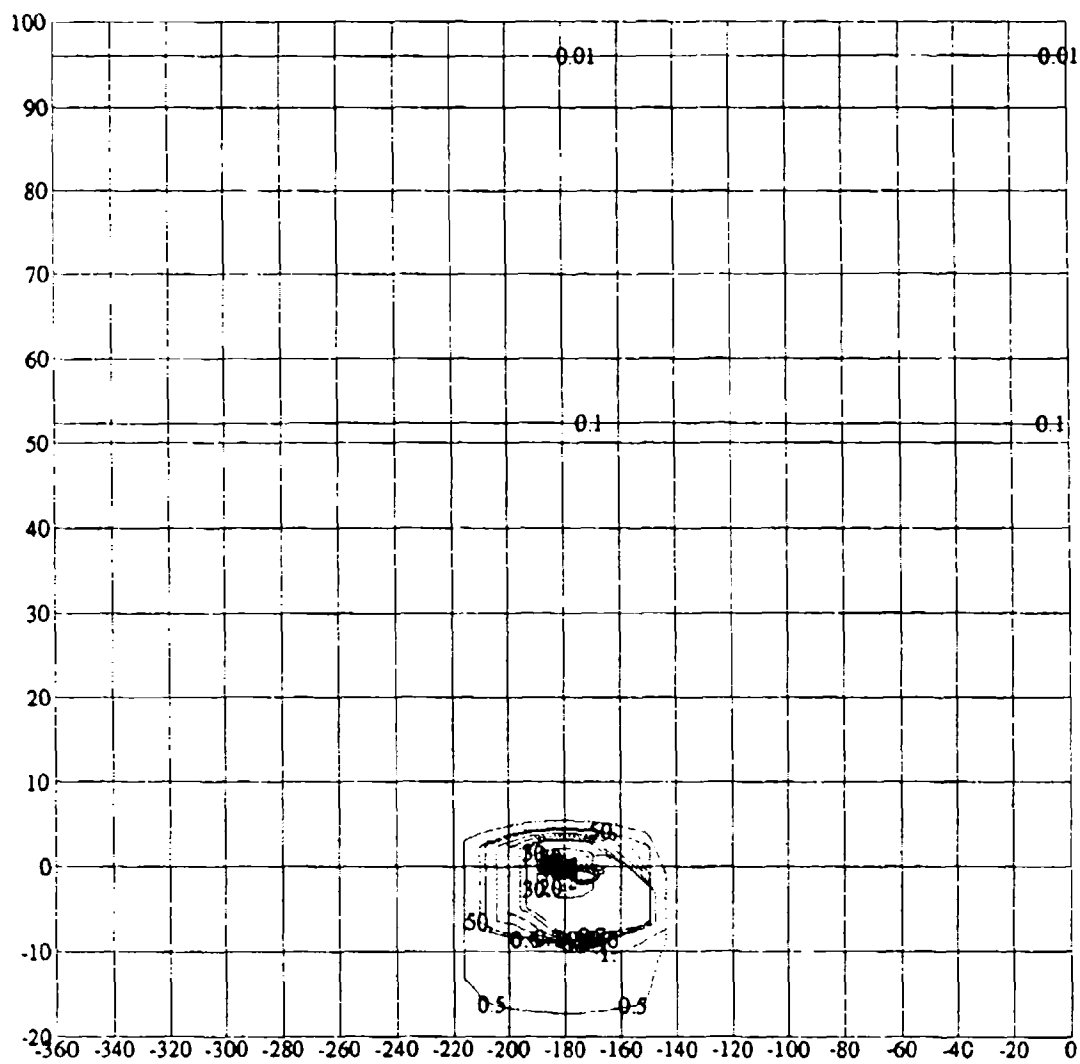
Figure E.9 Channel 3 Disturbance Bounds

E-10

Appendix F. QFT Compensators

This appendix contains the compensators designed in Chapter *V*.

F.1 Channel 1 compensator, g_1

$$\frac{(s+0.3)(s+0.25\pm0.433)(s+3)(s+9)(s+1.14\pm3.747)(s+200)}{s(s+2)(s+0.32\pm3.184)(s+90\pm4.02D-6)(s+135\pm65.38)(s+1100)} \qquad \text{(F-1)}$$

F.2 Channel 2 compensator, g_2

$$\frac{(s+0.25)(s+0.75)(s+1.2)(s+1.3)}{s(s+0.98\pm1)(s+10)(s+20)(s+120)} \qquad \text{(F-2)}$$

F.3 Channel 3 compensator g_3

$$\frac{(s+0.05)(s+0.1)(s+0.2)(s+0.6)(s+1.5\pm2.6)(s+5)(s+30)}{s(s+2.5D-4)(s+0.6\pm1.91)(s+10)(s+35\pm35.707)(s+37.5\pm64.95)} \qquad \text{(F-3)}$$

Bibliography

1. The Boeing Company. *Summary of the Stability, Control and Flying Qualities Information for All the -135 Series Airplanes.* Technical Report D3-9090 REV LTR A, Wichita KS, October 1073.

2. D'Azzo, John J. and Constantine H. Houpis. *Linear Control System Analysis and Design, Conventional and Modern* (Third Edition). McGraw-Hill, 1988.

3. Houpis, Constantine H. *Quantitative Feedback Theory (QFT)--Technique for Designing Multivariable Control Systems.* Technical Report AFWAL-TR-86-3107, Wright-Patterson AFB, OH: Flight Dynamics Laboratory, January 1987.

4. Sating, Richard R. *QFT CAD Package.* MS thesis, Air Force Institute of Technology, Wright-Patterson AFB, OH, March 1992.

5. Boeing Computer Services, Seattle, WA 98124-0346. *EASY5x - User's Guide,* January 1992

6. Blakelock H. John. *Automatic Control of Aircraft and Missiles* (Second Edition). Wiley-Interscience, 1991.

7. MATRIX$_x$ CAD/CAE Program, Integrated Systems Inc., South Matick, MA, 01760.

8. Pachter, Meir, "Personal Conversation, Correspondence and Class Notes." Professor of Electrical Engineering, Air Force Institute of Technology, Wright-Patterson AFB, OH, May 1992 through June 1993.

9. Houpis, Constantine H., "Personal Conversation, Correspondence and Class Notes." Professor of Electrical Engineering, Air Force Institute of Technology, Wright-Patterson AFB, OH, May 1990 through June 1993.

10. Roskam, Jan. *Airplane Flight Dynamics and Automatic Flight Controls, Part I.* Roskam Aviation and Engineering Corp., 1982.

11. Military Specification - Definition of Atmospheric Disturbance Model Form. MIL-STD 1797(USAF) APPENDIX A. 31 March 1987.

Vita

Captain Dennis Trosen was born on 10 August 1962 in Detroit, Michigan. He graduated from Waterford Township High School, Waterford Township Michigan in 1980. He attended Michigan Technological University and received his Bachelor of Science in Electrical Engineering in May of 1984. He received his commission from Officer Training School in August 1984. He was first assigned to the 6585th Test Group at Holloman AFB New Mexico were he was a guidance system component test engineer and then program manager for the Advanced Guidance Technology test program. In 1990 he was reassigned to the Foreign Aerospace Science and Technology Center at Wright-Patterson AFB Ohio, where he performed technology analysis of foreign C^3 systems. In June 1992, he entered the School of Engineering Air Force Institute of Technology studying for a Masters of Science degree in Electrical Engineering. Upon graduation from AFIT he will be assigned to Wright Laboratory at Wright-Patterson AFB, Ohio.

Permanent address: 124 Exmoor
                       Waterford, Michigan 48054

REPORT DOCUMENTATION PAGE

Public reporting burden for this collection of information is estimated to average 1 hour per response, including the time for reviewing instructions, searching existing data sources, gathering and maintaining the data needed, and completing and reviewing the collection of information. Send comments regarding this burden estimate or any other aspect of this collection of information, including suggestions for reducing this burden, to Washington Headquarters Services, Directorate for Information Operations and Reports, 1215 Jefferson Davis Highway, Suite 1204, Arlington, VA 22202-4302, and to the Office of Management and Budget, Paperwork Reduction Project (0704-0188), Washington, DC 20503

1. AGENCY USE ONLY (Leave blank)	2. REPORT DATE 7 June 1993	3. REPORT TYPE AND DATES COVERED Master's Thesis

4. TITLE AND SUBTITLE
DEVELOPMENT OF AN AIR-TO-AIR REFUELING AUTOMATIC FLIGHT CONTROL SYSTEM USING QUANTITATIVE FEEDBACK THEORY

5. FUNDING NUMBERS

6. AUTHOR(S)
Dennis W. Trosen

7. PERFORMING ORGANIZATION NAME(S) AND ADDRESS(ES)
Air Force Institute of Technology, WPAFB OH 45433-6583

8. PERFORMING ORGANIZATION REPORT NUMBER
AFIT/GE/ENG/93J-03

9. SPONSORING/MONITORING AGENCY NAME(S) AND ADDRESS(ES)
Wright Laboratory
FIGS
WPAFB OH 45433-6583

10. SPONSORING/MONITORING AGENCY REPORT NUMBER

11. SUPPLEMENTARY NOTES

12a. DISTRIBUTION AVAILABILITY STATEMENT
Distribution Unlimited

12b. DISTRIBUTION CODE

13. ABSTRACT (Maximum 200 words)

Abstract

Quantitative Feedback Theory and the improved method Quantitative Feedback Theory are enhanced to include the rejection of disturbance at the system output. The enhanced Quantitative Feedback Theory and improved method Quantitative Feedback Theory processes are applied to the design of an automatic flight control system to regulate position of the C-135B fuel receiving aircraft relative to the tanker during air-to-air refueling. A simple feedback control system is developed that will achieve stable position regulation. State-space aircraft models are generated. An "inner loop" autopilot is designed to reduce the plant cutoff frequency and provide the system inputs for the Quantitative Feedback Theory compensators. Disturbance models representing disturbance due to wind gusts and refueling are developed. The flight control system is designed using the enhanced Quantitative Feedback Theory equations. Linear simulations are performed on MATRIX, and nonlinear simulations are run on EASY5x. The results of the simulations show excellent results. The simulation results indicate that air-to-air automatic flight control system are technically achievable, and that implementation in USAF aircraft is possible.

14. SUBJECT TERMS
QFT, flight control, air-to-air refueling, disturbance rejection, regulation control

15. NUMBER OF PAGES
125

16. PRICE CODE

17. SECURITY CLASSIFICATION OF REPORT UNCLASSIFIED	18. SECURITY CLASSIFICATION OF THIS PAGE UNCLASSIFIED	19. SECURITY CLASSIFICATION OF ABSTRACT UNCLASSIFIED	20. LIMITATION OF ABSTRACT UL

NSN 7540-01-280-5500

GENERAL INSTRUCTIONS FOR COMPLETING SF 298

The Report Documentation Page (RDP) is used in announcing and cataloging reports. It is important that this information be consistent with the rest of the report, particularly the cover and title page. Instructions for filling in each block of the form follow. It is important to *stay within the lines* to meet *optical scanning requirements*.

Block 1. Agency Use Only *(Leave blank)*

Block 2. Report Date. Full publication date including day, month, and year, if available (e.g. 1 Jan 88). Must cite at least the year.

Block 3. Type of Report and Dates Covered. State whether report is interim, final, etc. If applicable, enter inclusive report dates (e.g. 10 Jun 87 - 30 Jun 88).

Block 4. Title and Subtitle. A title is taken from the part of the report that provides the most meaningful and complete information. When a report is prepared in more than one volume, repeat the primary title, add volume number, and include subtitle for the specific volume. On classified documents enter the title classification in parentheses.

Block 5. Funding Numbers. To include contract and grant numbers; may include program element number(s), project number(s), task number(s), and work unit number(s). Use the following labels.

C	- Contract	PR	-	Project
G	- Grant	TA	-	Task
PE	- Program Element	WU	-	Work Unit Accession No

Block 6. Author(s). Name(s) of person(s) responsible for writing the report, performing the research, or credited with the content of the report. If editor or compiler, this should follow the name(s).

Block 7. Performing Organization Name(s) and Address(es). Self-explanatory.

Block 8. Performing Organization Report Number. Enter the unique alphanumeric report number(s) assigned by the organization performing the report.

Block 9. Sponsoring/Monitoring Agency Name(s) and Address(es). Self-explanatory.

Block 10. Sponsoring/Monitoring Agency Report Number. *(If known)*

Block 11. Supplementary Notes. Enter information not included elsewhere such as: Prepared in cooperation with...; Trans of...; To be published in... When a report is revised, include a statement whether the new report supersedes or supplements the older report.

Block 12a. Distribution/Availability Statement. Denotes public availability or limitations. Cite any availability to the public. Enter additional limitations or special markings in all capitals (e.g. NOFORN, REL, ITAR).

- **DOD** - See DoDD 5230.24, "Distribution Statements on Technical Documents."
- **DOE** - See authorities.
- **NASA** - See Handbook NHB 2200.2.
- **NTIS** - Leave blank.

Block 12b. Distribution Code.

- **DOD** - Leave blank.
- **DOE** - Enter DOE distribution categories from the Standard Distribution for Unclassified Scientific and Technical Reports.
- **NASA** - Leave blank.
- **NTIS** - Leave blank.

Block 13. Abstract. Include a brief *(Maximum 200 words)* factual summary of the most significant information contained in the report.

Block 14. Subject Terms. Keywords or phrases identifying major subjects in the report.

Block 15. Number of Pages. Enter the total number of pages.

Block 16. Price Code. Enter appropriate price code *(NTIS only)*.

Blocks 17. - 19. Security Classifications. Self-explanatory. Enter U.S. Security Classification in accordance with U.S. Security Regulations (i.e., UNCLASSIFIED). If form contains classified information, stamp classification on the top and bottom of the page.

Block 20. Limitation of Abstract. This block must be completed to assign a limitation to the abstract. Enter either UL (unlimited) or SAR (same as report). An entry in this block is necessary if the abstract is to be limited. If blank, the abstract is assumed to be unlimited.